University of Kentucky
UKnowledge

Theses and Dissertations--Earth and Environmental Sciences

Earth and Environmental Sciences

2023

THE APPALACHIAN SYSTEM OF BASINS AND PLATFORMS AS A TECTONOSTRATIGRAPHIC ANALOGUE TO THE BARENTS SEA SHELF: WHERE ARCTIC MEETS THE APPALACHIANS

Gustavo De Aguiar Martins
University of Kentucky, gustavogeologist@gmail.com
Author ORCID Identifier:
https://orcid.org/0000-0002-8608-2363
Digital Object Identifier: https://doi.org/10.13023/etd.2023.374

Right click to open a feedback form in a new tab to let us know how this document benefits you.

Recommended Citation

De Aguiar Martins, Gustavo, "THE APPALACHIAN SYSTEM OF BASINS AND PLATFORMS AS A TECTONOSTRATIGRAPHIC ANALOGUE TO THE BARENTS SEA SHELF: WHERE ARCTIC MEETS THE APPALACHIANS" (2023). *Theses and Dissertations--Earth and Environmental Sciences*. 101.
https://uknowledge.uky.edu/ees_etds/101

This Doctoral Dissertation is brought to you for free and open access by the Earth and Environmental Sciences at UKnowledge. It has been accepted for inclusion in Theses and Dissertations--Earth and Environmental Sciences by an authorized administrator of UKnowledge. For more information, please contact UKnowledge@lsv.uky.edu.

STUDENT AGREEMENT:

I represent that my thesis or dissertation and abstract are my original work. Proper attribution has been given to all outside sources. I understand that I am solely responsible for obtaining any needed copyright permissions. I have obtained needed written permission statement(s) from the owner(s) of each third-party copyrighted matter to be included in my work, allowing electronic distribution (if such use is not permitted by the fair use doctrine) which will be submitted to UKnowledge as Additional File.

I hereby grant to The University of Kentucky and its agents the irrevocable, non-exclusive, and royalty-free license to archive and make accessible my work in whole or in part in all forms of media, now or hereafter known. I agree that the document mentioned above may be made available immediately for worldwide access unless an embargo applies.

I retain all other ownership rights to the copyright of my work. I also retain the right to use in future works (such as articles or books) all or part of my work. I understand that I am free to register the copyright to my work.

REVIEW, APPROVAL AND ACCEPTANCE

The document mentioned above has been reviewed and accepted by the student's advisor, on behalf of the advisory committee, and by the Director of Graduate Studies (DGS), on behalf of the program; we verify that this is the final, approved version of the student's thesis including all changes required by the advisory committee. The undersigned agree to abide by the statements above.

Gustavo De Aguiar Martins, Student

Dr. Frank R. Ettensohn, Major Professor

Dr. Michael McGlue, Director of Graduate Studies

THE APPALACHIAN SYSTEM OF BASINS AND PLATFORMS AS A TECTONOSTRATIGRAPHIC ANALOGUE TO THE BARENTS SEA SHELF: WHERE ARCTIC MEETS THE APPALACHIANS

DISSERTATION

A dissertation submitted in partial fulfillment of the
requirements for the degree of Doctor of Philosophy in the
College of Arts and Sciences
at the University of Kentucky

By
Gustavo De Aguiar Martins
Lexington, Kentucky
Director: Dr. Frank R. Ettensohn, Professor of Geosciences
Lexington, Kentucky
2023

Copyright © Gustavo De Aguiar Martins 2023
https://orcid.org/0000-0002-8608-2363

ABSTRACT OF DISSERTATION

THE APPALACHIAN SYSTEM OF BASINS AND PLATFORMS AS A TECTONOSTRATIGRAPHIC ANALOGUE TO THE BARENTS SEA SHELF: WHERE ARCTIC MEETS THE APPALACHIANS

Divided between Norway and Russia, the Barents Sea shelf (BSS) is an ~1.4 million km^2 Arctic province, containing significant hydrocarbon accumulations. However, much of the area is frontier, and geologic data are often restricted or unavailable. One strategy to mitigate lack of geologic data is the use of analogues from well-known, mature basins. Even though there have been attempts to use analogues to study the geology of the BSS, such use is limited. Moreover, no analogue, to my knowledge, has been capable of addressing the regional tectonostratigraphic development of the shelf as a whole.

In this research, the Appalachian system of basins and platforms and its included flexural stratigraphic sequences are defined as a tectonostratigraphic analogue, aiding the interpretation of BSS tectonostratigraphic evolution. Although temporally and paleogeographically different, both the Appalachian and BSS areas reflect collisional regimes, characterized by early subduction-related orogenies that concluded with a final collisional event. In the Appalachian foreland basin and adjacent intracratonic areas, each orogeny was defined by one or more, unconformity-bound, flexural stratigraphic sequences, called "tectophase" sequences.

The BSS tectonostratigraphic succession exhibits several unconformity-bound stratigraphic sequences that are comparable to tectophase sequences from the Appalachian area. These BSS sequences begin with black shales and end with molasse-like wedges of clastic sediments, which suggest flexural responses to orogeny. Much of this succession was deposited across structural elements that were likely reactivated by far-field responses to periods of Uralian–Pai–Khoi–Novaya Zemlya (Late Permian to Middle Jurassic) tectonism, involving the collision of Siberia-Kazakhstania with northern Baltican parts of Pangea. This widespread structural reactivation is discussed herein by applying the backstripping method for analysis of structural mechanisms, based on sediment thicknesses across various BSS structural elements. As in the Appalachian area, BSS structural reactivation occurred in various ways and times during ongoing Uralian–Pai–Khoi–Novaya Zemlya tectonism. In this context, the only part of the BSS collisional succession with sufficient lithologic data for regional studies is the Upper Triassic–Lower Jurassic (Carnian–Hettangian) stratigraphic succession. This succession includes erosional surfaces, as well as open-marine, marginal-marine and fluvio-deltaic deposits, and the

varying nature and thicknesses of these sediments across the several BSS structural elements suggest far-field reactivation by the coeval Novaya Zemlya Orogeny.

The Appalachian tectophase cycle is herein used to define pulses (tectophases) of deformational loading and possible sedimentary responses to foreland-basin and forebulge development. Although many BSS models suggest that tectonism in the area did not begin until the Late Triassic–Early Jurassic transition, sedimentary responses similar to those in the Appalachian tectophase model suggest that tectonism may have begun as early as Late Triassic (Norian) time. Even though many questions remain, the use of analogues external to the BSS, has not been a widespread practice. However, mature collisional settings like the Appalachian and BSS areas typically exhibit similar large-scale processes, meaning that analogues from one may provide new sources of information about the other.

KEYWORDS: Appalachian Basin, Barents Sea shelf, tectophases, tectonostratigraphy, foreland basins, Novaya Zemlya.

Gustavo De Aguiar Martins

05/07/2023

Date

THE APPALACHIAN SYSTEM OF BASINS AND PLATFORMS AS A TECTONOSTRATIGRAPHIC ANALOGUE TO THE BARENTS SEA SHELF: WHERE ARCTIC MEETS THE APPALACHIANS

By
Gustavo De Aguiar Martins

Dr. Frank R. Ettensohn
Director of Dissertation

Dr. Michael McGlue
Director of Graduate Studies

05/7/2023
Date

DEDICATION

To all international students. We can move mountains.

ACKNOWLEDGMENTS

I would like to thank Frank Ettensohn and Stig-Morten Knutsen, whom I see as true friends and from whom I have learned much, even beyond the geosciences. If there are two lessons I have learned from Frank Ettensohn, they are the importance of devoting time to a student and to never treat a question with arrogance regardless of who is asking. If there are two lessons I have learned from Stig-Morten Knutsen, they are the importance of investing in people and to avoid focusing on the word "problem."

I am grateful to the Norwegian Petroleum Directorate for project funding. Without their trust and willingness to take a risk, this research would likely not have been possible. I hope one day to give back, perhaps as part of their organization. I am also grateful to the University of Kentucky Department of Earth and Environmental Sciences for the opportunity to pursue the degree. I would like to thank my doctoral committee, Alice Turkington, Ryan Thigpen, and Steve Greb for their advice. I would like to thank the many Russian geologists for their kindness, specially Sergey Drachev. I give special thanks to Bjørn Lundschien for help with the shallow cores, to Marina Kustoya for help with the Russian language, and to Edward Woolery for advice and support.

Thanks to my family and to all who have directly or indirectly supported me; you know who you are! A special thanks to my American brother Joel Schiffer for the 10 years of friendship, and to Magne Bergo for teaching me the Norwegian language and for the fun conversations. Finally, I would like to acknowledge myself — and why not? Having had an original research idea that resulted in establishing a long-term cooperation between Kentucky's flagship university and the Norwegian Petroleum Directorate, while finding solutions during Covid time, is to me the very embodiment of the "American" dream.

TABLE OF CONTENTS

ACKNOWLEDGMENTS iii

LIST OF TABLES vi

LIST OF FIGURES vii

CHAPTER 1. INTRODUCTION 1

CHAPTER 2. THE APPALACHIAN AREA AS A TECTONOSTRATIGRAPHIC ANALOGUE FOR THE BARENTS SEA SHELF 11

2.1 Introduction 11
2.1.1 Analogue potential and testing 14

2.2 Geological setting 16
2.2.1 Barents Sea shelf 16
2.2.2 Uralian-Pai-Khoi-Novaya Zemlya orogeny 19
2.2.3 Appalachian Basin 21

2.3 Appalachian Basin and BSS analogues 23
2.3.1 Large-scale tectonic analogues 23
2.3.2 Tectonic processes analogues 25
2.3.3 Foreland-basin analogues 28
2.3.4 Intracratonic-basin analogues 34

2.4 Summary 36

CHAPTER 3. USE OF BACKSTRIPPING IN THE TRIASSIC–MIDDLE JURASSIC, SOUTH-CENTRAL BARENTS SEA SHELF SUCCESSION TO UNDERSTAND REGIONAL TECTONIC MECHANISMS AND STRUCTURAL RESPONSES 53

3.1 Introduction 53

3.2 Regional setting 55

3.3 Materials and method 58
3.3.1 Backstripping method 58
3.3.2 Backstripping parameters and equations 60

3.4 Results 62

3.5 Discussion 68
3.5.1 Tectonic mechanisms 69
3.5.2 Structural trends 71
3.5.3 Basin development 72

3.6 Conclusions 74

CHAPTER 4. INTERPRETING THE UPPER TRIASSIC–LOWER JURASSIC SEDIMENTARY SUCCESSION ACROSS THE SOUTH-CENTRAL BARENTS SEA SHELF: AN EXERCISE IN COMPRESSIONAL, TECTONOSTRATIGRAPHIC ANALOGUE MODELLING 101

4.1 Introduction *101*
4.1.1 Sedimentary cyclicity in foreland basins 104
4.1.2 The tectophase cycle 105

4.2 Materials and methods *107*

4.3 Regional setting *108*
4.3.1 Structural development 108
4.3.2 Tectonostratigraphy 109

4.4 Results *112*
4.4.1 Thickness variations 112
4.4.2 Wireline succession analysis 113
4.4.3 Unconformities 116

4.5 Discussion and conclusions *117*
4.5.1 Tectophase sequences 118
4.5.2 Evidence for foreland-basin development 118
4.5.3 Tectophase 1 (Norian–Rhaetian) 119
4.5.4 Tectophase 2 (Rhaetian–Hettangian) 121
4.5.5 Limitations 121
4.5.6 Conclusions 122

CHAPTER 5. CONCLUSIONS 136

APPENDIX 138

REFERENCES 146

VITA: GUSTAVO MARTINS 173

LIST OF TABLES

Table 2.1. Schematic comparison between the Appalachian and Barent Sea shelf areas in terms of general features, tectonics, stratigraphy and palaeogeography. 40

Table 2.2. General comparison between the Appalachian and Barents Sea shelf areas in terms of timing and tectonic events. 42

Table 3.1. General information for wells from the NBSS and RBSS used in this study. The following are NBSS formations: Ha = Havert; Kl = Klappmyss; Ko = Kobbe; Sn = Snadd; Fr = Fruholmen; Tu = Tubåen; No = Nordmela; and St = Stø. The following are RBSS stages: O=Olenekian; A = Anisian; L = Ladinian; C = Carnian; N = Norian; C–N = Carnian–Norian; R = Rhaetian; H–T = Hettangian–Toarcian; P–T = Pliensbachian–Toarcian; and A–B = Aalenian–Bathonian. 76

Table 3.2. General parameters used for calculating average grain densities, average porosities-at-surface, and average compaction coefficients. 79

Table 3.3. General parameters used in NBSS calculations. Average grain densities, porosities-at-surface and compaction coefficients are from Table 3.2. 80

Table 3.4. General parameters used in RBSS calculations. Average grain densities, porosities-at-surface and compaction coefficients are from Table 3.2. 85

Table 3.5. Main backstripping equations. 88

Table 3.6. Analyzed structural elements grouped by geometrical similarity, as well as by associated deflections and their characteristics. 89

Table 4.1. Thicknesses for RBSS, Pechora Sea, and Timan-Pechora Late Triassic sedimentary units approximately equivalent to the NBSS early Norian–Rhaetian Fruholmen Formation. 124

Table 4.2. Maximum and minimum Fruholmen Formation thicknesses across selected NBSS structural elements. 125

Table 4.3. Selected wireline logs used to compose a NBSS stratigraphic and correlation section. 126

LIST OF FIGURES

Figure 2.1. Map (a) main structural elements and major shale-play systems in the eastern, central, and northern United States. Data were compiled from the U.S. Energy Information and Administration EIA (2021, sedimentary basins and organic-rich plays); Tetra Tech (1981, arches and sags); Repetski et al. (2008, Paleozoic structures); and Sims et al. (2008, Precambrian structures). Map (b) main BSS structural elements. The red lines illustrate a highly schematic structural lineament framework (NPD, 2021). The solid purple line is the offshore boundary (NPD, 2017) between the Norwegian (western) and Russian (eastern) BSS sectors. Structural elements were compiled from the NPD (2021). 44

Figure 2.2. Schematic chronostratigraphic and lithostratigraphic diagram for eastern areas of the Norwegian BSS and a generalized stratigraphic column for eastern Svalbard (modified from NPD, 2017)..... 45

Figure 2.3. Schematic tectonostratigraphic section of eastern Spitsbergen (1); BSS (2–4; 7–13); Novaya Zemlya (5; 6; 14); Pechora Basin (15; 16) and northeastern Timan-Pechora Basin (17). Key references, but not the only references, used in constructing the section include: Timan-Pechora Basin (e.g., Abrams et al., 1999; Prischepa et al., 2011; Schenk, 2011); Pechora Basin (e.g., Ivanova, 1997; Norina et al., 2014; Suvorova & Matveeva, 2014; Zhuravlev et al., 2014); Novaya Zemlya (e.g., Drachev, 2016; Henriksen et al., 2011; Nakrem, 2007; Zhang et al., 2018); BSS (e.g.,Burguto et al., 2016; Dalland et al., 1988; Grogan et al., 1999; Johansen et al., 1993; Larssen et al., 2002; Leonchik & Senin, 2010; Margulis, 2008; NPD, 2017; Olaussen et al., 2018; Polyakova, 2015; Smelror et al., 2009; Stoupakova et al., 2011; Tugarova et al., 2008; Ustritskiy & Tugarova, 2013); eastern Spitsbergen (e.g., Dallmann et al., 2015; Nicolaisen et al., 2019; Riis et al., 2008; Stemmerik & Worsley, 2005)..... 46

Figure 2.4. (a) Extent of the Uralide fold belt and associated facies; Ordovician to Middle Carboniferous deposits are pre-orogenic, mostly platform, sequences (e.g., Proust et al., 1998; Evdokimov et al., 2000). (b) Major Hercynian-age fold belts involved in the final amalgamation of Pangea (modified from Proust et al., 1998). (c) Paleogeographic reconstruction illustrating the convergence of Laurussia and Siberia-Kazakhstania during Artinskian time (modified from Reid et al., 2007). 47

Figure 2.5. Schematic northwest-southeast cross section across the north-central Appalachian foreland basin (modified from Ettensohn et al., 2019)..... 48

Figure 2.6. Cross section showing the interpreted Devonian–Jurassic succession in the BSS, as well as major structural elements, structural reactivation, and salt mobilization due to westward compression from the Novaya Zemlya Orogeny (modified from Müller et al., 2019). 48

Figure 2.7. Sequential schematic diagrams showing flexural relationships among foreland-basin formation, sediment infill and deformational loading. (a) Basin-bulge formation and migration with subaqueous deformational loading and little clastic influx.

(b) Major surficial deformational loading with major clastic influx (modified from Ettensohn et al., 2019). 49

Figure 2.8. Schematic lithologic succession representing a generalized tectophase cycle at the outcrop scale with a eustatic curve for early subduction-type orogenies using the Appalachian, Taconic tectophase and ages as an example (modified from Ettensohn et al., 2019). 49

Figure 2.9. Complete Mississippian Neoacadian tectophase sequence from the Appalachian Basin showing the stage in the tectophase model to the right and the accompanying stratigraphic response to the left. (a) Same as Figures 2.7a and 2.8, parts 1, 2, 3. (b and c) Same as Figure 2.7b and Figure 2.8, part 4. (d) Same as Figure 2.8, part 5. (e) Same as Figure 2.8, parts 6, 7f, Figure 2.8, part 1, upper unconformity and new Alleghanian tectophase (modified from Ettensohn et al., 2012). 50

Figure 2.10. Schematic, southwest-northeast, Middle–Upper Ordovician section paralleling the strike of the Appalachian Basin and showing repetition of foreland-basin tectophase cycles for the Taconian tectophases (modified from Ettensohn et al., 2019). 51

Figure 2.11. Model a) Highly schematic cross-section illustrating Devonian–Mississippian black shales in east-central United States and basin yoking (modified from Ettensohn, 1992). Model b) Highly schematic cross section illustrating the Late Permian–Middle Jurassic tectonostratigraphic succession in the BSS area, illustrated using an Appalachian-type tectonostratigraphic model. 52

Figure 3.1. Main BSS structural elements. HB = Hammerfest Basin; LH = Loppa High; BP = Bjarmeland Platform; NB = Nordkapp Basin; FP = Finnmark Platform; FHA = Fersmanovskaya High area; FH = Fedynsky High; KMA = Kola Monocline area; and SBB = South Barents Basin (modified from Martins et al., 2022). 91

Figure 3.2. Top figure—Cross section schematically illustrating Upper Devonian–Late Jurassic strata across Svalbard (column 1), NBSS (columns 2–7), RBSS (columns 8–9); and Novaya Zemlya (column 10) (modified from Martins et al., 2022). Bottom figure—Simplified stratigraphic correlation for Triassic units across Svalbard, Franz Josef Land, NBSS, RBSS, and Novaya Zemlya (modified from Gilmullina et al., 2021). 92

Figure 3.3. Basic concepts and outputs of the backstripping method (modified from Angevine et al., 1990; Kneller, 1991; Roberts et al., 1998; and Watts, 2012). A) Each sedimentary unit is removed from the most recent (Time 4; T4) to the oldest stratum (Time 0; T0). B) Vertical movement of the datum in time after the sedimentary load is progressively removed. C) Backstripping elements for tectonostratigraphic interpretation (modified from Angevine et al., 1990; and Kneller, 1991). D) Example of high-resolution interpretation (modified from Watts, 2012). 93

Figure 3.4. Tectonic (blue) and datum (orange) subsidence curves for target BSS structural elements. 98

Figure 3.5. Schematic illustration showing main tectonic curve trends of targeted BSS structural elements. The lengths of the arrows and columns represent the duration of each main curve trend and are temporally correlated to the International Stratigraphic Chart (Cohen et al., 2022). The reddish arrow represents the westwardly migrating Novaya Zemlya orogenic events. The green areas represent the location of Late Paleozoic, North Atlantic, rifting events (Gabrielsen et al., 2016), whereas the red ellipse represents areas with mainly intracratonic subsidence mechanisms (Gac et al., 2013). 99

Figure 3.6. Highly schematic and extrapolated maps illustrating the main BSS structural trends observed in Fig. 3.5.) Early Triassic time; B) Middle Triassic time; C) Late Triassic time; and D) Early Jurassic time. The purple area represents the area likely affected by the Siberian Superplume (Puchkov, 2018; Puchkov et al., 2021)..... 100

Figure 4.1. (A) Geographic location, (B) Main BSS structural elements, and (C) Hydrocarbon exploration well locations with data applied in the study. AH=Admiralty High; AS=Albanovskaya Saddle; BB=Bjørnøya Basin; BP=Bjarmeland Platform; DH=Demidovskaya High; EBB=East Barents Basin; FEH=Fersmanovskaya High; FH=Fedinsky High; ; FP=Finnmark Platform; GH=Gardarbanken High; HB=Hammerfest Basin; HI=Hopen Island; KB=Korothaika Basin; KKL=Kong Karls Land; KKP=Kong Karl Platform; KM=Kola Monocline; LH=Loppa High; LS=Ludlovskaya Saddle; NB=Nordkapp Basin; NBB=North Barents Basin; OB=Olga Basin; PH=Polarrev High; PSB=Pechora Sea Basin; PSH=Perseu High; SB=Sørkapp Basin; SBB=South Barents Basin; SH=Sentralbanken High; SS=Shtokman Saddle; STH=Stappen High; TB=Tromsø Basin; and TPB=Timan-Pechora Basin..... 127

Figure 4.2. (A) and (B) Schematic tectonostratigraphic model illustrating deposition and structural reactivation during phases of active loading and relaxation. (C) Schematic lithologic succession representing an ideal tectophase cycle at outcrop scale with the associated eustatic curve. (D), (E), and (F) Schematic flexural model illustrating phases of deformational loading, loading-type relaxation, and unloading-type relaxation. Figures modified from Ettensohn et al., 2019..... 128

Figure 4.3. Stratigraphic compilation and interpreted depositional environments from selected BSS locations and adjacent areas. Key references include Dalland et al., (1988); Mørk (1989); Johansen et al. (1993); Grogan et al. (1999); Riis et al., (2008); Smelror et al. (2009); Stoupakova et al. (2011); Lundschien et al. (2014); Norina et al. (2014); Ryseth, 2014; Spina et al. (2015); Burguto et al. (2016); Fleming et al. (2016); Lerch et al. (2016); Sobornov and Astafiev (2017); Olaussen et al. (2018); Khudoley et al. (2019); Paterson et al. (2016); Paterson and Mangerud (2017, 2019); Line et al. (2020); Gilmullina et al. (2021); and Martins et al. (2022). Formation names and ages are compiled from Dibner and Krylova (1963); Embry (1992); Mørk (1999); Schenk (2011); Lord et al. (2014); Paterson and Mangerud (2017, 2019); Line et al. (2020); and Gilmullina et al. (2021)..... 129

Figure 4.4. Thickness values of the Fruholmen Formation in 78 NBSS wells relative to structural elements. BP=Bjarmeland Platform; BFC= Bjørnøyrenna Fault Complex; EL/HA=East Loppa/Hoop area; FB= Fingerdjupet Basin; FP=Finnmark Platform;

HB=Hammerfest Basin; LH=Loppa High; MFC= Måsøy Fault Complex; and NB=Nordkapp Basin. 130

Figure 4.5. Maximum and minimum thicknesses for the Fruholmen Formation on the NBSS (brown), for approximately equivalent deposits on the RBSS (blue), and for the Pechora Sea and Timan-Pechora areas (black). 131

Figure 4.6. NBSS wireline-log correlation. Well 7120/12-1 is the Fruholmen reference well used for correlation. HB=Hammerfest Basin; LH=Loppa High; BP=Bjarmeland Platform; NB=Nordkapp Basin; NFP= northern Finnmark Plaftform; and EBP=eastern Bjarmeland Platform. 132

Figure 4.7. Thicknesses for the Akkar Member (dark gray) and Reke plus Krabbe members (yellow) in the various wireline logs used in the correlation line. 133

Figure 4.8. Photographs of cores from shallow boreholes 7533/2-U-2 and 7934/8-U-1 (Fig. 4.1). (A) Rhaetian-Hettangian unconformity; (B) Contact between the Slottet Bed and De Geerdalen Formation; (C) Contact between the Slottet Bed and De Geerdalen Formation; and (D) Transition between the Slottet Bed and organic-rich shales equivalent to the Akkar Member. 134

Figure 4.9. Integrative BSS map schematically illustrating the depozones associated with the two Novaya Zemlya tectophases. 135

Figure 4.10 Norian–Rhaetian foreland-basin development and depozones across the southern BSS and adjacent areas. Maximum and minimum thicknesses (numbered columns) for the Fruholmen Formation on the NBSS (brown), for approximately equivalent deposits on the RBSS (blue), and the Pechora Sea and Timan-Pechora basins (black). Foreland depozone nomenclature is from DeCelles and Gilles (1996). 135

CHAPTER 1. INTRODUCTION

Humans have the mental ability to "overlap" shapes of known characteristics. This phenomena is defined as *pareidolia*, which is the ability to see shapes and structures in everyday objects (e.g., Palmer et al., 2020). For example, a cloud may look like a bird to an observer because the shape of a bird is known. Similarly, analogue science uses well-known references for comparison with and to better understand unknown targets (e.g., use of a modern tiger as an analogue to understand a Pleistocene sabretooth tiger).

In the *Cambridge Dictionary*, "analogue" is defined as "something that is similar to or can be used instead of something else," but this definition is commonly too broad for scientific purposes. According to the *Collins Dictionary*, for example, a biological analogue is defined as "an organ or part analogous to each other," whereas a chemical analogue is "one group of chemical compounds similar in structure but different in respect to elemental composition." Clearly, chemical analogues include both similarities and differences, whereas biological analogues may focus on similarities only. Analogues as a tool for comparative modelling are used in many situations beyond natural sciences; for example, the Project Management Institute (PMI) teaches that "Analogous Estimating" is "a method for estimating the duration of cost of an activity or a project by using historical data from a similar activity of project" (PMI, 2017). This diversity in the use of the term "analogue" shows that analogue use is nearly universal in any area of human knowledge.

In the Earth Sciences, however, the definition of the word "analogue" varies within its many subspecialities. For example, Sun et al. (2021) defined an analogue as "comparable fields and reservoirs relevant to a specific question or set of questions," whereas Schellart and Strak (2016) stated that an analogue is "a modelling approach that

is used in Earth Sciences to investigate geological phenomena and geodynamic processes in a laboratory at convenient time and length scales." In planetary sciences, Foucher et al. (2021) stated that "the precise signification of an analogue may differ, but the term is invariably used to denote a terrestrial site, material or object having similar composition and/or properties to a given extraterrestrial site, material or object." Clearly, every subspeciality contains its very own definition of the word, thus, making it difficult to use the term consistently. Additionally, analogues very often fail, or, according to Howell et al. (2014), "the model not correctly predicting an outcome." However, I draw attention to the fact that analogues will always be seen as imperfect, because they address largely unknown and/or controversial targets. Because analogue failure is always to be expected, the following should always be considered in the use of an analogue: 1) the need to continuously test and calibrate the analogue, and 2) the need to determine what parts of the analogue work and what parts do not.

The above leads to the following question: Why use an analogue? For example, sedimentary basin A may be defined as analogous to basin B. However, will this analogue realistically impact exploratory decisions, prospecting, and geologic knowledge of basin B? Should analogues be seen as a "geocuriosity" or are they functional? If not functional, is there potential for uses other than resource exploration? For example, analogues have tremendous educational potential to facilitate the visualization and explanation of complicated geologic processes. With these considerations in mind, I would like to present the following definition for use of the term in Earth Sciences: An analogue is a well-known reference model capable of simplifying, comparing, representing, and/or illustrating geologic features and processes in ways that facilitate communication with both specialists

and non-specialists. Such analogues may have industrial potential and can be used to better understand a poorly known area where lack of data, data inaccessibility, and/or lack of specialized expertise hinder understanding.

Even though the Barents Sea shelf (BSS) is likely the most well-studied, offshore, Arctic province, the area remains largely frontier and at times geologically controversial. Moreover, approximately half of the BSS (eastern areas) is controlled by Russia, where access is largely restricted; in contrast, the western half is open Norwegian territory. Because of the enormous size of the area, resource potential, and international politics, data for regional studies, which could link both parts of the shelf, are very difficult to obtain. Very few research groups have access to Russian datasets, publications are few and often in Russian, and presentation of data is often very schematic. Moreover, the COVID-19 pandemic and Ukrainian-Russian conflict have only enhanced these difficulties by isolating the Russian BSS and restricting the diversity of interpretations and authors who work there. Ironically, these challenges present a fertile ground for the use of analogues.

To date, the only attempted, large-scale analogue for the BSS is the work of Cecchi et al. (1995), who used the Marathon system of Permian basins and platforms (Paradox, Delaware, and Midland basins) as an analogue for Permian carbonate and facies development in southwestern parts of the BSS. Even though various aspects of their comparison are useful, the analogue is somewhat ambiguous because the tectonic settings are different, and the aerial extent excludes Russian parts of the shelf. Moreover, the analogue does not explain the sudden development of a thick siliciclastic succession that overlies carbonate deposits across the entire BSS during Permian–Early Mesozoic time.

In this study, the well-known Appalachian system of basins and platforms (ASBP) is proposed to be a suitable analogue for the regional BSS. In the eastern U.S., the ASBP traditionally consists of the Appalachian orogen and Appalachian foreland basin, as well as the Illinois and Michigan intracratonic basins, and intervening platforms, a usage which is similar to definitions presented by Hatcher et al. (1989) and Ettensohn et al. (2019). Some authors also include both the bounding Ouachita and Marathon fold and thrust belts across the south and southwestern U.S. in the ASBP (e.g., Thomas, 1985; Dennison, 1989; Viele, 1989; Miall and Blakey, 2019).

Located in the Russian and Norwegian Arctic, the BSS system of basins and platforms also represents a geologic system that was largely controlled by compressional tectonics and geodynamics. The BSS is bounded by fold and thrust belts, which were responsible for triggering the development of foreland and intracratonic basins across the shelf (Faleide et al., 1984; Smelror et al., 2009; Drachev, 2016).

The ASBP has a tremendous comparative potential for the BSS, because it provides potential analogues to: 1) the Caledonian orogeny and orogenic collapse; 2) the Uralian-Pai-Khoi-Novaya Zemlya orogeny and far-field tectonic responses in adjacent basins; 3) continental break-up and oceanic opening/closure; and 4) plume uplift and exhumation. Although this study only focuses on item 2 above, brief explanations for other parts of the above analogue model are presented.

The Appalachians are often interpreted to be a part of the "Appalachian-Caledonian" fold and thrust belt system, which formed through subduction of the Iapetus and Rheic oceans, orogenic build-up, and subsequent orogenic collapse (e.g., Ziegler, 1989; McKerrow et al., 2000; Gee et al., 2008; Ettensohn, 2008; Miall and Blakey, 2019).

Because the Caledonian orogeny is also a relevant part of the BSS tectonic evolution, the ASBP provides direct regional analogues to the Caledonian orogeny and associated processes there. Likewise, the ABSP is the result of complete Wilson cycles (Iapetus and Rheic cycles; Ettensohn et al., 2019), which is also the case in the BSS (Iapetus cycle, western margin; Uralian cycle, eastern margin) (e.g., Torsvik and Cocks, 2017). Because both ABSP and BSS areas experienced cycles of oceanic opening and closing (Wilson cycles), ABSP tectonic and geodynamic processes and the resulting stratigraphy, can be used or tested against BSS stratigraphic successions representative of similar geologic history. Similarly, the ABSP underwent widespread uplift, erosion and exhumation as a result of magmatic processes associated with the breakup of the Atlantic Ocean (Ettensohn et al., 2019). In the BSS, North Atlantic magmatic processes have also been interpreted to have triggered uplift, erosion, and exhumation of regional significance (e.g., Henriksen et al., 2011).

In the literature, the first mention of an analogous relationship between the Appalachian and Uralian orogens (Uralian cycle) was that by Puchkov (1979). Similarly, Puchkov (2002) noted the potential similarity of collisional mechanisms relative to promontories and embayments like those in the Appalachian area. Although the possibility of analogues is noted, these ideas are presented only as general suggestions (e.g., Puchkov, 2002, 2009, 2010; Hatcher, 2014). Only a few studies have formally compared both orogens (e.g., Artyushkov and Bær, 1983; Kruse and McNutt, 1988; Matte, 2002), and of these, only Kruse and McNutt (1988) offered detailed comparisons between the Appalachians and Urals by using gravity and deep-seismic techniques. However, Kruse and McNutt (1988) only focused their comparison on south-central Uralian areas. In the

BSS area, a part of the northern Uralian system, formal comparison with the ASBP has never been done. Ritzmann and Faleide (2009) very briefly suggested the possibility of BSS intracratonic mechanisms like those in the Appalachian area. After studying intracratonic mechanisms in the Russian BSS, Gac et al. (2013) stated: "we propose that a similar mechanism explains the formation of other intracratonic basins such as the Michigan, Illinois, and Williston basins, which formed during the Early Paleozoic (Klein and Hsui, 1987) contemporaneous with the main phase of the Appalachian orogeny." This statement refers to the idea that foreland flexure (Appalachian Basin) and intracratonic subsidence (Michigan and Illinois basins) were both coeval with Appalachian orogenies at times.

Even though several authors have raised the potential of using ASBP analogues in the Uralian system of basins and platforms, which the BSS is largely a part of, few have attempted detailed comparisons. This study herein defines and uses ASBP tectonostratigraphy as an analogue to the Late Devonian–Middle Jurassic BSS succession to determine if development of the latter can be explained in terms of analogous ASBP tectonostratigraphic processes (e.g., tectophases). Hence, this Ph. D. research is pioneering, because it is the first attempt to formally define the Appalachian-BSS analogue. The definition and usage of the ASBP as an analogue to the BSS is presented in three papers, which are included as separate chapters in this dissertation. The abstracts for each chapter are presented below.

Chapter 2, which was published in *Basin Research* (Martins et al., 2022) and nominated for best early career paper of that journal in 2022, presents a systematic comparison of both areas, brings the analogue potential to focus, suggests analogous

flexural relationships, and briefly reviews the tectonostratigraphy and geologic history of both areas. The US Appalachian Basin and the Arctic Norwegian and Russian BSS areas are two strategic provinces for the energy industry. The Appalachian Basin is a well-studied, mature, onshore basin, whereas the offshore BSS is still considered a frontier area. This study suggests that the Appalachian Basin may be an appropriate analogue for understanding the BSS and contribute to development of a tectonostratigraphic framework for the area. Although the Appalachian and BSS areas reflect different times and settings, both areas began as passive margins that were subsequently subjected to subduction and continent collision associated with the closure of an adjacent ocean basin. As a result, both areas exhibit multi-phase subduction-type orogenies, a rising hinterland that sourced sediments, and a foreland-basin sedimentary system that periodically overflowed onto an adjacent intracratonic area of basins and platforms with underlying basement structures. Foreland-basin sedimentary systems in the Mid-to-Late Palaeozoic Appalachian Basin are composed of unconformity-bound cycles related to specific orogenic pulses called tectophases. Each tectophase gave rise to a distinct sequence of lithologies related to flexural events in the orogen. In this study, similar sequences are recognized in both BSS foreland-basin and adjacent intracratonic sedimentary sequences that formed in response to the Late Palaeozoic–Mesozoic Uralian–Pai–Khoi–Novaya Zemlya Orogeny, suggesting that the processes generating the sequences are analogous to the tectophase cycles in the Appalachian Basin. Hence, this pioneering use of the Appalachian area and its succession as large-scale tectonostratigraphic analogues for the BSS may further enhance understanding of Upper Palaeozoic to Middle Jurassic stratigraphy across the BSS.

Chapter 3, which was published in *Tectonophysics* (Martins et al., 2023a), presents a backstripping analysis of Triassic–Middle Jurassic strata across the south-central BSS to identify the existence of far-field reactivation of intracratonic structures. Across the ASBP, it is well-known that structural reactivation of basement structures by orogeny was important for sedimentary control in different areas at different times (Ettensohn et al., 2019). Hence, Martins et al. (2023a) aimed to assess the likelihood of differential structural reactivation across the BSS and to determine if these mechanisms could be tied to regional orogenic events. To my knowledge, this study represents the largest backstripping study in BSS literature. Because of its economic importance for hydrocarbon development, the tectonostratigraphic development of the Triassic–Middle Jurassic succession across the BSS has been of particular interest. Much of this succession was deposited across Timanian (late Neoproterozoic–early Cambrian)- to Caledonian (at least Devonian)-age structural elements that were later reactivated by far-field responses to periods of Uralian–Pai–Khoi–Novaya Zemlya and North Atlantic tectonism. The timing and nature of these far-field responses are analyzed in this study by applying the backstripping method for analysis of tectonic mechanisms and structural responses, based on stratigraphic thicknesses across multiple south-central BSS structural elements. Based on ten tectonic subsidence curves from these structural elements generated by backstripping calculations, it is suggested that structural reactivation occurred at various times during latest Permian to Middle Jurassic time. The many tectonic mechanisms interpreted in several BSS backstripping curves suggest that the mechanisms were not homogeneous and that the stress regimes under which these structures reactivated were diverse. The backstripping analysis also shows that among the majority of structural elements analyzed, subsidence predominated across the

southern BSS during Early–Middle Triassic time, followed largely by uplift in Late Triassic time, and subsequently, by subsidence in Jurassic time. Tectonostratigraphic interpretations extracted from the backstripping curves suggest that regional structural reactivation generated by Novaya Zemlya compressional tectonism was significant during at least Late Triassic–Early Jurassic time.

Chapter 4, which is being refereed for *Frontiers in Earth Science (Sedimentology, Stratigraphy and Diagenesis)* (Martins et al., 2023b), presents a stratigraphic analysis of Late Triassic–Middle Jurassic sedimentary thicknesses across the south-central BSS using Appalachian models. Across the ASBP, foreland depozones (e.g., foredeep, forebulge and backbulge) triggered by flexure are reflected in the lithologic composition and thicknesses in the stratigraphy that can be characterized as tectophases (e.g., black shales; Ettensohn et al., 2019). Using the tectophase model, Martins et al. (2023b) applied Appalachian flexural models to determine the likelihood of similar foreland-basin depozones, based on the Upper Triassic–Lower Jurassic stratigraphy and thicknesses variations across the BSS. The Upper Triassic–Lower Jurassic succession across the BSS is part of an important petroleum system that represents various depositional settings and tectonostratigraphic events. Even though this succession is overall well-understood, interconnections between these elements and possible tectonic triggers are unclear. This study discusses new interpretations that focus on relationships between the stratigraphic succession across the south-central Barents Sea shelf (BSS) and Novaya Zemlya collisional tectonics. By applying the tectonostratigraphic "tectophase model" from the Appalachian Basin to analyze this succession, the presence of foreland-basin depozones and associated processes related to compressional tectonics in an adjacent orogen are suggested. Across the BSS, the

tectophase model is used to address unconformity development, lithostratigraphic succession, and reactivation of structures. Additionally, the analogue model suggests tectonostratigraphic responses to two episodes (tectophases) of Novaya Zemlya tectonism, reflected in coeval BSS stratigraphy. Overall, this tectonostratigraphic study aligns with other research suggesting a Late Triassic inception for an episode of Novaya Zemlya compressional tectonism, which influenced larger parts of the BSS through far-field structural reactivation and flexural responses.

CHAPTER 2. THE APPALACHIAN AREA AS A TECTONOSTRATIGRAPHIC ANALOGUE FOR THE BARENTS SEA SHELF

2.1 Introduction

The use of analogues is recognised as an important tool in providing solutions for qualitative and quantitative problems pertinent to both academia and the energy industry (e.g., Howell et al., 2014; Schellart and Strak, 2016; Sun et al., 2021). Analogues are especially desirable when dealing with areas where geological uncertainties predominate. Use of geological analogues typically involves using a well-known geological system, area or process (the standard) to help explain possible similarities between the standard and a target of interest. For example, Ulmishek (1986) suggested that the assessment of undiscovered hydrocarbon resources in poorly known areas (targets of interest) should be based on comparative analysis of geologic elements and processes in a well-explored analogue area (standard). In this study, the well-known geological evolution of the onshore, east central, US Appalachian region (Figure 2.1a), including the foreland basin and adjacent intracratonic area, is the standard, whereas the Barents Sea shelf (BSS; Figure 2.1b) is the target area of interest. The BSS is part of the Norwegian (western BSS) and Russian (eastern BSS) Arctic continental shelf and currently represents a frontier province—in particular the northern sectors—for hydrocarbon exploration, and for future carbon storage capture (NPD, 2017).

The BSS is commonly characterised as a large tectonic element within the Arctic system of platforms and basins (e.g., Drachev, 2016). Even though the BSS is a well-studied Arctic region, research focusing on external, large-scale, tectonostratigraphic analogues to the overall setting and development of the BSS remains scarce. Hence, the overarching goal of this paper is to investigate possible analogue relationships between the

U.S. Appalachian and BSS systems of basins and platforms. Elements of the Appalachian system (Figure 2.1a) have been previously used as possible analogues for the nearby Timan–Pechora Basin (e.g., Artyushkov and Baer, 1986), and earlier generic comparisons of the Appalachian orogen with the Caledonian and Uralian orogens have been attempted (Allen and Allen, 2013; Arthaud and Matte, 1977; Artyushkov and Baer, 1983, 1985; Brown et al., 2004, 2006; Hatcher, 2010; Knapp et al., 1998; Kruse and McNutt, 1988; Matte, 2002; Puchkov, 2009). For example, Puchkov (2009) briefly suggested that evolution of the Uralian Orogeny was like that of the Taconian and Alleghanian orogenies in the Appalachian area but went no further in defining the analogue. Difficulties in developing suitable regional external analogues for the offshore BSS probably result from lack of familiarity with possible analogue basins and the fact that the BSS is not as well explored as other regions. In fact, Scott (2007) published a report entitled, 'Eastern Barents Sea-Novaya Zemlya-Kara Sea tectonic relationships: The search for an appropriate analogue', which highlights the importance of finding suitable analogues for the BSS.

Accessibility to BSS data can also be difficult. In the Norwegian sector, data from several exploration-wells and seismic surveys are available also through the Norwegian Petroleum Directorate (NPD). However, wells concentrate in southwestern-most areas and a large majority did not reach Palaeozoic strata. Moreover, the northern sector (>74°30′N) has not yet been opened for petroleum activity (NPD, 2017), and seismic quality is often poor. Moreover, most available seismic surveys are only two-dimensional. In the Russian sector, exploratory data tend to be concentrated in southern areas and are very difficult to obtain except what is published. Unlike the Norwegian Svalbard archipelago (Figure 2.1), access to the Russian Novaya Zemlya archipelago is restricted. Clearly, the above situation

makes it challenging to generate large-scale studies capable of integrating both sectors of the BSS. As a result, BSS problems, such as far-field tectonics, halokinesis, energy potential, stratigraphic facies, regional tectonism, among others, remain more unresolved to the north. In trying to resolve these issues, several analogues have been used at various scales, but with varying degrees of success. What has been lacking, however, is a large-scale, analogue-generated model to integrate all these aspects across the BSS. Hence, in this study we present the Appalachian foreland basin and adjacent intracratonic areas as such a large-scale analogue capable of treating all these aspects together, thus, representing another instrument in the BSS analogue toolbox.

The geology and tectonostratigraphy of both Appalachian and BSS areas are largely the result of their development within the classic framework of the Wilson cycle (Ettensohn et al., 2019; Puchkov, 2009; Wilson, 1966), which necessarily includes such large-scale tectonic elements as passive margins, foreland basins and intracratonic platforms (e.g., Beaumont, 1981; Price, 1973; Walcott, 1970). The Appalachian foreland basin and adjacent intracratonic platforms and basins are considered sources of potential analogues for comparison, because they represent the 'type-area' of the Wilson cycle (Ettensohn et al., 2019; Wilson, 1966) and also the 'type-area" for related tectonostratigraphic sequences (Hatcher et al., 1989; Tollo et al., 2010). Consequently, the Wilson cycle and the resulting tectonostratigraphic sequences provide the foundation for testing this hypothesis of basin analogues.

Hence, the overarching goal of this paper is to define and test the above analogue hypothesis by providing a review of the main tectonostratigraphic features of the BSS and systematically comparing them with those of the Appalachian foreland basin and adjacent

intracratonic areas. Because no seismic data were available for this study, our interpretations are based largely on published literature.

2.1.1 Analogue potential and testing

Geologic studies frequently rely on analogues because the development of rocks and structures can rarely be observed directly (Alexander, 1993). This is true for the BSS because: (1) the area is mostly submerged; (2) seismic imaging to the north is often poor; (3) well data north of 74°30′N are often limited or non-existent; (4) most wells do not hit basement; (5) Russian data are mostly inaccessible; (6) structural elements are widespread and frequently affected sedimentation; and (7) several orogenic events affected the area and overlapped in time and space (see section 2). Hence, choosing analogues applicable at both local and regional scales and capable of integrating both shelf sectors is difficult. For example, an analogue employed to understand the Nordkapp Basin, a rift basin (Figure 2.1), may fail in explaining the South Barents foreland basin. To help with addressing such challenges, after examining several basinal areas, we chose the following key aspects of the Appalachian area for comparison with the target BSS area: (1) areal extent; (2) evidence for multiple tectonic events of similar types and durations; (3) presence of coeval, far-field, structural reactivation; and (4) presence of foreland-basin and an adjacent intracratonic areas with distinctive tectonostratigraphic sequences. Testing for each of these aspects required a systematic comparison of the standard (Appalachian area) with the target (BSS; see Table 2.1).

Relative to areal extent, although not equal, the extent of the Appalachian area (0.93 million km^2) approaches that of the BSS (1.4 million km^2). Furthermore, in both areas,

tectonic events largely tie to key Pangean Wilson cycles. In the Appalachian area, the cycle involved opening and closure of the Iapetus and Rheic oceans, whereas in the BSS area the cycle involved opening and closure of the Iapetus and Uralian oceans, both of which triggered multiple, diachronous, continent-margin orogenies (e.g., Hatcher, 2010; Matte, 2002; Puchkov, 2009; Ziegler, 1989). In fact, Puchkov (2009) noted that the duration of the Uralian Orogeny (ca. 214 Ma; Middle Devonian–Middle Jurassic; eastern BSS) is comparable to that of the Appalachian orogenies (ca. 217; Middle Ordovician–Permian; Appalachian area). Moreover, in both areas, subduction-type orogenies preceded final continent-continent collision. Importantly, these orogenies also reactivated widespread basement structures, which, on the BSS, are largely Precambrian to Caledonian in age (Anell et al., 2013), and in the Appalachian area, are Precambrian to Cambrian in age (Ettensohn et al., 2019). Similarly, these tectonic events resulted in distinctive, geometrically comparable, tectonostratigraphic successions of carbonates and clastics that can be characterised in similar terms in both areas (cf., Ettensohn et al., 2019; NPD, 2017; see Section 2). Nonetheless, challenges related to different palaeogeography, palaeoclimate and timing remain. However, these challenges do not necessarily invalidate the basic tectonic mechanisms that underpin the analogous development of both areas.

Although the tectonic development and stratigraphic framework of the Appalachian area are already well-known (e.g., Ettensohn et al., 2019), these same aspects of the BSS, especially for the eastern Russian sector, are incompletely known. Our first step, then, in testing analogies was to understand the regional stratigraphy of the BSS. This was accomplished through an extensive review of the literature and NPD archives, which resulted in a stratigraphic chart/section that encompasses most of the BSS (see Section 2).

Searching this chart/section for cyclic, unconformity-bound, stratigraphic responses, comparable with those in the Appalachian area represented a critical test of the analogue, because presence of such cycles is evidence of similar tectonic mechanisms, which were already developed for the Appalachian area (see Section 3). In the end, application of Appalachian tectonostratigraphy as an analogue allowed the interpretation of the late Palaeozoic to Middle Jurassic BSS succession in terms of flexural tectonics.

2.2 Geological setting

2.2.1 Barents Sea shelf

The BSS covers approximately 1.4 million km^2 and comprises the sea-areas with average water-depths of about 230 m located between northern Norway, Svalbard, Franz Joseph Land, and Novaya Zemlya (Figure 2.1b). The regional structural framework includes large basins west of Novaya Zemlya, which gently pass westward into an extensive platform area with smaller basins (Marello et al., 2013; Figure 2.1b). The very southeastern end of the BSS is defined as the Timan-Pechora Basin, which continues onshore areas (Stephenson et al., 2006; Stoupakova et al., 2011). The eastern and western areas of the BSS are delimited by an overall N–S monoclinal structure that roughly corresponds with the offshore boundary between the Norwegian and Russian sectors (Faleide et al., 2017; Worsley, 2008; Figure 2.1b). The geologic evolution of the eastern BSS was mainly influenced by the Uralian Orogeny (e.g., Petrov et al., 2008), whereas the western BSS had multiple influences, including Caledonian and Uralian orogenic events, followed by the late Mesozoic–Palaeogene opening of the North Atlantic (e.g., Worsley, 2008).

The eastern BSS sector consists of two very deep basins (Figure 2.1b), with thicknesses of possibly more than 20 km in the South Barents Basin and 12 km in the North Barents Basin (Gee, 2005; Ivanova et al., 2006; Klitzke et al., 2015; Shipilov, 2010), which cover a basement of most likely Timanian (Late Proterozoic–Early Cambrian) origin (Drachev, 2016; Gee et al., 2006; Kuznetsov, 2006). Timanian basement structures trend NW–SE and are truncated by Uralian and Caledonian structures on the eastern and western margins of the BSS, respectively (Gernigon et al., 2018; Pease et al., 2014). The western BSS sector exhibits many smaller basins and intervening platforms, with sedimentary thicknesses of at least 10 km (Faleide et al., 1984). These western basins have a basement of likely Caledonian origin (Corfu et al., 2014; Gee et al., 2010; Klitzke et al., 2019), originating from the Silurian–Devonian continental collision of Baltica and Laurentia that formed the supercontinent Laurussia (McKerrow et al., 2000; Miall and Blakey, 2019; Torsvik and Cocks, 2017; Ziegler, 1989). The dominant Caledonian structural trends are N–S and NE–SW (Gee et al., 2008; Gernigon et al., 2014; Figure 2.1b).

In general, the tectonostratigraphic framework of the BSS is represented by a clastic-carbonate-clastic succession (Figures 2.2 and 2.3) that reflects complex relationships among tectonics, eustasy, palaeogeography, and palaeoclimate. Ordovician to Middle Devonian rocks have only been identified in the eastern BSS basins and include organic-rich rocks that sourced large volumes of hydrocarbons (Alsgaard, 1993; Guo et al., 2010; He et al., 2012; Polyakova, 2015; Stoupakova et al., 2011, 2015). During Early Devonian to Early Carboniferous time, the BSS migrated out of equatorial and into subtropical conditions (Lopes et al., 2016; Worsley, 2008). Continental and marginal-marine clastics were deposited in western parts of the shelf (Figures 2.2 and 3B′-B″), while

widespread carbonate sedimentation predominated in shallow-marine basins across the eastern parts of the shelf (Dallmann et al., 2015; Stemmerik and Worsley, 2005; Figure 2.3C-C′, B-B′). Ongoing sea-level rise, regional uplift and development of half-grabens favoured deposition of thick warm-water carbonate successions, including buildups and lagoonal evaporites on the BSS during Carboniferous and Early Permian time (Blomeier et al., 2009; Rafaelsen et al., 2008; Stemmerik et al., 1994; Stemmerik and Worsley, 2005; Figures 2.2 and 2.3). In the eastern BSS during Late Carboniferous–Early Permian time, black, phosphate-bearing, siliceous, radiolarian-rich, shales grade eastward into turbidite deposits (Smelror et al., 2009; Figures 2.2 and 2.3).

On the western BSS, Upper Carboniferous to Lower Permian deposits include algal build-ups and limestones locally intercalated with evaporites (Dallmann et al., 2015). By Early Mid Permian time, the BSS had migrated into more temperate latitudes, contributing to the shift in regional deposition from shallow, warm-water to deeper-water carbonates and spiculitic cherts (Matysik et al., 2018; Stemmerik, 2000; Figures 2.2 and 2.3). Moreover, Upper Permian petroleum source-prone, calcareous, silica-rich, black shales have been identified in both the Norwegian and Russian Barents Sea shelves (Figures 2.2 and 3), having thicknesses of ca. 100 and 350 m respectively (Henriksen et al., 2011; Konyukhov, 2016). During Late Permian–Early Triassic time, the Uralian Orogeny culminated, resulting in rapid crustal subsidence and deposition of flysch-and molasse-like sediments in the eastern BSS (Faleide et al., 1984; Golonka and Ford, 2000; Nikishin et al., 1996; Figure 2.3). As the Uralides evolved, large volumes of clastics, initially consisting of prolific organic-rich muds (Figures 2.2 and 2.3), were deposited across the BSS (Anell et al., 2014, 2016; Brekke et al., 1999; Johansen et al., 1993; Konyukhov, 2016;

Lundschien et al., 2014; Riis et al., 2008; Uchman et al., 2016). During Mid Triassic–Early Jurassic time, uplifted Uralian source areas to the east contributed large volumes of prograding clastic sediments, whereas on parts of the western shelf, deposition of source-prone black shales predominated (Georgiev et al., 2017; Ohm et al., 2008; Polyakova, 2015; Stupakova et al., 2012; Figures 2.2 and 2.3). During Late Jurassic to earliest Cretaceous time, Kimmeridgian rifting and deposition of organic-rich black shales marked the inception of North Atlantic tectonism across the BSS (Figures 2.2 and 2.3; Faleide et al., 2008; Henriksen et al., 2011; Lopatin et al., 2003; Serck et al., 2017). Events associated with the opening of the North Atlantic Ocean may have started as early as Late Palaeozoic–earliest Triassic and persisted into Cenozoic time (Amantov and Fjeldskaar, 2018; Knutsen and Larsen, 1997; Ryseth et al., 2003; Stemmerik and Worsley, 2005).

2.2.2 Uralian-Pai-Khoi-Novaya Zemlya orogeny

The traditionally named 'Uralian–Pai–Khoi–Novaya Zemlya' Orogeny (Volkov, 1963), was the product of the collision of Siberia and Kazakhstania with the Baltic margin of Laurussia (Brown et al., 2004; Pease et al., 2014; Puchkov, 1997, 2003; Torsvik and Cocks, 2017). The Uralide belt is today represented by a N-S linear belt, at least 2,500 km in length (Figure 2.4a), which represents the Palaeozoic collision of at least two intra-oceanic arcs at the eastern margin of Baltica, followed by continent-continent collision (Brown, Spadea, et al., 2006; Puchkov, 2009).

Broadly viewed, the orogeny developed in Palaeozoic (Ordovician–Permian) and Mesozoic (Triassic–Jurassic) stages (Puchkov and Ivanov, 2020). The Palaeozoic stage in the BSS area is tied to the closure of the Uralian Ocean during Early Carboniferous to

Permian time, with the main orogenic phase taking place in Late Permian to Early Triassic time (Ershova et al., 2015; Petrov et al., 2016; Smelror and Petrov, 2018). The foreland basin for this stage of collision was concentrated in the present-day Novaya Zemlya area and was filled with dark shales, flysch-like and molasse-like sediments (Figures 2.2–2.4; Brown, Spadea, et al., 2006; Puchkov, 2009; Reid et al., 2007).

The late stages (at least Late Mesozoic) of the Uralian Orogeny are often called the Pai-Khoi-Novaya Zemlya Orogeny (Puchkov and Ivanov, 2020; Smelror and Petrov, 2018). Pai-Khoi (Figures 2.1b and 2.4) is a complex structural area between what is now the Novaya Zemlya archipelago and the northernmost Ural Mountains (Timonin et al., 2004). Novaya Zemlya (Figures 2.1b and 2.4) is an arc-shaped archipelago, which has been interpreted as the result of the Late Triassic to Early Jurassic collision of Siberia, which acted as a transpressional indenter, with a former continental embayment on the northeastern margin of Baltica (Curtis et al., 2018; Faleide et al., 2017; Lopatin et al., 2001; Petrov et al., 2008; Puchkov and Ivanov, 2020; Scott et al., 2010; Smelror and Petrov, 2018; Smelror et al., 2009). During this phase of orogeny, what had been a Late Palaeozoic foreland basin became inverted as a fold-thrust belt and pushed westward onto the margin of Baltica as the current, arc-shaped Novaya Zemlya archipelago. Puchkov (2009) interpreted this Mesozoic phase to represent the terminal collision in the Uralides. The resultant Novaya Zemlya fold belt (archipelago) is approximately 1,200 km in length (Figure 2.4a), represents the amalgamation of several allochthons and exposes Precambrian to Early Triassic successions (Filatova and Khain, 2010; Toro et al., 2016; Zhang et al., 2018). The geographic position of the archipelago suggests that it represents a northward continuation of the Uralian Orogeny, but such a possibility is still debated (Buiter and

Torsvik, 2007; Dedeev, 1959; O'Leary et al., 2004; Otto and Bailey, 1995; Pease et al., 2014; Scott et al., 2010; Smelror and Petrov, 2018; Toro et al., 2016; Volkov, 1963). Although a major tectonic analysis of Novaya Zemlya is beyond the scope of this paper, it is important to be aware that the development of the Novaya Zemlya fold belt significantly influenced the tectonostratigraphy on the BSS.

2.2.3 Appalachian Basin

The Appalachian Basin represents a large-scale, composite foreland basin associated with the amalgamation of Pangea (e.g., Hatcher et al., 1989). The Appalachian Basin is approximately 2,050 km in length and is about 530 km at its broadest point and includes an area of approximately 536,000 km^2 (Colton, 1970). The stratigraphic succession is wholly Palaeozoic, with thicknesses of nearly 600–900
m on its western flank and more than 13,700 km on its eastern flank, and a total sedimentary volume of about 2,300,000 km^3 (Ettensohn et al., 2019). Large intracratonic basins occur to the west (Figure 2.1a), and to the east, the Appalachian Mountain belt has a NE-SW orientation and a length of 3,000 km (Hatcher, 2010). Moreover, some workers include the Ouachita fold belt (Figure 2.4b) as a structural extension of the Appalachian system that extends southwestward for an additional 2,100 km (Denison, 1989; Miall and Blakey, 2019; Thomas, 1985; Viele, 1989). In a broad view, the Appalachian Basin and adjacent intracratonic areas reflect subsidence accompanying a series of terrane collisions with the Appalachian margin during at least five orogenies (Ettensohn et al., 2019). These tectonic events contributed to the development of Pangea and represent one complete Wilson cycle (Hatcher, 2010; Miall and Blakey, 2019; Stockmal et al., 1998).

The tectonostratigraphic framework of U.S. parts of the Appalachian Basin is represented by a clastic-carbonate-clastic succession (Figure 2.5), which reflects complex relationships among tectonics, eustasy, palaeogeography and palaeoclimate. The succession began with the deposition of continental clastics in rift basins formed during the initiation of the Iapetan cycle during Late Precambrian–Early Cambrian time (Curtis and Faure, 1997; Gao et al., 2000). Laurentia shifted southward from its Late Precambrian equatorial position, and by Cambro–Ordovician time, the Appalachian margin had reached subtropical, arid latitudes, contributing to thick carbonate successions along the passive margin (Miall and Blakey, 2019; Torsvik and Cocks, 2017; Figure 2.5). By the Early–Middle Ordovician transition, island-arc collision with promontories on the Appalachian margin generated the Taconian Orogeny and a concomitant regional unconformity across large parts of Laurentia (Finney et al., 1996; Park et al., 2010; Sloss, 1963; Figure 2.5). At the time, the Appalachian region remained within arid latitudes (Torsvik and Cocks, 2017) and produced a foreland-basin succession including black-shale deposition of excellent petroleum potential within and beyond the foreland basin (Ettensohn et al., 2019; Park et al., 2010). The Appalachian margin remained in arid latitudes until Late Mississippian time, and during this period, experienced a series of orogenic events, the Salinic and Acadian/Neoacadian orogenies (Ettensohn et al., 2019; Hatcher, 2010; Miall and Blakey, 2019). These orogenic events generated foreland-basin deposits that include widespread black-shales, as well as coarser-clastic and carbonate sequences that comprise one of the most prolific petroleum systems within the foreland and adjacent intracratonic basins (Cluff and Dickerson, 1982; Ettensohn, 1985; Ettensohn and Lierman, 2012; Konyukhov, 2014; Roen, 1984; Figures 2.1a and 2.5). By Late Mississippian–Early Pennsylvanian time,

the Appalachian margin moved into the tropical, equatorial belt (Torsvik and Cocks, 2017). At the same time, continent-continent collision with Gondwana generated the Alleghanian Orogeny (Hercynian-Variscan), and a fold-thrust belt that filled the adjacent foreland basin with a coal-rich clastic blanket that prograded more than 1,000 km westward across the craton (Ettensohn et al., 2019; Greb et al., 2008; Hatcher et al., 1989; Figure 2.5). By Late Triassic–Jurassic time, global plate-tectonic reconfiguration led to widespread rifting along the former Appalachian Mountain belt, initiating the Atlantic Wilson cycle (Miall and Blakey, 2019).

2.3 Appalachian Basin and BSS analogues

2.3.1 Large-scale tectonic analogues

It is very true that perfect analogues do not exist (Alexander, 1993), but on a broad scale, as imperfect as they are, as comparisons, analogues can still prove to be very useful. Howell et al. (2014) have noted that at the largest scales analogues of size and geometry of geological features may be effective ways to begin the comparison of two areas, and such a comparison can be done between the Appalachian and BSS regions (Table 2.1). Both areas contain basins filled with thick sedimentary successions and include regions exhibiting foreland and hinterland physiographic domains. Both hinterlands exhibit multi-generational mountain belts that formed through diachronous subduction/collisional events associated with ocean closure. In the Appalachian region, the Iapetus and Rheic oceans closed during several Palaeozoic collisions with peri-Gondwanan microcontinents and Gondwana (e.g., Hatcher et al., 2007). Closure of the Iapetus Ocean continued northward into the western BSS region with collision of Baltica and Laurentia to form the minor

supercontinent Laurussia and the Arctic–North Atlantic Caledonides (e.g., Corfu et al., 2014).

Although the BSS is about one-third larger than the Appalachian region, both areas exhibit similar large-scale tectonic features (Figure 2.1; Table 2.1). For the Palaeozoic, Appalachian hinterland (now mostly eroded), the analogous BSS feature is the Late Palaeozoic–Mesozoic Uralian and Novaya Zemlya hinterland, suggested by Puchkov (2002) to be structurally analogous features. Cratonward (west) of the Appalachian hinterland is the Appalachian foreland basin, which was superimposed on Late Precambrian precursor rift basins (Rome Trough, Figure 2.1a; Ettensohn, 2008). Similarly, cratonward of the Uralian hinterland is an extensive foreland-basin belt extending from the Caspian Sea to Novaya Zemlya (Figure 2.4c), including Novaya Zemlya itself in Late Palaeozoic time and later incorporating the South and North Barents basinal areas in Permo-Triassic time and again in Late Triassic–Jurassic time (Müller et al., 2019; Nikishin et al., 2002). The Uralian succession across the BSS was similarly superimposed on Caledonian and Timanian basement structures.

Cratonward of the Appalachian Basin is a transitional area, represented by the Cincinnati Arch (Figure 2.1a), interpreted to have been a Pennsylvanian–Permian, Alleghanian bulge (Tankard, 1986), which resembles the broad monoclinal structure between the western and eastern BSS sectors interpreted here to be a transitional bulge-like zone. Others have interpreted even larger areas of the western BSS to have been a Jurassic, Uralian–Pai–Khoi–Novaya Zemlya bulge (e.g., Müller et al., 2019; Figure 2.6). West of the Alleghanian bulge area in the Appalachian region is a broad, foreland zone of large intracratonic basins and intervening platform areas, most of which probably began as

reactivated rift basins (Klein and Hsui, 1987). This broad intracratonic region is rife with older basement structures (Figure 2.1a), which were periodically reactivated by far-field tectonics during the various Appalachian orogenies (Ettensohn et al., 2019). In the Norwegian BSS, a broad platform system, basins and uplifts are similarly underlain by Caledonian, basement structures, which may have been reactivated by far-field tectonics during the Uralian Orogeny (Anell et al., 2013).

Like tectonics, the palaeoclimatic evolution in both areas is comparable because the succession of palaeoclimates represents a shift from humid to arid, and again to humid conditions (Table 2.1). It is important to note that even though the succession of palaeoclimates in both areas was similar, the palaeogeographic position was not. In a broad view, the humid conditions in the Appalachian area were due to its more equatorial position, whereas the BSS was influenced by both equatorial and highly temperate zones as the area moved to its current geographic location (Miall and Blakey, 2019). Such tectonic and palaeoclimate similarities led to the development of largely comparable stratigraphic successions, which include multiple regional unconformities and the persistence of carbonate platforms (Figures 2.2, 2.3 and 2.5; Table 2.1).

2.3.2 Tectonic processes analogues

The similarities between Appalachian and BSS regions reflect largely comparable tectonic histories. The Palaeozoic development of the Appalachian region reflects the closure of seaway and continent–continent collision (Hatcher, 2010). After development of a Cambro-Ordovician, carbonate-rich, passive margin, a mid-Ordovician to Mississippian phase involving the westward, subduction-related collision of island arcs and

peri-Gondwanan terranes generated several marine, facies-rich foreland basins, which migrated westward in space and time (Ettensohn, 2008). During the four orogenies involved, the accompanying foreland basins developed cyclic, unconformity-bound, sedimentary sequences in response to the orogeny; these sedimentary sequences have been termed tectophase cycles by Johnson (1971) and Ettensohn et al. (2019). Far-field forces during subduction promulgated the reactivation of extensive basement rift systems across the adjacent foreland. This phase ended with continent–continent collision and the generation of an extensive, Pennsylvanian–Permian clastic wedge (Figure 2.5). Subsequent Late Triassic–Jurassic rifting and sedimentation ended the Appalachian Wilson cycle and marked the inception of the Atlantic cycle (Ettensohn et al., 2019). The evolution of the Appalachian area can be condensed into eight stages, which are summarised in Table 2.2

If the Appalachian evolution (Table 2.2) is seen as a large-scale analogue to the BSS area, then similar evolutionary stages should be observed in both areas. Although the Arctic–North Atlantic Caledonides generated the basement in western parts of the BSS and many of the structures therein, we will not include them in this comparative analysis, because the resulting sedimentary succession was largely eroded (Nikishin et al., 1996). Instead, we will use the well-preserved Late Palaeozoic–Mesozoic UralianPai–Khoi–Novaya Zemlya succession and structures on the BSS, because, as in the Appalachian area, they are the products of diachronous collisional events associated with the closure of the Uralian Ocean (Puchkov, 2009).

In the BSS, several basement structures were developed during the Timanian and Caledonian orogenies, and these were later reactivated by the collapse of the Caledonides, and during the Uralian–Pai–Khoi–Novaya Zemlya Orogeny (Anell et al., 2013). This event

corresponds to stages 1 and 2 in the Appalachian area (Table 2.2), where a regional framework of pre-Appalachian basement structures was reactivated by the multiple Appalachian orogenies (Ettensohn, 2008). In both areas, orogenic collapse triggered relaxation, rifting and erosion, and widespread deposition of mainly continental-clastic sequences (Figures 2.2, 2.3 and 2.5; Table 2.2). Next, in the BSS region, a Late Mississippian to Early Permian, carbonate rich stable platform developed behind a Middle Devonian island arc above the westward subduction of the Uralian oceanic plate on the eastern BSS area (e.g., Smelror et al., 2009; Ziegler, 1989; Figures 2.2 and 2.3). This event corresponds to stage 3 in the Appalachian area (Table 2.2), where a stable platform rich in carbonate rocks developed during the Middle Cambrian–Early Ordovician (Figure 2.5).

By Pennsylvanian time, major subduction, involving arc collision on the eastern BSS region (Nikishin et al., 1996; Ziegler, 1989), is represented by a regional Late Carboniferous–Permian unconformity (Figure 2.3), which marks the inception of crustal loading in the Novaya Zemlya/eastern BSS region. This event corresponds to stage 4 in the Appalachian area (Table 2.2), where crustal loading triggered by the Taconian Orogeny is represented by a regional Middle Ordovician unconformity (Figure 2.5). The increasing crustal loading in the Novaya Zemlya/ eastern BSS area eventually triggered widespread deformational loading, which is represented by the extensive deposition of cherty limestones to black shales (Figure 2.3), representing basal foreland-basin sequences. This event corresponds to stage 5 in the Appalachian area (Table 2.2), where the inception of the Appalachian foreland basin (Ettensohn et al., 2019) is represented by the deposition of carbonates and black shales overlying the Middle Ordovician unconformity (Figure 2.5). Following crustal loading, the Novaya Zemlya/eastern BSS area rebounded. Widespread

flysch-like and molasse-like sequences were deposited in that area during Permian to Late Triassic time and are represented by black shales and marine to marginal-marine clastics (Figure 2.3). This event corresponds to stage 6 in the Appalachian area (Table 2.2), which was repeated during each Appalachian orogenic pulse and explains the deposition of multiple foreland successions (Ettensohn et al., 2019; Figure 2.5). In the BSS, at least two phases of crustal loading and relaxation are apparent during at least Late Triassic time (Figure 2.3). Lastly, one final tectonic pulse thrusted Novaya Zemlya on top of the eastern BSS (Petrov et al., 2008), generating a regional Triassic–Jurassic unconformity and resulting in the deposition of Lower–Middle Jurassic marine, marginal-marine and terrestrial clastic sequences (Figure 2.3); this represents the termination of the Uralian–Pai–Khoi–Novaya Zemlya cycle (Henriksen et al., 2011; Petrov et al., 2008). This event corresponds to stage 7 in the Appalachian area (Table 2.2), during which Pennsylvanian–Permian continental collision (Alleghanian Orogeny) triggered regional unconformity development and a subsequent, largely terrestrial, clastic wedge (Figure 2.5), which represents the termination of the Appalachian cycle (Ettensohn et al., 2019). In the BSS area, Late Jurassic–Eocene rifting, associated with the opening of the North Atlantic Ocean and the polar basin to the far west and north, respectively, became the dominant tectonic process. These events correspond to stage 8 in the Appalachian area (Table 2.2), during which Late Triassic–Jurassic rifting is associated with the opening of the Atlantic Ocean.

2.3.3 Foreland-basin analogues

Foreland basins represent a flexural crustal response to an advancing deformational load, the erosion of which largely provides the infilling sediments (Quinlan and Beaumont,

1984). Such foreland crustal responses may propagate across distances of more than 1,000 km (Beaumont, 1981; DeCelles and Giles, 1996) and reflect a dynamic relationship between tectonics and depositional regime (Figure 2.7a,b). Deformational loading in the form of a fold and thrust belt develops in response to orogeny, generating subsidence in front of the load, as a subsiding foreland basin and an uplifted peripheral bulge on the distal edge of the foreland basin. Uplift on the bulge typically generates an unconformity, and as the load migrates cratonward, the basin, bulge and contained sediments will also migrate cratonward (Figure 2.7; Quinlan and Beaumont, 1984).

The tectonic setting of the Appalachian Basin has been used to construct tectonostratigraphic models for foreland-basin sedimentation (Ettensohn, 1991, 2004, 2008; Ettensohn et al., 2019; Johnson, 1971), and following similar lines of thought, Johnson (1971) used the concept of 'tectophase cycles' to predict, discuss and illustrate the tectonostratigraphic succession of a foreland basin. Inasmuch as subduction-related orogenies occur in a series of deformational pulses or 'tectophases' (Camacho et al., 2005; Jamieson and Beaumont, 1988; Johnson, 1971), each tectophase will generate a typical sequence of lithologies (Figure 2.8), representing isostatic responses to the changing deformational load. In collisional orogenies, however, lower parts of a typical cycle are wholly overwhelmed by widespread, thin-skinned uplift and accompanying terrestrial sedimentation, as in the Appalachian Alleghanian Orogeny. Several examples of tectophase sequences are present in the Appalachian Basin (Ettensohn et al., 2019), but the Mississippian sequence, a stratigraphic response to the Neoacadian Orogeny (Figure 2.9), probably provides the best example of the model.

According to Ettensohn et al. (2019), a typical foreland-basin sequence (Figure 2.8) begins with a regional unconformity marking bulge uplift and moveout (Figures 2.8 and 2.9a). In addition to these regional, sequence-bounding unconformities, more localised unconformities may also occur due to far-field reactivation of local basement structures. Bulge uplift and moveout is followed by initial subsidence typically represented by the rapid deposition of shallow-water carbonates or sands (Figure 2.8), but this phase may be absent where subsidence is very rapid (Figure 2.9a). Once load migration ceases and the load becomes static, subsidence outpaces sedimentation, as most of the load is subaqueous and generates little clastic sediment (Figure 2.7a). As a result, mostly fine-grained organic matter from the water column accumulates. Many foreland-basin source rocks originate in this fashion (Ettensohn, 1997; Ulmishek and Klemme, 1990).

As surficial relief and complete drainage nets develop, clastic sediments from the adjacent load fill the foreland basin with 'flysch-like' sediments represented by deep-to shallow-marine, clastic deposits (Figures 2.7b, 2.8 and 2.9b). Once filled, the basin passes through a short 'equilibrium' phase, during which basin fill and eroded source areas are at or near base level; distal parts of the basin may experience sediment starvation at this time (Figure 2.9c). In the Mississippian example from the Appalachian Basin (Figure 2.9), equilibrium carbonates predominate during this phase because of unique subtropical, lowstand conditions in the area (Figure 2.9d). However, this phase may be minimal or absent in different climatic or non-lowstand conditions. The equilibrium phase is followed by a relaxation phase when proximal parts of the foreland basin and adjacent 'unloaded' source areas (Figure 2.9d) undergo rebound (Figure 2.9e), and previously deposited sediments are cannibalized. This phase is dominated by widespread deposition of finer-

grained, marginal-marine, post-orogenic, clastic sediments, which often include redbeds and coals. These 'molasse-like' sediments (Figure 2.8) end the tectophase cycle and are typically truncated by a regional unconformity marking the inception of the next tectophase. Tectonostratigraphic sequences like the tectophase cycle have been recognised in several other foreland basins (Allen et al., 1991; Coakley and Watts, 1991; Sinclair et al., 1991; Su et al., 2009).

However, each foreland basin is different in the number of cycles, each of which reflects an orogenic event. For example, the Alpine foreland basin exhibits only one cycle (Allen et al., 1991; Sinclair et al., 1991), whereas the Appalachian Basin exhibits 13 such cycles reflecting five orogenies, of which cycles beginning with the Ordovician Utica (Figure 2.10) and Devonian Marcellus (Figure 2.11a) black shales are best known for their hydrocarbon potential. Of special interest relative to foreland-basin cycles are the two Taconian tectophase cycles in the Appalachian Basin (Figure 2.10). Figure 2.10 illustrates one ideal case of well-developed cycles in an along-strike section that shows how orogeny and accompanying cycles migrate in space and time (south to north), as well as the varying tectonostratigraphic responses in each of the two cycles. On the BSS, we have recognised three such tectophase successions (Figure 2.3) reflecting two major orogenic events.

Using Appalachian Basin models (Figures 2.8–2.11a) as a basis, a schematic cross-section illustrating the tectonostratigraphic development of the Late Permian–Middle Jurassic succession across the BSS is presented (Figure 2.11b). This model illustrates multiple tectonic pulses in the eastern BSS region and a largely southeastern to northwestern progradation of deeper-marine shales and clastic wedges. The formation names correspond to the Norwegian nomenclature currently adopted by the Norwegian

Petroleum Directorate. At least three major clastic wedges were deposited during Late Permian, Triassic, Late Triassic (Norian) and Middle Jurassic times (Figure 2.11b). To our knowledge, the only wedge with a 'formal' name is the 'Triassic Boreal Ocean Delta', (Klausen et al., 2019; Figure 2.11b). The unconformities in red are the result of tectonic pulses caused by the Uralian–Pai–Khoi–Novaya Zemlya Orogeny on the eastern BSS region. So, as not to be mistaken for a tectophase-bounding unconformity, it is important to note that the green, Permo-Triassic unconformity in Figure 2.11b, used as a datum herein, is related to regional uplift accompanying the Permo-Triassic super-plume event (Drachev, 2016), which was responsible for extrusion of the Siberian Traps in the West Siberian Basin (Saunders et al., 2007). In the rest of this section, we will examine the Late Permian–Middle Jurassic BSS cycles (Figures 2.2, 2.3 and 2.11b), considering the Appalachian Basin models pictured above (Figures 2.8–2.11a).

As previously mentioned, the tectophase cycles are based on the presence of unconformities and a distinct overlying stratigraphic sequence (Figure 2.8). In the Appalachian cycles, the basal unconformities and overlying succession typically become younger in space andtime cratonward (Figure 2.11a). Similarly, in the BSS, the first tectophase (Figure 2.3; purple) is represented by the development of a basal Uralian unconformity in the east during Late Carboniferous (Bashkirian–Gzhelian) time (Figure 2.3; columns 5, 6, 14), which migrates westward, becoming progressively younger into Early Permian (Kungurian) time (Figure 2.3). Rocks on top of the basal unconformity are typically transgressive carbonates or black shales in Appalachian sections and represent rapid subsidence (Figures 2.8 and 2.10). Likewise, in the BSS section, Lower to Upper Permian (Kungurian–Wuchiapingian) deeper water carbonates and spiculites and Permo-

Triassic black shales reflect transgression and rapid subsidence atop the unconformity (Figures 2.2, 2.3 and 2.11b), representing major deformational loading in the Uralides. Once loading halts, relaxation sets in and widespread erosion in the now uplifted orogen results in basin infilling with flysch-like clastics followed by molasse-like sediments, which are well observed in the Appalachian area (Figures 2.8–2.11a). On the BSS, Late Carboniferous to Permian, deeper water, black shales do grade upward into flysch-like clastics of the Sassendal and lowermost Kapp Toscana groups (Figures 2.2, 2.3 and 2.11b), but at the Permo-Triassic transition, a prominent unconformity, most likely associated with regional uplift caused by the Permo-Triassic plume event, extensively truncates the section (Figures 2.3 and 2.11b). By Early Triassic (Induan) time, the unconformity is succeeded by thick, molasse-like sedimentation, including marginal-marine, cyclically alternating, black shales and clastics with later fluvio-deltaic facies and coal (Figures 2.3 and 2.11b), suggesting local pulses of thrust movement in the nearby orogen like those noted in the Acadian section (Figure 2.11a).

In the Appalachian Acadian sequence, the molasse-like sediments were deposited more proximally in the Catskill and Price-Pocono 'Deltas' (Ettensohn, 2004). On the BSS, the very prominent molasse-like sequence comprises the 'Triassic Boreal Ocean Delta' (Figure 2.11b), which is purported to be the largest deltaic complex of its type in the Earth's history (Klausen et al., 2019). These deltaic sequences were abruptly uplifted and capped by a Late Triassic, mid-Norian unconformity that signaled the advent of another tectophase, representing the advent of folding and thrusting of the Novaya Zemlya archipelago upon the BSS or the Novaya Zemlya Orogeny (Henriksen et al., 2011; Petrov et al., 2008). This tectophase (Figure 2.3; orange) is represented by a typical sequence of

organic-rich, flysch-like and molasse-like sediments and only lasted for about 20 m.y. from mid-Norian time to the Triassic-Jurassic boundary (Figures 2.3 and 2.11b). Rocks from this tectophase were abruptly truncated along a widespread, regional unconformity at the Triassic–Jurassic boundary (Figures 2.3 and 2.11b). This unconformity apparently characterizes the inception of another tectophase (Figure 2.3; black), which represents the final transpressional collision and indentation of a segment of Siberian crust into Baltica in the Novaya Zemlya archipelago (Curtis et al., 2018; Drachev et al., 2010). Like the Alleghanian collisional orogeny (Figure 2.5), this final collision generated a large wedge of alternating terrestrial and marginal-marine clastic sediments without lower parts of the cycle as in the Appalachian Basin (Table 2.2, Stage 7; Figures 2.2, 2.3 and 2.5). Sedimentation persisted for about 35 m.y. until Middle Jurassic (Bathonian) time, when uplift related to the opening of the Atlantic generated another unconformity (Figures 2.3 and 2.11b), overlain by deep-water, Atlantic-type oceanic shales (Henriksen et al., 2011), which effectively terminated the Uralian–Pai–Khoi–Novaya Zemlya tectonostratigraphic succession on the BSS.

2.3.4 Intracratonic-basin analogues

Intracratonic basins are areas within the craton that have experienced broad, long-period, regional-scale sagging, with most lacking a rapid, initial subsidence phase (Armitage and Allen, 2010; Klein and Hsui, 1987; Xie and Heller, 2009). These basins are generally described as having sedimentary thicknesses of less than 5 km, and rarely 6–7 km, exhibiting a generally saucer-like geometry, lacking major syn-tectonic faults, and experiencing only occasional post-sedimentary faulting (Allen and Armitage, 2012; Xie

and Heller, 2009). These characteristics are probably oversimplified because of the variety of subsidence mechanisms and geometries associated with these basins (An and Assump..o, 2006; Armitage and Allen, 2010; Cloetingh and Burov, 2011; Gac et al., 2013; Klein and Hsui, 1987; Ritzmann and Faleide, 2009; Ulmishek and Klemme, 1990). In the U.S. Illinois and Michigan basins (Figure 2.1a), subsidence mechanisms are related to much earlier phases of rifting (Kolata and Nelson, 1991; McBride and Kolata, 1999), and subsequent flexural stresses are associated with nearby orogenic activity (Cloetingh and Burov, 2011). Interestingly, Gac et al. (2013) concluded that the eastern BSS basins were largely formed by mechanisms like those forming the Illinois and Michigan basins, which were contemporaneous with Appalachian orogenies.

Stratigraphic successions in intracratonic basins are predominantly terrestrial to shallow-water origin, which suggests that sedimentation effectively kept pace with subsidence (Allen and Armitage, 2012). Moreover, intracratonic stratigraphic successions can at times be tied to the development of adjacent foreland basins (Ettensohn, 1985, 1992; Figure 2.11a). In fact, the same flexural stresses controlling foreland-basin sedimentation may also influence patterns of cratonic sedimentation some distance from the foreland basin, making it difficult to distinguish the intracratonic from the foreland tectonostratigraphic sequences (Ettensohn et al., 2019). Widespread source-rock deposition can also occur (Vyssotski et al., 2012), but some overfill and regional progradation of foreland tectonostratigraphic sequences far onto the adjacent craton, as in the Appalachian system (Figure 2.11a). The persistent large-scale cratonward progradation of the Uralian–Pai–Khoi–Novaya Zemlya succession (Figure 2.11b, southeastern Triassic–Jurassic clastic sequences) contributed to the filling of intracratonic basins in the western

BSS and Russian-Norwegian BSS transitional areas (e.g., Olga and eastern Nordkapp basins; Figures 2.1b, 2.2, 2.3 and 2.11b), intertonguing with local intracratonic stratigraphic sequences.

Because of the several formation mechanisms possible (Allen and Armitage, 2012), the tectonostratigraphic nature of intracratonic basins can be unclear (Lindsay et al., 1993). However, based on work in the Appalachian area (e.g., Quinlan and Beaumont, 1984), it is also important to understand that some intracratonic basins may experience periodic interactions with adjacent foreland basins, resulting in periods of yoking (Ettensohn and Lierman, 2015) and intracratonic subsidence (Howell and van der Pluijm, 1990) related to orogenic activity in the adjacent orogen. Hence, if development of intracratonic basins in the eastern BSS area is like that in the Appalachian area, as suggested by Gac et al. (2013) for the BSS, then processes from Appalachian intracratonic areas may well provide analogues, especially relative to subsidence rates (Smelror et al., 2009), fault reactivation (Anell et al., 2013) and foreland-basin- like stratigraphic successions on the BSS (Figure 2.3).

2.4 Summary

Using the features and history of a well-known area as analogues to understand a lesser-known area is a widely used technique in the geologic sciences and industry. Even though the studied areas may be widely separated and represent different times and places, external analogues may compensate for a lack of in-place data and provide new perspectives. Clearly, analogues are not perfect, but in areas of limited or unavailable knowledge, they should be examined as one of the first sources of information. To our

knowledge, basin areas external to the BSS and adjacent areas have not been widely used as analogues to the BSS. Inasmuch as both the Appalachian and BSS areas record the closure of an ocean or oceans and reflect the final stages of a Wilson cycle during the formation of Pangea, it is reasonable to expect the possibilities of at least large-scale analogues.

The main challenges in transposing Appalachian models to the BSS are the differences in timing, palaeogeography, and palaeoclimate. Even though the timing of tectonic events in the two areas is not the same, overall temporal differences should not affect the use of large-scale Appalachian analogues in the BSS area, because both areas experienced a very similar tectonic history. Similarly, the palaeogeographic placement in time of both areas was not identical, but the succession of resulting palaeoclimates in both areas was nearly the same and resulted in large-scale clastic-carbonate-clastic successions, which broadly reflect a similar sequence of non-marine, marine, non-marine depositional settings. Moreover, both basins experienced times of rapid subsidence that led to the accumulation of thick stratigraphic sequences.

Assuming that Appalachian and BSS (Uralian) successions are tectonostratigraphically analogous and are largely the products of flexural interactions (loading and relaxation), then Appalachian tectonostratigraphic flexural models (e.g., tectophase cycles) should be applicable to the BSS. For example, using the Appalachian tectophase model merely transposes a Lower Permian-to-Jurassic succession of units on the BSS for a Lower-to-Upper Palaeozoic successions of units in the Appalachian area. In this context, units from the Norwegian BSS would largely represent more distal cratonic areas, whereas units from the Russian BSS and Novaya Zemlya would constitute more

proximal intracratonic, bulge-related, and foreland-basin areas. Hence, an Appalachian model effectively provides critical background when analysing BSS regional unconformities, organic-rich rocks, petroleum systems, stratigraphic geometries, basin filling, correlation, tectonic timing and helps with integrating the regional tectonostratigraphy of both Norwegian and Russian BSS sectors.

The Palaeozoic Appalachian succession is the result of complex interactions among foreland basins, intracratonic basins, platform systems, and the widespread reactivation of Precambrian structures, which facilitated interactions between foreland and intracratonic basins. Similarly, the Upper Permian-to-Middle Jurassic BSS succession is the result of large-scale interactions among similar features of a younger age. In the BSS area, the Upper Palaeozoic sequence generally begins with a major bounding unconformity, overlain in succession by organic-rich marine shales, flysch-like clastics, and molasse-like clastics, and is subsequently truncated by an unconformity. This succession is analogous to those in several Appalachian foreland basins and adjacent intracratonic areas and is herein interpreted to be parts of unconformity-bound tectophase cycles related to flexural interactions with the orogen.

The large-scale setting with a deformed precursor basement, a closing ocean, a collisional orogen and resulting foreland and intracratonic basins is much the same in both areas. What is new in this analysis is the recognition of tectonostratigraphic cycles in the BSS succession that reflect flexural responses typical of Appalachian tectophase cycles. The idea that the existing BSS stratigraphy can now be related to distinct phases of Uralian orogeny is relatively new and especially critical in understanding the BSS succession in a tectonostratigraphic framework. This understanding is clearly a product of using

Appalachian tectonostratigraphic analogues and provides a foundation on which to develop the study of related BSS petroleum systems. This, we hope, will provide an additional tool for hydrocarbon exploration and in finding suitable carbon-capture and storage targets across the BSS.

Table 2.1. Schematic comparison between the Appalachian and Barent Sea shelf areas in terms of general features, tectonics, stratigraphy and palaeogeography.

Items	Appalachian area	Barents Sea shelf area
Approximate area (km^2)	0.93 million (Appalachian foreland and intracratonic areas)	1.4 million (shelf area)
Present-day setting	Continental	Mostly Offshore
Approximate maximum thickness (km)	13.7 (Appalachian Basin); 6.0 (Illinois Basin); and 4.3 (Michigan Basin)	Unknown. More than 20 km is believed in the South Barents Basin. At least 10 km in western basins.
Exploration status	Mature	Mostly frontier
Tectonics		
Structural elements (present day)	Foreland and intracratonic basins; structural highs and platforms. Nine superimposed foreland basins	Foreland, intracratonic, rift and strike-slip basins. Structural highs and platforms. Abundance of structural highs
Diachronous collisional events associated with oceanic closure	Closure of Iapetus and Rheic Oceans	Closure of Iapetus and Uralian Oceans
Stratigraphy		
Overall succession	Clastic-carbonate-clastic	Clastic-carbonate-clastic
Foreland basin succession	Easily identified. Several superimposed foreland basins.	Not easily identified. At least one Mesozoic and one Palaeozoic basin
Unconformities	Multiple. Local and regional	Multiple. Local and regional
Level of foreland preservation	Very good. Most foreland lithologies are preserved regionally	Variable. The Palaeozoic foreland basin(s) were structurally inverted by thrusting and destroyed by erosion
Carbonate platforms	Warm water (stable platform, abundant); salt is not abundant; cold water (following the beginning of collision); chert is present at local to basinal scale	Warm water (stable platform, abundant); salt is common to abundant; cold water (following the beginning of collision); chert is present at a regional scale
Palaeogeography		
Overall palaeoclimate succession	Humid-arid-humid	Humid-arid-humid

Palaeogeography		
Palaeocontinent development in time	Laurentia-Laurussia-central Pangea	Baltica-Laurussia-northern Pangea
Influence of major glaciation	Ordovician, Devonian, and Permo-Carboniferous	Permo-Carboniferous and Late Cenozoic

Table 2.2. General comparison between the Appalachian and Barents Sea shelf areas in terms of timing and tectonic events.

	Appalachian area		Barents Sea shelf area	
Stages	Timing	Event	Timing	Event
1. Basement precursors	Precambrian	Presence of Precambrian basement structures	Late Precambrian–Late Devonian	Presence of Timanian and Caledonian basement structures
2. Orogenic collapse and relaxation	Late Precambrian–early Cambrian	Relaxation, rifting, erosion, and deposition of continental clastics	Late Devonian–Early Carboniferous	Caledonian relaxation, rifting, erosion, and deposition of continental clastics (western BSS)
3. Stable platform development	Middle Cambrian–Early Ordovician	Stable platform development	Late Carboniferous–Early Permian	Stable platform development (behind offshore arc to the east)
4. Inception of subduction-type orogeny (s) with bulge migration	Early–Middle Ordovician	Inception of Taconian Orogeny with unconformity and initiation of basal tectophase	Early Permian	Pennsylvanian inception of orogeny with unconformity and initiation of basal tectophase
5. Deformational loading and platform subsidence to develop a foreland basin (one or more tectophases)	Middle Ordovician–Mississippian (during four orogenies and nine tectophases)	Deformational loading and platform subsidence (marine black shales during each of nine tectophases)	Permian–earliest Triassic (at least one tectophase during one orogeny)	Deformational loading and platform subsidence (cherty limestones to black shales)
6. Relaxation through infilling of foreland basin with syn-and	Late Ordovician–Mississippian (during four orogenies and	Infilling of foreland and some intracratonic basins with syn-and	Permian–Late Triassic	Infilling of foreland and some intracratonic basins with syn-and

	Appalachian area		Barents Sea shelf area	
post-orogenic clastics; termination of tectophase	nine tectophases)	post-orogenic clastics (flysch- and molasse-like clastics during each of nine tectophases)		post-orogenic clastics (flysch-and molasse-like clastics during at least one tectophase)
7. Final ocean closure and continental collision with major unconformity development, overlain by a largely terrestrial clastic wedge	Pennsylvanian–Permian	Mississippian-Pennsylvanian unconformity, overlain by a largely terrestrial clastic wedge, migrating far beyond the foreland basin	Lower–Middle Jurassic	Triassic-Jurassic unconformity, overlain by a largely terrestrial clastic wedge, migrating far beyond the foreland basin
8. Beginning of Atlantic cycle	Late Triassic–Jurassic	Orogenic collapse, rift development and infill	Late Jurassic–Eocene	Transpression on western part of BSS and oceanic flooding

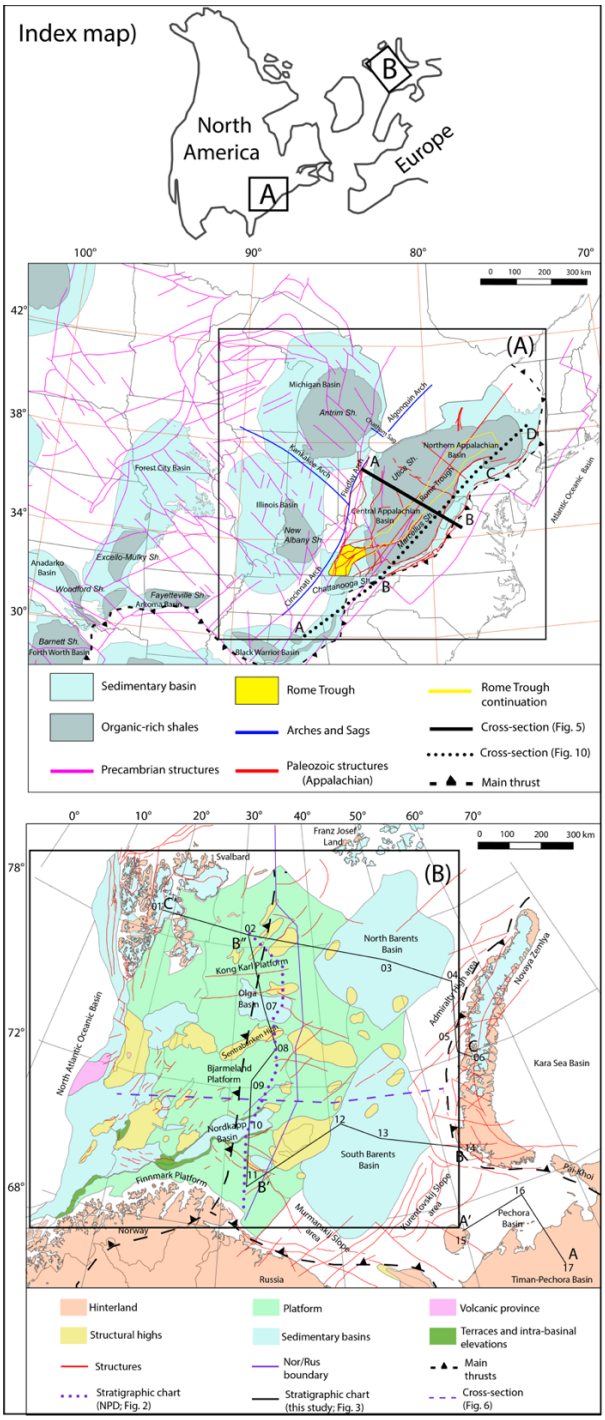

Figure 2.1. Map (a) main structural elements and major shale-play systems in the eastern, central, and northern United States. Data were compiled from the U.S. Energy Information and Administration EIA (2021, sedimentary basins and organic-rich plays); Tetra Tech (1981, arches and sags); Repetski et al. (2008, Paleozoic structures); and Sims et al. (2008, Precambrian structures). Map (b) main BSS structural elements. The red lines illustrate a highly schematic structural lineament framework (NPD, 2021). The solid purple line is the offshore boundary (NPD, 2017) between the Norwegian (western) and Russian (eastern) BSS sectors. Structural elements were compiled from the NPD (2021).

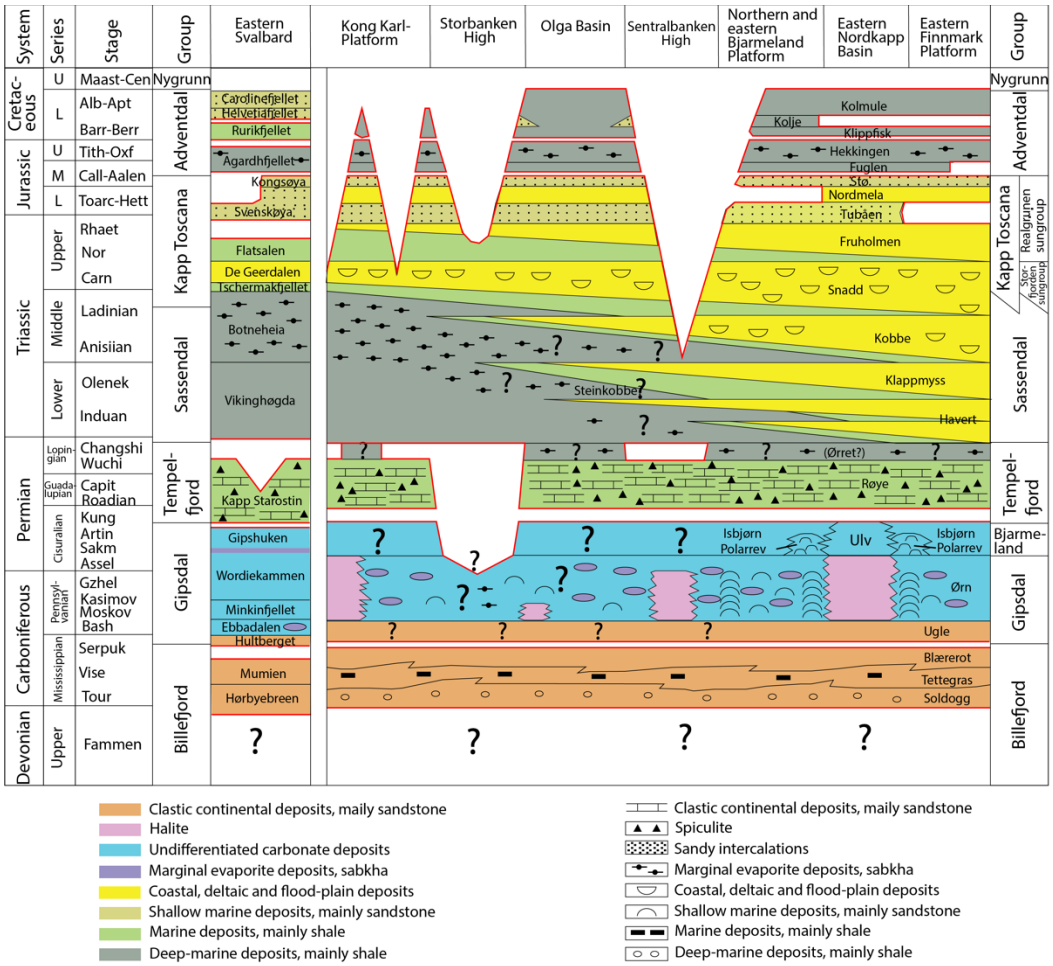

Figure 2.2. Schematic chronostratigraphic and lithostratigraphic diagram for eastern areas of the Norwegian BSS and a generalized stratigraphic column for eastern Svalbard (modified from NPD, 2017).

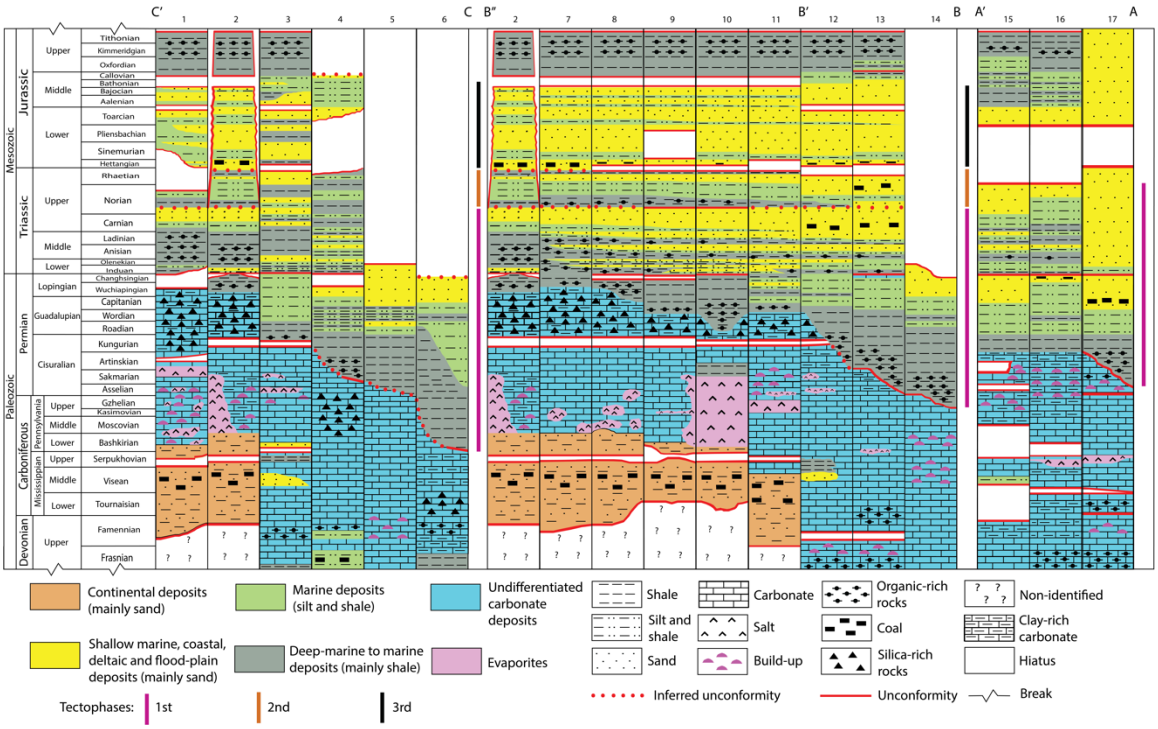

Figure 2.3. Schematic tectonostratigraphic section of eastern Spitsbergen (1); BSS (2–4; 7–13); Novaya Zemlya (5; 6; 14); Pechora Basin (15; 16) and northeastern Timan-Pechora Basin (17). Key references, but not the only references, used in constructing the section include: Timan-Pechora Basin (e.g., Abrams et al., 1999; Prischepa et al., 2011; Schenk, 2011); Pechora Basin (e.g., Ivanova, 1997; Norina et al., 2014; Suvorova & Matveeva, 2014; Zhuravlev et al., 2014); Novaya Zemlya (e.g., Drachev, 2016; Henriksen et al., 2011; Nakrem, 2007; Zhang et al., 2018); BSS (e.g.,Burguto et al., 2016; Dalland et al., 1988; Grogan et al., 1999; Johansen et al., 1993; Larssen et al., 2002; Leonchik & Senin, 2010; Margulis, 2008; NPD, 2017; Olaussen et al., 2018; Polyakova, 2015; Smelror et al., 2009; Stoupakova et al., 2011; Tugarova et al., 2008; Ustritskiy & Tugarova, 2013); eastern Spitsbergen (e.g., Dallmann et al., 2015; Nicolaisen et al., 2019; Riis et al., 2008; Stemmerik & Worsley, 2005).

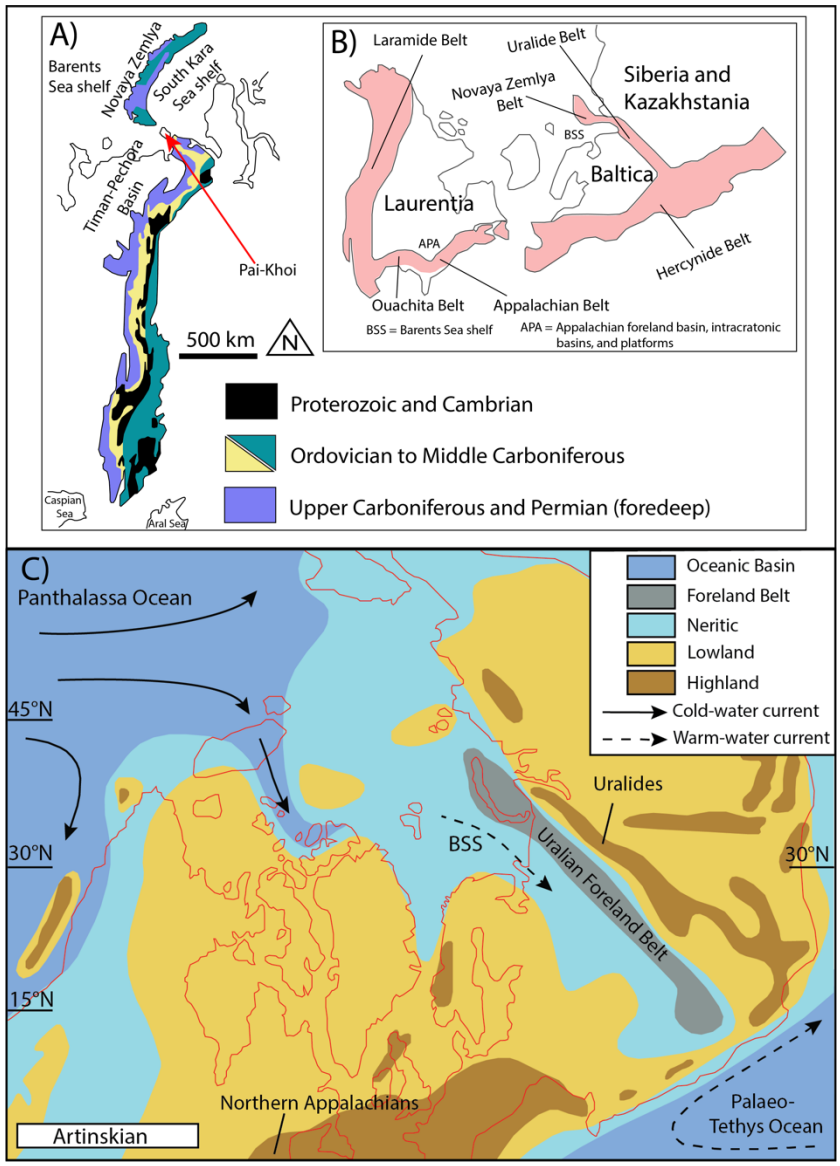

Figure 2.4. (a) Extent of the Uralide fold belt and associated facies; Ordovician to Middle Carboniferous deposits are pre-orogenic, mostly platform, sequences (e.g., Proust et al., 1998; Evdokimov et al., 2000). (b) Major Hercynian-age fold belts involved in the final amalgamation of Pangea (modified from Proust et al., 1998). (c) Paleogeographic reconstruction illustrating the convergence of Laurussia and Siberia-Kazakhstania during Artinskian time (modified from Reid et al., 2007).

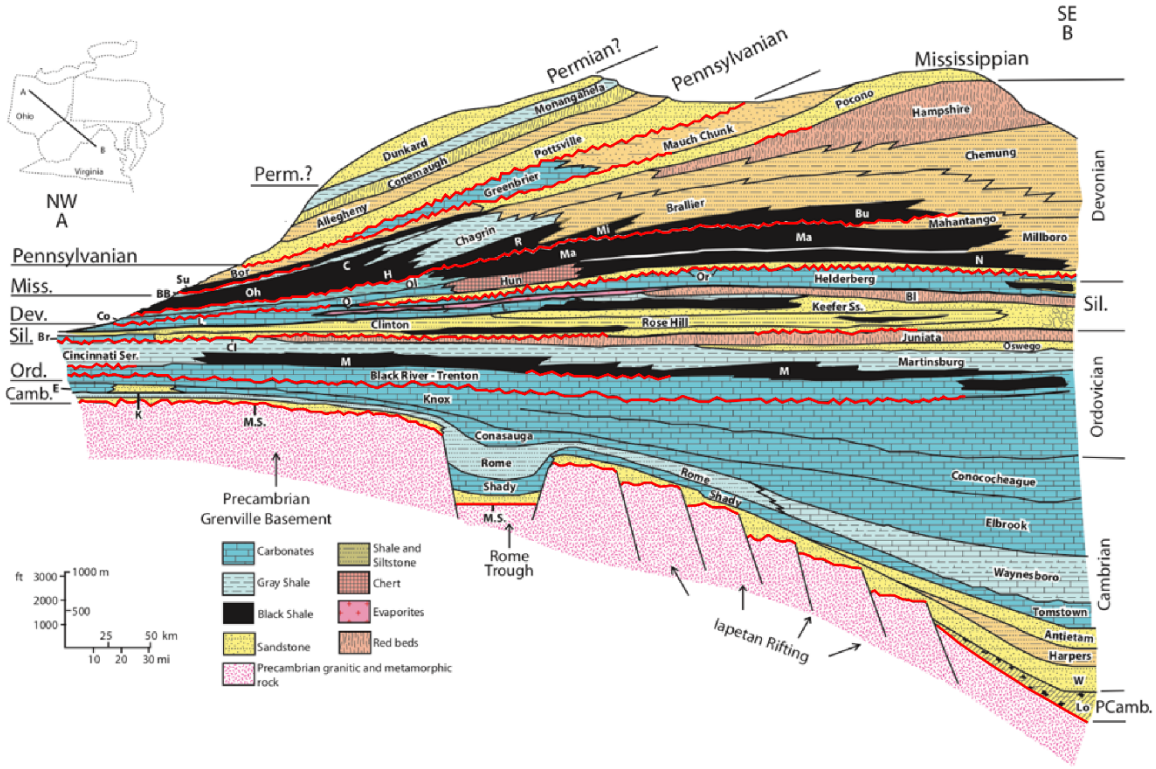

Figure 2.5. Schematic northwest-southeast cross section across the north-central Appalachian foreland basin (modified from Ettensohn et al., 2019).

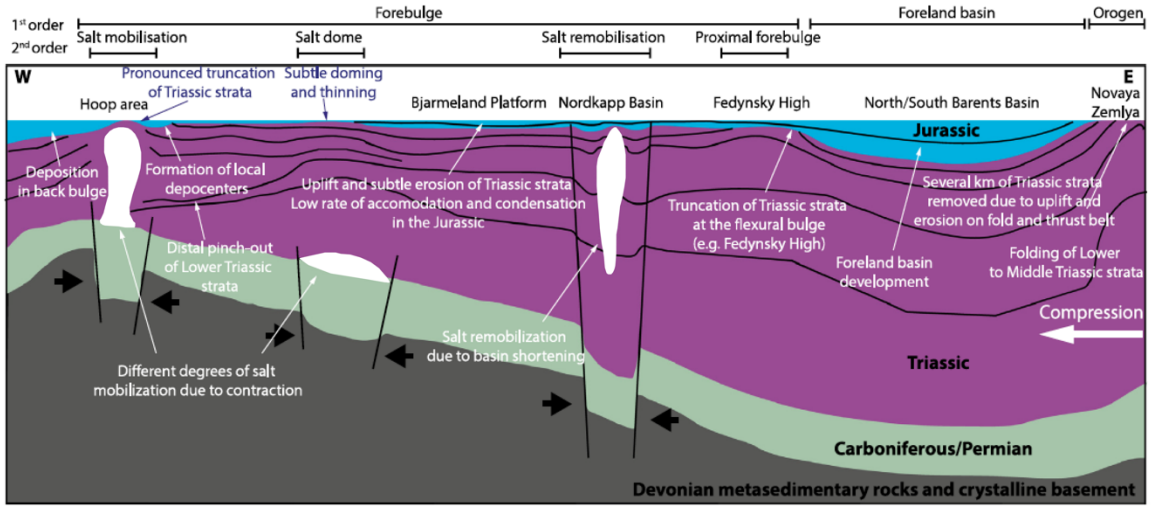

Figure 2.6. Cross section showing the interpreted Devonian–Jurassic succession in the BSS, as well as major structural elements, structural reactivation, and salt mobilization due to westward compression from the Novaya Zemlya Orogeny (modified from Müller et al., 2019).

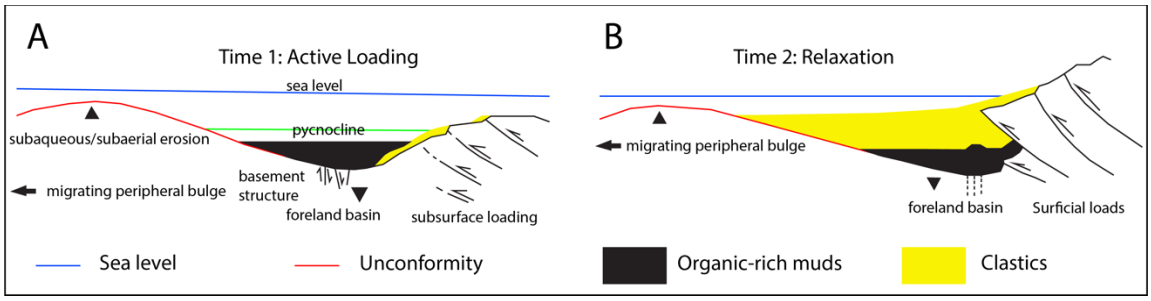

Figure 2.7. Sequential schematic diagrams showing flexural relationships among foreland-basin formation, sediment infill and deformational loading. (a) Basin-bulge formation and migration with subaqueous deformational loading and little clastic influx. (b) Major surficial deformational loading with major clastic influx (modified from Ettensohn et al., 2019).

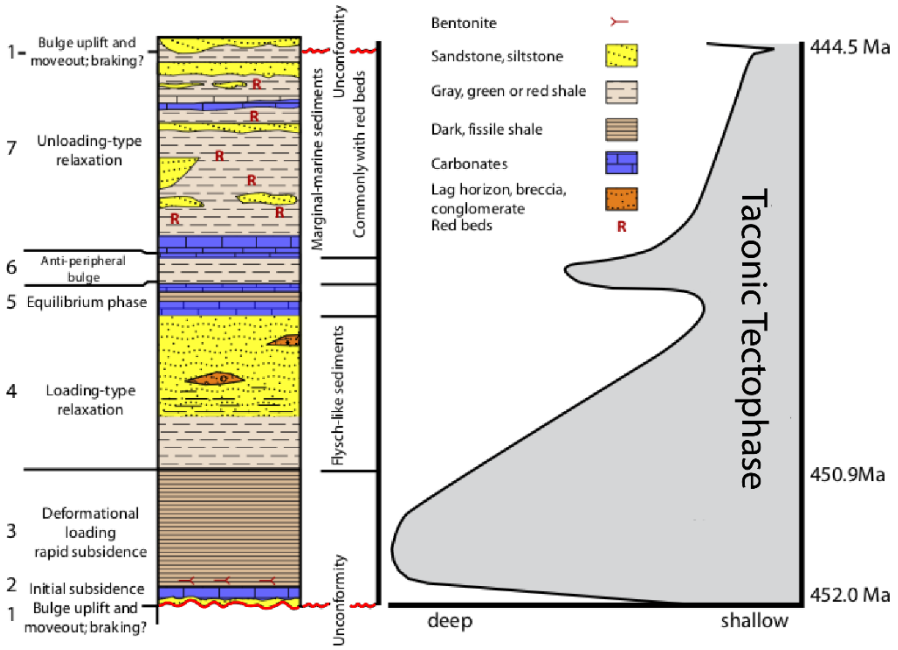

Figure 2.8. Schematic lithologic succession representing a generalized tectophase cycle at the outcrop scale with a eustatic curve for early subduction-type orogenies using the Appalachian, Taconic tectophase and ages as an example (modified from Ettensohn et al., 2019).

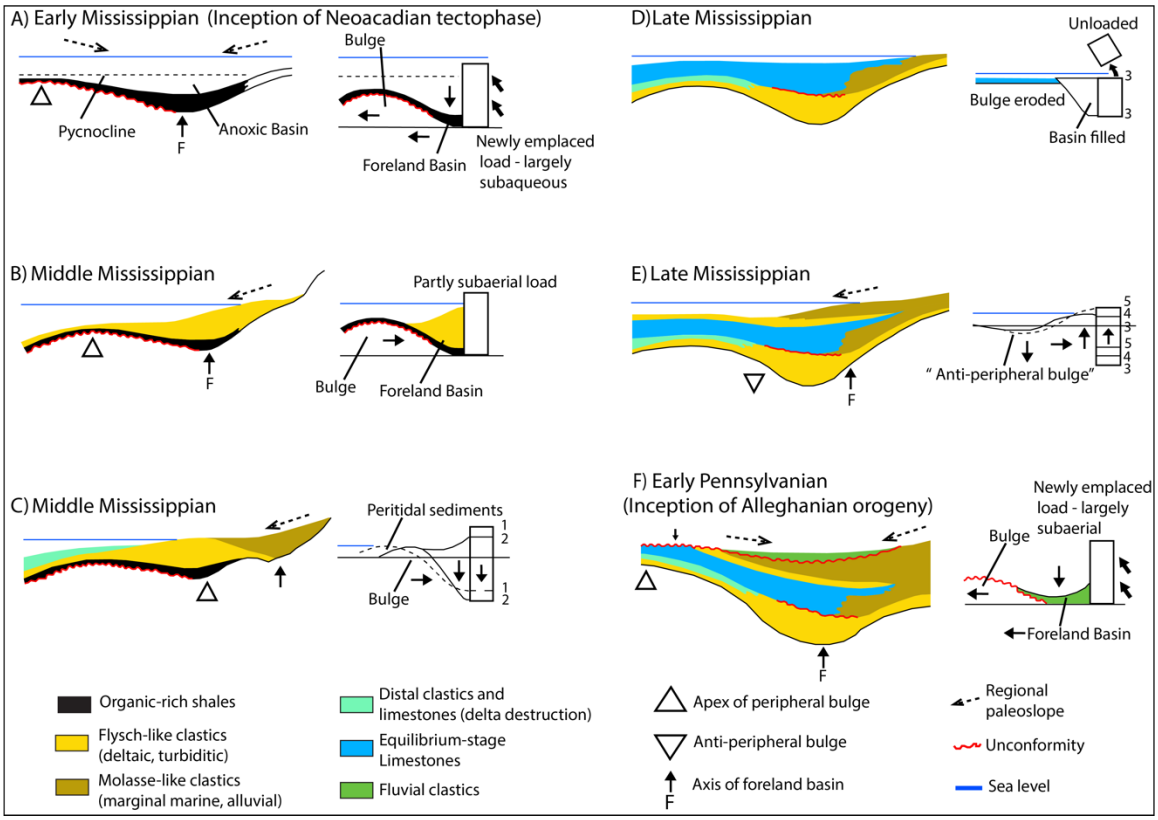

Figure 2.9. Complete Mississippian Neoacadian tectophase sequence from the Appalachian Basin showing the stage in the tectophase model to the right and the accompanying stratigraphic response to the left. (a) Same as Figures 2.7a and 2.8, parts 1, 2, 3. (b and c) Same as Figure 2.7b and Figure 2.8, part 4. (d) Same as Figure 2.8, part 5. (e) Same as Figure 2.8, parts 6, 7f, Figure 2.8, part 1, upper unconformity and new Alleghanian tectophase (modified from Ettensohn et al., 2012).

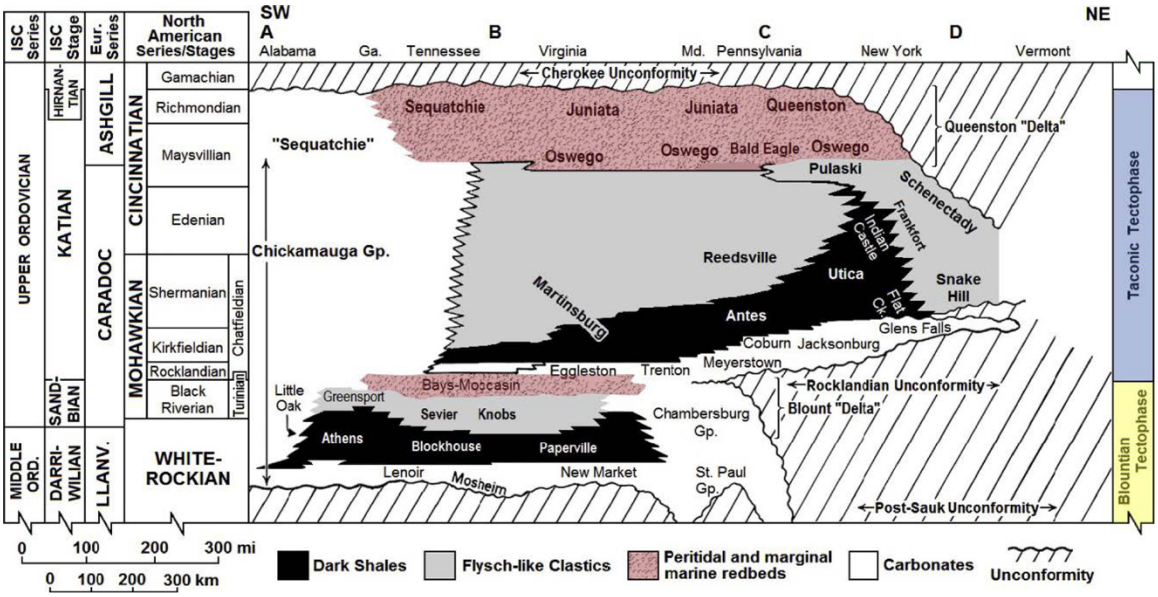

Figure 2.10. Schematic, southwest-northeast, Middle–Upper Ordovician section paralleling the strike of the Appalachian Basin and showing repetition of foreland-basin tectophase cycles for the Taconian tectophases (modified from Ettensohn et al., 2019).

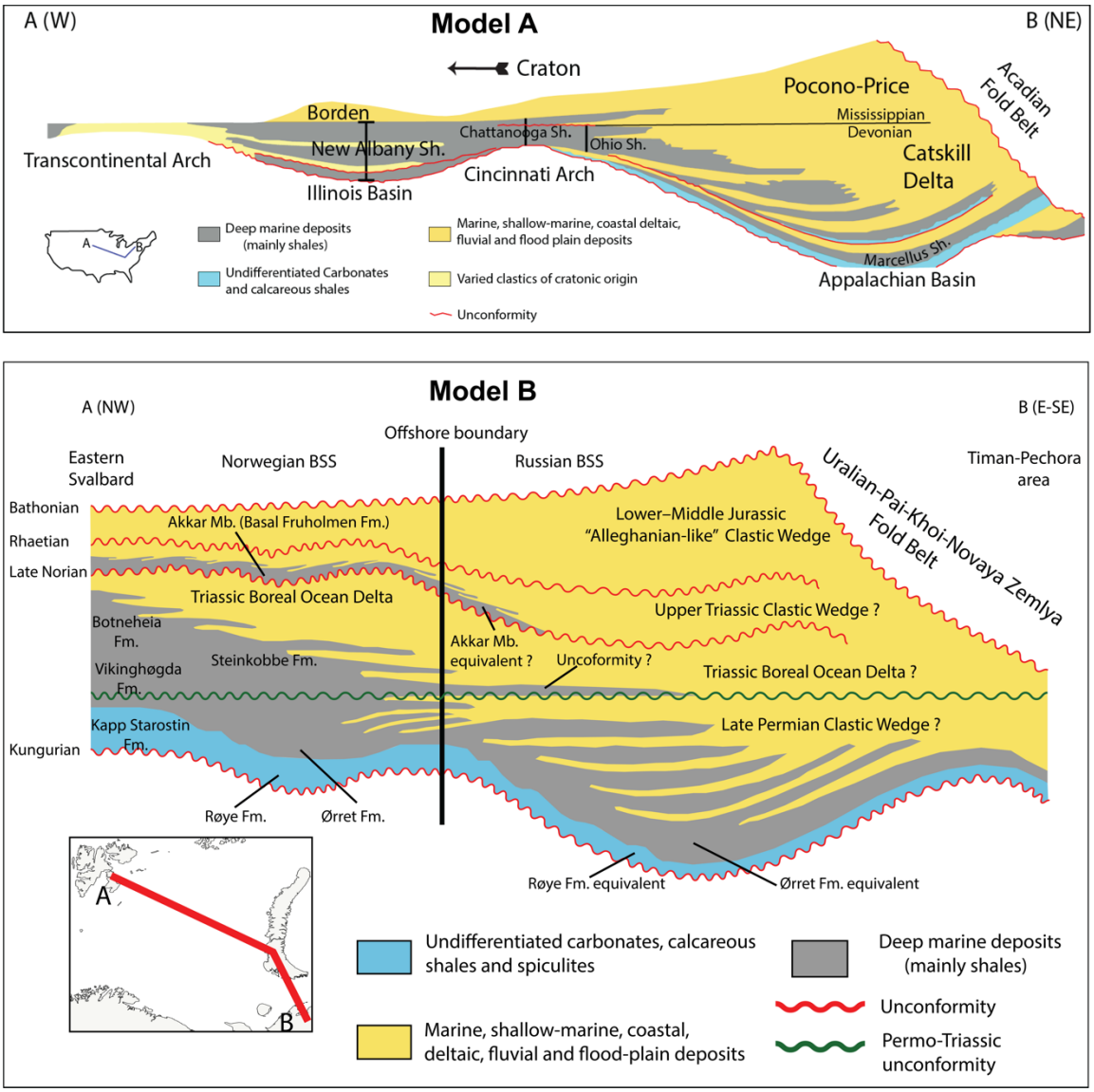

Figure 2.11. Model a) Highly schematic cross-section illustrating Devonian–Mississippian black shales in east-central United States and basin yoking (modified from Ettensohn, 1992). Model b) Highly schematic cross section illustrating the Late Permian–Middle Jurassic tectonostratigraphic succession in the BSS area, illustrated using an Appalachian-type tectonostratigraphic model.

CHAPTER 3. USE OF BACKSTRIPPING IN THE TRIASSIC–MIDDLE JURASSIC, SOUTH-CENTRAL BARENTS SEA SHELF SUCCESSION TO UNDERSTAND REGIONAL TECTONIC MECHANISMS AND STRUCTURAL RESPONSES

3.1 Introduction

The Barents Sea shelf (BSS) is a vast Arctic epicontinental shelf, which is divided into Norwegian (NBSS) and Russian (RBSS) sectors (Fig. 3.1). The shelf is located between northern Norway, northwestern Russia, Svalbard, Franz Joseph Land, and Novaya Zemlya, and covers an area of ~1.4 million km^2 with an average water depth of ~230 m. The area has been studied also as part of hydrocarbon exploration, which has been ongoing since the 1970s, but geologic uncertainties, including the large-scale tectonostratigraphic evolution of the latest Permian–Middle Jurassic succession, remain (e.g., Müller et al., 2019).

The structural framework across the BSS is diverse and includes rifts, intracratonic and foreland basins, platforms, and structural highs (e.g., Gabrielsen et al., 1990; Faleide et al., 2017), which were reactivated during Paleozoic–Middle Mesozoic tectonism (e.g., Martins et al., 2022). The backstripping method (e.g., Sclater and Christie, 1980; Allen and Allen, 2013) is a technique that can add additional understanding to the nature of tectonic events and large-scale structural reactivation in any basin type by using the sedimentation history across structural elements with well control (Xie and Heller, 2009). In the NBSS, well data are mostly available, but exploratory drilling is concentrated in the south, whereas in the north (>74◦30′ N lat.), deep drilling has not yet been permitted. In the RBSS, well data are scarce, are commonly unavailable to the public, and often do not penetrate Paleozoic sediments.

Understanding BSS structural activity and its implications for tectonostratigraphy is fundamental for producing and refining geodynamic models. Hence, the main goals of this paper are: 1) use the backstripping method (Allen and Allen, 2013) to interpret possible Triassic–Middle mechanisms in terms of known large-scale BSS tectonic history. Because of the disparate temporal and spatial nature of BSS structural reactivation, the method can be used to interpret tectonic mechanisms by analyzing and extracting variations in the rate of subsidence from the curves and treating them simultaneously in terms of tectonics (e.g., Xie and Heller, 2009). Although NBSS and RBSS tectonics have been long studied, much work remains to understand how various structures respond to these events, particularly those related to compressional tectonics (e.g., Petrov et al., 2008; Henriksen et al., 2011; Olaussen et al., 2018; Müller et al., 2019). To our knowledge, no study has attempted to use the backstripping method on the BSS on this scale.

It is important to keep in mind that this study does not aim to integrate alternative datasets (e.g., seismic; biostratigraphy), but to focus exclusively on traditional backstripping methods, for which well data are required (e.g., Sclater and Christie, 1980; Allen and Allen, 2013). Examples of tectonostratigraphic studies targeting a similar Triassic–Middle Jurassic BSS succession using methodologies and datasets other than backstripping are Lundschien et al. (2014); Klausen et al. (2016); Olaussen et al. (2018); Khudoley et al. (2019); Müller et al. (2019); Gilmullina et al. (2021a, 2021b), and Martins et al. (2022).

3.2 Regional setting

In broad view, the RBSS includes two very large basins (Fig. 3.1) with sediment thicknesses reaching up to 20+ kilometers, and a roughly N-S structural trend (Ivanova et al., 2006; Kuznetsov, 2006; Shipilov, 2010; Pease et al., 2014; Drachev, 2016). The NBSS generally includes platforms and smaller basins with sediment thicknesses of 10+ km with roughly N-S and NE-SW structural trends (Gee et al., 2008, 2010; Corfu et al., 2014; Gernigon et al., 2014; Klitzke et al., 2019). The current BSS structural framework is the product of several tectonic events, including the Timanian (Ediacaran–Early Cambrian), Caledonian (Late Ordovician–Early Devonian), and Uralian-Pai-Khoi-Novaya Zemlya (Middle Carboniferous–Middle Jurassic) orogenies, as well as subsequent, protracted extensional episodes (rifting) culminating in Early Eocene continental breakup and sea-floor spreading (Nikishin et al., 1996; Petrov et al., 2008; Drachev, 2016; Faleide et al., 2017; Smelror and Petrov, 2018; Lasabuda et al., 2021; Martins et al., 2022). Detailed description of the structural elements used in this study (Fig. 3.1) can be found in Gabrielsen et al. (1990), Stoupakova et al. (2011), Anell et al. (2016), and Drachev (2016).

The Timanian and Caledonian orogenies consolidated the basement in the RBSS and NBSS, respectively, whereas central areas represent a transitional basement zone (Drachev, 2016; Klitzke et al., 2019). During Devonian–Carboniferous time, various extensional basins developed in the NBSS in a largely intracratonic domain and were structurally controlled by the Devonian collapse of the Caledonides and later proto- North Atlantic rifting events (Faleide et al., 1984; Seidler et al., 2004; Stemmerik and Worsley, 2005; Marello et al., 2013; Gasser, 2014; Faleide et al., 2017; Olaussen et al., 2018). In these

basins, continental sediments followed by warm-water carbonates accumulated (Fig. 3.2; Columns 1–7).

In the RBSS, during Devonian–Carboniferous time, ongoing closure of the Uralian Ocean generated a Devonian back-arc province (Puchkov et al., 2021). Next, final closure of the Uralian Ocean occurred by at least latest Early Carboniferous time, and the coeval amalgamation of Baltica, Siberia and Kazakhstania into Pangea triggered the Uralian-Pai-Khoi- Novaya Zemlya orogeny (e.g., Ziegler, 1989; Nikishin et al., 1996; Torsvik and Cocks, 2017). This collision was diachronous (Late Carboniferous–Permian), propagating northward from southern central Asia during Carboniferous (late Bashkirian) time towards the Pai-Khoi and likely Novaya Zemlya areas by Permian (Late Hercynian?) time (Puchkov, 2009; Filatova and Khain, 2010; Korago et al., 2022), and eventually triggered fast foreland-type subsidence in Novaya Zemlya and coeval intracratonic subsidence in the RBSS (e.g., Martins et al., 2022) (Fig. 3.1). In these basins, carbonates and deep-water shales accumulated (Fig. 3.2; Columns 8–10), but by Late Permian time, sedimentation of silica-rich carbonates and deep-marine deposits predominated across the BSS (Fig. 3.2).

At the Permo-Triassic transition, emplacement of the Siberian superplume triggered widespread hinterland uplift, thus enhancing the already ongoing erosion of the Uralides (Puchkov et al., 2021; Gilmullina et al., 2021a) and contributing to widespread deltaic progradation across the BSS (Riis et al., 2008; Glørstad-Clark et al., 2011; Fleming et al., 2016; Klausen et al., 2019; Gilmullina et al., 2021b) (Fig. 3.2). Meanwhile, the Novaya Zemlya basin had closed by at least Late Permian–Early Triassic time (Petrov et al., 2008).

During Triassic time, the NBSS represented parts of a large platform area, with complex offshore-marine and fluvio-deltaic deposition, whereas the RBSS basins

experienced rapid subsidence in more proximal areas dominated by fluvio-deltaic sedimentation (Uchman et al., 2016; Klausen et al., 2015, 2019; Gilmullina et al., 2021a, 2021b). Even though deep-marine to fluvio-deltaic sedimentation persisted during the entire Triassic time (Fig. 3.2), marine incursions often pushed the delta-top far eastward (e.g., Johansen et al., 1993; Henriksen et al., 2011; Eide et al., 2017). By at least Late Triassic–Early Jurassic time, westward thrusting of the Novaya Zemlya archipelago on top of the RBSS formed an arcuate fold belt (Fig. 3.1), representing the final continental collision of Siberia with northeastern Baltica (Nikishin et al., 1996; Lopatin et al., 2001; Petrov et al., 2008; Drachev et al., 2010; Scott et al., 2010; Faleide et al., 2017; Curtis et al., 2018; Puchkov and Ivanov, 2020). The Triassic succession is likely the most well-understood stratigraphic system in the BSS and adjacent areas and has been recently regionally correlated in terms of ages and units (Gilmullina et al., 2021a) (Fig. 3.2).

Even though a Late Triassic age is favored in the literature, the timing of Novaya Zemlya tectonism is still being debated. The most recent Novaya Zemlya study by Korago et al. (2022) interpreted a Late Hercynian (?) (Permian)–early Cimmerian (at least Early Jurassic) timing. However, earlier authors, using various methodologies (e.g., seismic, paleomagnetics, geochronology of granitic rocks, and apatite fission track), interpreted the timing of orogeny as Permian (e.g., Filatova and Khain, 2010; Shatsillo, 2015), Early Triassic (e.g., Gudlaugsson et al., 1998; Scotese and Wright, 2018), Middle Triassic (e.g., Smelror et al., 2009; Nikishin et al., 2011; Norina et al., 2014), and Late Triassic (e.g., Klausen et al., 2016; Zhang et al., 2018; Müller et al., 2019). In Pai-Khoi (Fig. 3.1), Timonin et al. (2003) suggested that a phase of collision started as early as Late Permian time and culminated during Late Triassic time. Moreover, Scott et al. (2010) indicated that

phases of Mesozoic Novaya Zemlya deformation may have been superimposed on earlier, late Paleozoic deformation of Uralian age, suggesting that there is still a lack of clarity about the timing and nature of events. Regardless of the timing, thrusting of Novaya Zemlya led to the development of at least one, collisional foreland-basin in the RBSS, and the associated unconformity represents the most significant hiatus in the Triassic–Middle Jurassic, BSS succession (Müller et al., 2019; Martins et al., 2022).

During Early to Middle Jurassic time, alternating shallow-marine, coastal, deltaic, floodplain and deep-marine deposits covered the entire BSS (e.g., Olaussen et al., 1984; Dalland et al., 1988; NPD, 2017) (Fig. 3.2). By late Middle Jurassic time, major marine incursions and resulting deep-marine deposition represent the predominance of North Atlantic rifting across the area (Knutsen and Larsen, 1997; Lopatin et al., 2003; Serck et al., 2017; Fjeldskaar and Amantov, 2018).

3.3 Materials and method

3.3.1 Backstripping method

Generation of quantitative tectonic subsidence curves requires the plotting of stratigraphic data relative to both depth and geologic time, creating a graphic representation of the vertical movement of a stratigraphic horizon with respect to a basin datum (Kneller, 1991; Xie and Heller, 2009). The backstripping method generates such a representation after subtracting the effect of sediment loading to quantify tectonic subsidence by sequentially removing overlying strata (Fig. 3.3A). This process simulates the "decompaction" of underlying strata, thus recreating the original sedimentary porosity prior to compaction (Heidlauf et al., 1986; Cloetingh and Lankreijer, 1992; Allen and

Allen, 2013) and emulating the vertical movement of a datum through time. This method produces: 1) a tectonic subsidence curve (subsidence related to tectonism); and 2) a total subsidence curve (subsidence due to gradual sediment loading) (Beglinger et al., 2013) (Fig. 3.3B), and quantitatively estimates tectonic subsidence by using the stratigraphic succession in each well.

The backstripping method assumes that sedimentation took place in a water-filled basin because of the water column's contribution to subsidence (e.g., Allen and Allen, 2013; Beglinger et al., 2013). However, eustatic corrections are often not applied, and this has been the case with most studies that assumed the loss of porosity to be mostly due to mechanical compaction (Xie and Heller, 2009; Berra and Carminati, 2010; Baiyegunhi et al., 2017). These assumptions and data inaccuracies (e.g., age control) are the main limitations of the method (Xie and Heller, 2009). The main backstripping parameters are sedimentary thicknesses, porosity-at-surface, compaction coefficient, and mineralogical, water and mantle densities (Allen and Allen, 2013).

In the BSS, detailed regional paleobathymetric data is often insufficient. To provide some bathymetric reference, we estimated mean water-depth curves by analyzing the studied NBSS formations and RBSS sedimentary units in terms of lithology and sedimentary facies in each well, and based on the work of Glørstad-Clark et al. (2011), we assumed the following BSS depositional settings and water depths: 1) deep marine (500 m); 2) clinoform slope (400–250 m); 3) shallow marine (50 m); 4) delta front (25 m); 5) coastal plain (10 m); and 6) fluvial plain (0 m). These mean water-depth estimates are only provided as approximate references but are too general to use in the backstripping calculations.

The produced backstripping curves were analyzed in terms of geometric patterns, tectonic mechanisms, and unconformities (Fig. 3.3C), and were later interpreted in terms of known regional BSS Triassic–Middle Jurassic tectonics. According to Pitman III and Andrews (1985), Kneller (1991), Xie and Heller (2009) and Beglinger et al. (2013) (Fig. 3.3C), tectonic mechanisms and associated curve geometries are: 1) extensional (blue curve): produces a concave-up curve towards the time axis, representing shift from rapid fault-controlled subsidence to slower thermal subsidence; 2) strike-slip (green curve): produces variable U-shaped curves that show rapid, but short-lived, subsidence and/or uplift (transtension/transpression); and 3) flexural (red curve): produces an overall convex curve towards the time axis that reflects deformational loading typical of a fold-thrust belt. These patterns are, however, oversimplified and may be difficult to identify (Xie and Heller, 2009). Moreover, the backstripping curves can be interpreted in two ways. The most common (lower resolution) is to interpret the entire curve as one overall basin style (e.g., Xie and Heller, 2009). The least common (higher resolution) is to interpret smaller-order curve deflections as individual tectonic events (e.g., Watts, 2012; Fig. 3.3D).

3.3.2 Backstripping parameters and equations

In this study, ten wells were selected based on data availability, stratigraphic completeness, drilling depths, and thicknesses (Table 3.1) to generate the backstripping curves. Six wells are located in the NBSS, are in true-vertical-depth, and data from them are publicly available in NPD open files (NPD, 2022), whereas published data from four RBSS wells were obtained from VSEGEI reports (Astafiev et al., 2008; Burguto et al., 2016). The literature did not indicate if the RBSS wells are in true-vertical-depth, however,

the wells were drilled through sections having no significant dips. In this study, the top of the Permian System is considered the "datum" and functions as a reference level that can change vertically (Fig. 3.3A, B). For wells that did not penetrate Permian strata, the datum will then be the oldest post-Permian stratum penetrated (Table 3.1).

The petrophysical parameters needed for traditional backstripping calculations are sediment grain density, compaction coefficient, porosity-at-surface, and mantle and water densities (e.g., Allen and Allen, 2013) (Table 3.2). Even though the lithologic parameters of Sclater and Christie (1980) (Table 3.2) were obtained from the North Sea, these values have become standardized as appropriate for most BSS lithologies (Baig et al., 2016; Klausen and Helland-Hansen, 2018). All parameters were then calculated using values from Table 3.2, proportionate to the lithologic percentages in each NBSS formation and RBSS sedimentary unit, as noted in each well (Tables 3.3 and 3.4). Age values for each NBSS formation were obtained from Paterson and Mangerud (2019) and Gilmullina et al. (2021a), as well as from Astafiev et al. (2008) and Burguto et al. (2016) for RBSS sedimentary units. These ages were then calibrated relative to the absolute values in Cohen et al. (2022), and mean ages were then calculated (Tables 3.3 and 3.4).

Finally, all these parameters were processed in the following fashion (Allen and Allen, 2013): 1) calculating variations in porosity as a function of depth (Table 3.5; eq. 1); 2) decompacting sedimentary thickness (Table 3.5; eq. 2); 3) determining bulk densities for the entire sedimentary column (Table 3.5; eq. 3); and 4) quantifying tectonic subsidence (Table 3.5; eq. 4). These results were then plotted on a time-to-subsidence graph, generating both tectonic and total subsidence curves.

3.4 Results

Each of the backstripping curves (Fig. 3.4; A–J) was plotted on time-to-depth graphs and represents selected BSS wells on distinct BSS structural elements (Table 3.1; Fig. 3.1). However, the completeness of the target BSS succession (Triassic–Middle Jurassic; ~251 Ma to ~170 Ma) as found in each well varies (Table 3.1). To mitigate age uncertainties, mean ages for each targeted NBSS formation and RBSS sedimentary unit (Tables 3.3 and 3.4), plotted as dots on the curves (Fig. 3.4), were obtained from recent stratigraphic studies (e.g., Paterson and Mangerud, 2019; Gilmullina et al., 2021a) and later adjusted relative to the absolute ages provided in the most recent International Stratigraphic Chart (Cohen et al., 2022).

In Figure 3.4, each backstripping plot represents variations in the rate of subsidence on each independent BSS structural element (Fig. 3.1). The tectonic subsidence curves (blue) illustrate an idealized subsidence history that would have existed if no sediment filled the basin, thus emphasizing the tectonic mechanisms (Xie and Heller, 2009; Beglinger et al., 2013) (Fig. 3.3A, B). In contrast, the total subsidence curves (orange) illustrate the effects of sediment-induced loading, summed with tectonically driven subsidence (Beglinger et al., 2013). The water-depth curves (purple) represent paleobathymetric estimates based in lithology and sedimentary facies estimated from each well.

In this analysis, the backstripping curves are interpreted in terms of both lower (overall curve trend; red curves) and higher (relevant deflections and shorter duration trends; black curves) resolutions. Additionally, tectonostratigraphic interpretations (unconformity, non-deposition, and overprint) are indicated in the curves. The Rhaetian–

Hettangian unconformity (culmination of the Novaya Zemlya orogeny) is interpreted in the curves, considering the relationship between the backstripping curves and estimated water depth (Fig. 3.3C). In the discussion section, we will discuss these tectonostratigraphic interpretations in more detail and compare them with previous literature (e.g., Müller et al., 2019; Gilmullina et al., 2021a).

In Fig. 3.4A–J, the plots can be schematically grouped according to geometric similarities in the tectonic subsidence curve (Table 3.6). These groups are: 1) the Hammerfest Basin (HB) and Loppa High (LH) (Figs. 3.4A, B); 2) the western and eastern Bjarmeland platforms (WBP; EBP), Nordkapp Basin (NB), northeastern Finnmark Platform (NFP), and northwestern and southeastern Kola Monocline areas (NKMA; SKMA) (Figs. 3.4C, D, E, F, H, J); 3) Fersmanovskaya High area (FH) (Fig. 3.4G); and 4) South Barents Basin (SBB) (Fig. 3.4I). The longest-duration event is observed in the Souths Barents Basin (~30 Ma), whereas the Hammerfest Basin had the shortest (~2 Ma). Similarly, the strongest episode of subsidence is observed in the Nordkapp Basin (~1.34 km), whereas the weakest was identified in the eastern Bjarmeland Platform (0.05 km). Additionally, Table 3.6 presents the interpreted tectonic mechanisms of extension (E), flexure (F), and likelihood of transtension (Te) as well as the major characteristics observed in each relevant backstripping-curve deflection (age, duration, and subsidence).

For every plot, the mean and standard deviation for the tectonic subsidence (Tes Mean; Tes SD) and total subsidence (Tos Mean; Tos SD) were included and are also presented in Table 3.6. Dividing the standard deviation by the mean results in the coefficient of variation, which can be understood as a ratio between the standard deviation and the mean. Usually, a coefficient of variation value >1 is considered to represent a high

standard deviation relative to the mean. Except for the Loppa High (Table 3.6), the coefficient of variation per curve in each well is <1. It is possible that the high values for the Loppa High are due to low sampling because of the largely incomplete Triassic–Middle Jurassic succession found in this structural element (Table 3.1).

The Hammerfest Basin and Loppa High backstripping curves (Group 1; Table 3.6) are overall characterized by a slow tectonic subsidence that abruptly becomes very rapid and is immediately followed by abrupt uplift (Figs. 3.4A, B). Even though most of the succession in the Loppa High was eroded, both curves have similar overall curve geometric patterns. In the Hammerfest Basin (Fig. 3.4A), deflection 1 (250–248 Ma) represents a density contrast between clay- and sand-rich intervals (Klappmyss and Kobbe formations; Table 3.3). If this contrast is ignored, the resulting overall shape of the part of the curve containing this deflection is convex; thus, a flexural mechanism is illustrated (Fig. 3.3C). In the Hammerfest Basin and Loppa High, abrupt, rapid, short-lived subsidence (deflections 2 and 3) initially suggest a transtensional mechanism (Fig. 3.3C). According to Xie and Heller (2009), the magnitude and concave-shape of strike-slip curves are like those of passive margins, although subsidence rates are much faster. However, the abrupt overprint, observed at ~232 Ma, and poor preservation of the Loppa High succession prevent a more accurate determination of the tectonic mechanism. Because rifting processes were already operant on the NBSS (e.g., Klitzke et al., 2019), existence of extension and/or transtension at these locations is possible. In the Hammerfest Basin, following the abrupt uplift phase, the tectonic subsidence curve becomes nearly horizontal. Because the estimated water depth is about 0.1 km, the depth excludes sub-aerial exposure. Furthermore, the Rhaetian–Hettangian unconformity in this location (Fig. 3.4A) is not very

extensive due to creation of accommodation space, reflected by a possible subtle deflection in the tectonic subsidence curve at ~195 Ma.

The backstripping curves for the western and eastern Bjarmeland platforms, Nordkapp Basin, northeastern Finnmark Platform, and northwestern and southeastern Kola Monocline (Group 2; Figs. 3.4C, D, E, F, H, J; Table 3.6) areas are overall characterized by rapid tectonic subsidence that is either followed by uplift (Figs. 3.4C, D, E, F, H) or by flat-curve trend (Fig. 3.4J). In all these curves, an overall extensional mechanism is observed, reflected in the clear concave geometries and periods of rapid initial grading into slow subsidence (Fig. 3.3C). In Figures. 3.4F, H, and J, short pulses of abrupt uplift may represent distortions caused by intervals having a more sand-rich composition in contrast to underlying, very clay-rich, strata (Tables 3.3 and 3.4).

In Figures. 3.4C, D, E, F and H, rapid Early–Middle Triassic initial subsidence, followed by slower subsidence (deflections 4, 7, 8 and 10), is interrupted by abrupt uplift at ~232 Ma, which overprints the overall curve trends. The magnitude of this uplift varies from significant (Figs. 3.4C, E), to moderate (Figs. 3.4F, H), to subtle (Fig. 3.4D). Interestingly, the western Bjarmeland Platform exhibits significant uplift, whereas the eastern part of this same structural element (Fig. 3.1) shows only a very subtle uplift trend. In all curves of Group 2 (Table 3.6), the deflections show a concave geometry that represents rapid initial subsidence, which is indicative of extension (Fig. 3.3C). The eastern Bjarmeland Platform tectonic subsidence curve (Fig. 3.4D), however, exhibits a subtle, convex deflection at ~196 Ma (deflection 6), which indicates a flexural mechanism.

In Group 2, the timing and extension of the Rhaetian–Hettangian unconformity varies. The tectonic subsidence curve for the southeastern Kola Monocline (Fig. 3.4J)

exhibits the most significant erosive episode (at least ~212–188 Ma), whereas the least significant erosional episode (~197 Ma) is observed in the Nordkapp Basin (Fig. 3.4E). Flat-curve trends in the above curves at times of significant water depth may represent periods of non-deposition instead of sub-aerial exposure and sediment bypass (Figs. 3.4C, E, F). In the northeastern Kola Monocline area (Fig. 3.4H), a non-flat trend is observed in the tectonic subsidence curve, reflecting gentle subsidence. However, Burguto et al. (2016) interpreted an unconformity in the well succession for this structural element that represents the removal of at least the entire Rhaetian succession. Because of the lack of curve horizontality, it is difficult to accurately illustrate the extent of this unconformity in the plot. Hence, the extension of the erosional event in this curve is speculative and based solely in their interpretation of the well. In the southeastern Kola Monocline (Fig. 3.4J), a flat tectonic subsidence curve and lack of water depth allows the interpretation of a widespread unconformity. Even though water depth is minimal, and the tectonic subsidence curve is horizontal (Fig. 3.4J), ongoing subsidence, as indicated by the total subsidence curve, may preclude interpretations of more extensive erosion.

The Fermanovskaya High area backstripping curve (Group 3; Fig. 3.4G; Table 3.6) represents continuous tectonic subsidence, which is followed by uplift at 222 Ma and renewed subsidence at 187 Ma. The main curve deflection (deflection 9) illustrates a clear convex geometry, thus indicating flexure (Figs. 3.3C, 3.4G). The overall tectonic mechanism is difficult to determine because of the overprinting event; however, a flexural mechanism is suggested by its convex geometry and the steepness of the curve. Moreover, lack of flat tectonic-subsidence trends does not allow for interpretation of a Rhaetian unconformity and/or non-deposition (Figs. 3.3C, 3.4G). However, like the northeastern

Kola Monocline (Fig. 3.4H), Burguto et al. (2016) interpreted an unconformity that removed at least the entire Rhaetian interval in the well succession for this structural element. Hence, inclusion and magnitude of the Rhaetian erosional event in this curve are speculative and based solely in their interpretation of the well. Interestingly, the overall geometry of the tectonic subsidence curve for the Fersmanovskaya High area evokes that of a broad, "bulge-like" geometry (Fig. 3.4G).

The South Barents Basin backstripping curve (Group 4; Fig. 3.4I; Table 3.6) represents a very short initial period of subsidence, followed by uplift at 232 Ma, and again by subsidence at ~218 Ma, creating a "bulge-like" geometry. Like previous curves, the uplift observed at ~232 Ma is indicative of overprint. Both deflection 11 and the broad, convex shape of the overall curve suggest a flexural tectonic mechanism. In contrast to other plots in Figure 3.4, an indication of renewed subsidence is present at ~218 Ma, and the steepness of the curve shows that subsidence gradually increased into Hettangian (~200 Ma) time and persisted during the entire Jurassic time range included in the plot (from ~201 to ~170 Ma). Like other RBSS locations, the ongoing subsidence observed in the curves makes it difficult to determine the possible presence and magnitude of the Rhaetian–Hettangian unconformity. Astafiev et al. (2008) interpreted an unconformity in the well succession for this structural element, but Rhaetian strata were not entirely eroded from the well succession. Hence, inclusion of the erosional event in this curve is speculative and based solely in their interpretation of the well.

3.5 Discussion

Interpretations regarding Triassic–Middle Jurassic BSS tectonostratigraphy need to consider interactions between the Uralian (at least latest Paleozoic)-Pai-Khoi (at least latest Paleozoic to Late Triassic)- Novaya Zemlya (at least Late Triassic) orogeny, the Permo-Triassic Siberian superplume, and Late Paleozoic North Atlantic rifting events (e. g., Timonin et al., 2003; Henriksen et al., 2011; Faleide et al., 2017). Of these events, the Uralian-Pai-Khoi-Novaya Zemlya orogeny is the least understood, which often leads to disagreements and contradictions in the literature (e.g., Scott et al., 2010; Filatova and Khain, 2010; Drachev, 2016; Zhang et al., 2018; Müller et al., 2019; Korago et al., 2022). Even though resolving the timing of the Novaya Zemlya orogeny is beyond the scope of this paper, the backstripping curves in Figure 3.4 may be of use in addressing future topics like this.

Observations and backstripping results will be discussed in terms of overall tectonic mechanisms and how these interpretations can be correlated to the large-scale, Triassic–Middle Jurassic, tectonic development of the southern BSS. Even though our approach focuses on tectonic responses interpreted from tectonic subsidence curves, it is important to emphasize that non-tectonic, Permo-Triassic uplift of eastern hinterland areas triggered by the Siberian Superplume enhanced the already ongoing erosion of the Uralides, thus significantly increasing the output of sediments into the BSS system (e.g., Fleming et al., 2016; Gilmullina et al., 2021b; Puchkov et al., 2021). Therefore, it is important to consider sedimentary weight as a contributing factor to the accentuated subsidence observed in various total subsidence curves (Fig. 3.4).

3.5.1 Tectonic mechanisms

Following the collapse of the Caledonides, proto-North Atlantic rifting systems triggered NBSS extensional episodes during Middle Carboniferous, Carboniferous–Permian, and Late Permian–earliest Triassic times (e.g., Faleide et al., 2008; Blaich et al., 2017). Moreover, Caledonian collapse and lithospheric unloading may have triggered flexural responses during extension (e.g., Weissel and Karner, 1989). Hence, transtensional/extensional and flexural mechanisms interpreted from the Hammerfest Basin and Loppa High curves (Group 1; Figs. 3.1, 3.4A, B; Table 3.6) can be tied to these NBSS extensional episodes. Even though Late Permian–earliest Triassic tectonism is suggested to have been mainly concentrated at the Loppa High (e.g., Blaich et al., 2017), the Hammerfest Basin had a phase of Carboniferous extension and widespread Late Paleozoic sedimentation (Blaich et al., 2017; Henriksen et al., 2021). Hence, combination of extension, possible far-field reactivation of earlier extensional structures, and sedimentary accumulation can explain the abrupt and extensive subsidence observed in these curves (Figs. 3.4A, B).

Traditionally, tectonic-curve geometries showing brief, very rapid subsidence are indicative of transtension (Kneller, 1991; Xie and Heller, 2009) (Fig. 3.3C). Because the sharp curve "rebound," which may represent overprint (Figs. 3.4A, B), it is not possible to clearly determine if either transtension or extension occurred in the Hammerfest Basin and Loppa High area. Nevertheless, because of Caledonian collapse and proto-North Atlantic tectonic processes across at least western areas of the BSS (e.g., Faleide et al., 2008; Blaich et al., 2017), the possibility of extensional or transtensional mechanisms is feasible.

In the western and eastern Bjarmeland platforms, Nordkapp Basin, northeastern Finnmark Platform, and Kola Monocline area (Group 2; Figs. 3.1, 3.4C, D, E, F, H, J; Table 3.6), interpretations are tied to two distinct tectonic settings. In the NBSS, rapid Early Triassic to slow Middle Triassic tectonic subsidence (Figs. 3.4C, D, E, F) can be explained by Late Permian–earliest Triassic rifting, reactivation of Caledonian-age structures, and further thermal sag processes (e.g., Gernigon et al., 2014; Gabrielsen et al., 2016). In the RBSS, non-fault related subsidence triggered by phase changes in igneous bodies coeval to orogeny, has been suggested (e.g., Ritzmann and Faleide, 2009; Gac et al., 2014). This process was not restricted to the BSS, being well-known in the Appalachian area to represent intracratonic subsidence associated with the reactivation of earlier rift structures by Appalachian orogenies (e.g., Quinlan and Beaumont, 1984; de Klein and Hsui, 1987). According to Xie and Heller (2009), intracratonic backstripping geometries are very similar to those resulting from rifting. Similarly, Early–Middle Triassic tectonic mechanisms inferred from Figs. 3.4H and J are interpreted to represent intracratonic subsidence triggered earlier by the Uralian orogeny. This interpretation aligns with the reactivation of RBSS Devonian back-arc/extensional structures, rapid Permo-Triassic subsidence, and coeval Permo-Triassic Uralian stresses (e.g., Nikishin et al., 1996; Gac et al., 2016; Faleide et al., 2017).

In the Fersmanovskaya High area (Group 3; Fig. 3.4G; Table 3.6), though flexure is suggested, interpreting the tectonic mechanism is difficult because of abrupt uplift and overprint at approximately 222 Ma. However, in Group 4 (Table 3.6; Fig. 3.4I; Table 3.6), even though limited drilling depth precludes interpretation of tectonic mechanisms prior to Late Triassic time, the flexural mechanisms observed at ~218 Ma align with studies that

suggested the development of a foreland basin at this location (e.g., Petrov et al., 2008; Müller et al., 2019; Martins et al., 2022).

In plots 4A, B, F, H, and J, minor, short-lived tectonic-curve deflections representing "uplift" can be observed during Early to Middle Triassic time. In the Timan-Pechora Basin (Fig. 3.1), Lobkovsky et al. (1996) interpreted similar backstripping curve geometries to represent inversion events triggered by the propagation of Carboniferous–early Mesozoic Uralian compressional stresses, which overprinted coeval post-rift, post-Devonian, subsidence mechanisms in that basin. Though interpretations like those by Lobkovsky et al. (1996) are certainly feasible across the BSS (Martins et al., 2022), lack of Paleozoic deposits in most of BSS wells makes it difficult to confidently associate the observed minor Early to early-Middle Triassic deflections to Uralian compressional stresses or to distortions caused by minor local variation in sedimentary content (Tables 3.3 and 3.4) instead. To better understand the propagation of Uralian compressional stresses would require a much larger regional analysis, including basins across the entire Uralide belt, which is well beyond the scope of this study. However, the possibility of propagation of compressional stresses and overlapping with post-rifting or intracratonic subsidence in BSS basins should not be ignored.

3.5.2 Structural trends

The overall trends exhibited in the tectonic subsidence curves were simplified and transposed to a highly schematic map that allows comparison of all trends in space and time (Fig. 3.5). Using arrows to represent structural responses, the length of each arrow represents the approximate time duration of each major backstripping trend, up-or-down

arrows represent uplift or subsidence respectively, and the shapes of arrow heads reflect schematic trend magnitudes. Columns without arrowheads represent flat/near-flat curve geometries, which are interpreted as structural stability. In Figure 3.5, the green areas represent areas of major Late Paleozoic North Atlantic rifting (Gabrielsen et al., 2016), whereas the light red area represents major Permo-Triassic intracratonic subsidence (Gac et al., 2013). The timing of Novaya Zemlya orogeny is considered to be at least Late Triassic (reddish arrow). In Figure 3.5, Early–Middle Triassic widespread subsidence is reversed by Late Triassic uplift. During latest Triassic–Middle Jurassic time, most elements either show subsidence or stability. All these trends were then transposed to a series of highly schematic maps (Fig. 3.6), which are discussed in the next section.

3.5.3 Basin development

Early–Middle Triassic subsidence across the BSS (e.g., Henriksen et al., 2011; Figs. 3.4, 3.5, and 3.6A, B) was accompanied by widespread progradation across the shelf during this period, which has been interpreted to reflect the generation of more accommodation space (e.g., Fleming et al., 2016; Figs. 3.4 and 3.6). This sedimentary progradation was most likely the result of widespread uplift of eastern hinterland areas by the Siberian superplume (Gilmullina et al., 2021a, 2021b; Fig. 3.6A), which enhanced ongoing erosion and contributed to the progradation. The shift from rapid Early Triassic subsidence to decreasing rates of Middle Triassic subsidence, followed by abrupt Late Triassic uplift (Figs. 3.4, 3.5, and 3.6), aligns with studies that show varying rates of sediment supply through Triassic time (e.g., Gilmullina et al., 2021b). The abrupt uplift, recognized as early as ~232 Ma (Fig. 3.4) and the only tectonic event capable of triggering such regional uplift,

is the Novaya Zemlya orogeny (Figs. 3.5, and 3.6C). This idea that uplift was related to orogeny agrees with studies that indicate a Late Triassic orogenic timing (e.g., Drachev, 2016). Subtle latest Triassic–earliest Jurassic curve trends (e.g., Fig. 3.4D) can also be associated with this orogeny. In the Hammerfest Basin and Loppa High (Figs. 3.4A, B), however, the interpretation of Late Triassic orogenic uplift contradicts traditional interpretations (e.g., Henriksen et al., 2011; Indrevær et al., 2017); hence, more studies are needed to investigate the nature of the potential uplift suggested in the backstripping curves for these areas. The Novaya Zemlya orogeny has also been interpreted as the main cause for the generation of the Rhaetian–Hettangian unconformity (Müller et al., 2019). In the eastern Bjarmland and northeastern Finnmark platforms, and Kola Monocline area (Figs. 3.4D, F, H, J), the magnitude of this erosional event is like magnitudes presented by Müller et al. (2019) and Gilmullina et al. (2021a).

The backstripping curve trends from latest Permian–Middle Triassic time and comparison with the literature suggest that the NBSS was dominated by basin-development mechanisms associated with rifting and thermal-sag processes; in contrast, the RBSS reflects intracratonic subsidence triggered by compressional far-field forces at the same time (Figs. 3.4, 3.5 and 3.6). Moreover, during Late Triassic time, flexural subsidence in the South Barents Basin (Fig. 3.4I) and coeval, abrupt, uplift in the Fersmanovskaya High area (Fig. 3.4G) suggest the development of a foreland-basin system across these structural elements (Fig. 3.6C, D), in agreement with previous studies (e.g., Petrov et al., 2008; Müller et al., 2019). In addition, the total subsidence curve in Figure 3.4I indicates subsidence of ~1.1 km from ~218 to 170 Ma, which is on the same order as foreland thicknesses estimated by Suslova (2014) and Gilmullina et al. (2021a). During latest

Triassic–Middle Jurassic time, uplift and subsidence trends can be tied to Novaya Zemlya thrusting, as well as coeval development of foreland basins and intracratonic reactivation (Figs. 3.5 and 3.6). In the NBSS (Figs. 3.4A–F, 3.5 and 3.6), it is not clear if Late Triassic uplift represents bulge deflection (Müller et al., 2019), or if the bulge is restricted to the transitional NBSS/RBSS area (Olaussen et al., 2018). However, like Olaussen et al. (2018), we suggest that the transitional BSS area represents bulge uplift, whereas central-western NBSS uplift represents back-bulge structural readjustment to Novaya Zemlya compression. Clearly, more studies covering other methodologies are needed.

3.6 Conclusions

Understanding structural responses in the hydrocarbon-rich, Triassic–Middle Jurassic succession across the BSS requires more consideration of large-scale, diverse, tectonic triggers and the related reactivation of BSS structures. Thus, the integration of individual structural responses to regional events is important, and the backstripping method provides a means of modelling such responses and their timing. This backstripping treatment of BSS well data allows for the interpretation of low- and high-resolution tectonic mechanisms, as well as for trends of subsidence and uplift, which can be tied to the major BSS tectonostratigraphic events and to other BSS studies. Backstripping curves for ten, distinct, southern, BSS structural elements provide evidence of structural reactivation triggered largely by Uralian-Pai-Khoi- Novaya Zemlya and North Atlantic tectonism. Differences in the timing and type of structural response across the BSS likely reflect the geologic properties and stress regimes under which each specific BSS structure formed. These observations suggest that, despite similar triggers, BSS structural features often

responded independently. Even though tectonic overprint is a possible complicating factor, most Late Triassic uplift can be tied confidently to the later phases of the Uralian- Pai-Khoi-Novaya Zemlya orogeny.

In summary, this backstripping analysis illustrates the diverse nature and activity of southern BSS, Triassic–Middle Jurassic structural responses and tectonic mechanisms, as well as the likely tectonic triggering events. Moreover, the study shows that despite location, subsidence predominated across the southern BSS during Early–Middle Triassic time, followed largely by uplift in Late Triassic time, and subsequently by subsidence in Jurassic time. Even though many questions remain, and other analytical techniques need consideration, these results align with previous studies, which suggest that southern BSS structures were much more affected by Novaya Zemlya compressional tectonism than often assumed. Similar patterns and activity are likely in northern parts of the shelf, but confirmation must await more evidence.

Table 3.1. General information for wells from the NBSS and RBSS used in this study. The following are NBSS formations: Ha = Havert; Kl = Klappmyss; Ko = Kobbe; Sn = Snadd; Fr = Fruholmen; Tu = Tubåen; No = Nordmela; and St = Stø. The following are RBSS stages: O=Olenekian; A = Anisian; L = Ladinian; C = Carnian; N = Norian; C–N = Carnian–Norian; R = Rhaetian; H–T = Hettangian–Toarcian; P–T = Pliensbachian–Toarcian; and A–B = Aalenian–Bathonian.

Well	Location	Total Thickness (m)	Individual thicknesses (m)	Oldest target strata	Youngest target strata	Considered Datum
7120/1-1	Loppa High/NBSS	1711	Ha = 30; Kl = 58; Ko = 30; Sn = 1179; and Fr = 414	Havert Fm. (Induan)	Fruholmen Fm. (Norian–Rhaetian)	Ørret Fm. (Permian)
7120/9-2	Hammerfest Basin/NBSS	2985	Ha = 150; Kl = 561; Ko = 283; Sn = 1410; Fr = 262; Tu = 134; No = 108; and St = 77	Havert Fm. (Induan)	Stø _Fm. (late Pliensbachian–Bajocian)	Røye Fm. (Permian)
7224/2-1	western Bjarmeland Platform/NBSS	2049.49	Kl = 477.5; Ko = 536.5; Sn = 935.14; Fr = 77.88; No = 15; and St = 25	Klappmyss Fm. (Olenekian)	Stø _Fm. (late Pliensbachian–Bajocian)	Havert Fm. (Induan)
7228/2-1 S	Nordkapp Basin/NBSS	2437	Kl = 363; Ko = 969; Sn = 858; Fr = 119;	Klappmyss Fm. (Olenekian)	Stø _Fm. (late Pliensbachian–Bajocian)	Havert Fm. (Induan)

Well	Location	Total Thickness (m)	Individual thicknesses (m)	Oldest target strata	Youngest target strata	Considered Datum
			Tu = 58; No = 46; and St = 24			
7229/11-1	northeastern Finnmark Platform/NBSS	2610	Ha = 1075; Kl = 451; Ko = 511; Sn = 389; Fr = 131; No = 44; and St = 9	Havert Fm. (Induan)	Stø _Fm. (late Pliensbachian–Bajocian)	Ørret Fm. (Permian)
7335/3-1	eastern Bjarmeland Platform/ NBSS	1691	Kl = 650; Ko = 456; Sn = 361; Fr = 136; Tu = 21; No = 64; and St = 3	Klappmyss Fm. (Olenekian)	Stø _Fm. (late Pliensbachian–Bajocian)	Havert Fm. (Induan)
Fersmanovskaya-1	Fermanovskaya High area/ RBSS	1536	A = 143; L = 409; C–*N* = 621; H–*T* = 124; and A–B = 239	Anisian	Aalenian–Bajocian	Olenekian
Severo-Kildinskaya-80	northwestern Kola Monocline area (West Kola Saddle)/ RBSS	1709	O = 429; A = 477; L = 202; C = 265; *N* = 57; H–*T* = 103; and A–B = 176	Olenekian	Aalenian–Bajocian	Induan

Well	Location	Total Thickness (m)	Individual thicknesses (m)	Oldest target strata	Youngest target strata	Considered Datum
Arkticheskaya-1	South Barents Basin/RBSS	1684	C = 425; *N* = 229; *R* = 269; H–*T* = 402; and A–B = 359	Carnian	Aalenian–Bajocian	Ladinian
Murmanskaya-24	southeastern Kola Monocline area /RBSS	1454	A = 246; L = 157; C–*N* = 416; P–*T* = 287; and A–B = 348	Anisian	Aalenian–Bathonian	Olenekian

Table 3.2. General parameters used for calculating average grain densities, average porosities-at-surface, and average compaction coefficients.

General parameters			
Lithology	Grain density (kg/m□ _3)	Porosity-at-surface	Compaction coefficient
Claystones	2720	0.63	0.51
Siltstones	2720	0.63	0.51
Sandstones	2650	0.49	0.2
Limestones	2710	0.513	0.518
Mantle density (kg/m□ _3)		Water density (kg/m□ _3)	
3330		1030	

Table 3.3. General parameters used in NBSS calculations. Average grain densities, porosities-at-surface and compaction coefficients are from Table 3.2.

Norwegian Barents Sea shelf (NPD, 2022)						
Well number	Target formation	Mean age (Ma)	Lithology	Grain density (kg/m^{-3})	Porosity-at-surface	Compaction coefficient
7120/1-1 (Loppa High)	Havert	250.651	Siltstones (3%) and sandstones (97%)	2652	0.49	0.209
	Klappmyss	248.3	Claystones/siltstones (100%)	2720	0.63	0.51
	Kobbe	244.6	Claystones/siltstones (98%) and sandstones (2%)	2718	0.63	0.503
	Snadd	232.65	Claystones/siltstones (97%) and sandstones (3%) and limestones (<0.5%)	2717	0.62	0.5
	Fruholmen	215.4	Claystones/siltstones (89%) and sandstones (10%) and limestones (1%)	2712	0.61	0.479
7120/9-2 (Hammerfest Basin)	Havert	250.651	Claystones/siltstones (100%)	2720	0.63	0.51
	Klappmyss	248.3	Claystones/siltstones (100%)	2720	0.63	0.51

Norwegian Barents Sea shelf (NPD, 2022)						
	Kobbe	244.6	Claystones/siltstones (92%), and sandstones (8%)	2714	0.62	0.485
	Snadd	232.65	Claystones/siltstones (70%), sandstones (30%), limestones (<0.01%)	2699	0.58	0.417
	Fruholmen	215.4	Claystones/siltstones (25%) and sandstones (75%)	2667	0.52	0.277
	Tubåen	199.87	Siltstones (5%) and sandstones (95%)	2653	0.5	0.215
	Nordmela	187.12	Siltstones (7%) and sandstones (93%)	2654	0.5	0.221
	Stø	176	Siltstones (3%) and sandstones (97%)	2652	0.49	0.209
7224/2-1 (western Bjarmeland Platform)	Klappmyss	248.3	Claystones/siltstones (97%) and sandstones (3%) and limestones (<0.5%)	2717	0.62	0.5
	Kobbe	244.6	Claystones/siltstones (87%) and sandstones (11%) and limestones (2%)	2712	0.61	0.476
	Snadd	232.65	Claystones/siltstones (72%) and	2702	0.59	0.435

Norwegian Barents Sea shelf (NPD, 2022)						
			sandstones (24%) and limestones (4%)			
	Fruholmen	215.4	Claystones/siltstones (72%) and sandstones (18%) and limestones (10%)	2706	0.59	0.455
	Nordmela	187.12	Claystones/siltstones (10%) and limestones (90%)	2711	0.52	0.517
	Stø	176	Sandstones (100%)	2650	0.49	0.2
7228/2-1 S (Nordkapp Basin)	Klappmyss	248.3	Claystones/siltstones (98%) and sandstones (2%)	2718	0.63	0.503
	Kobbe	244.6	Claystones/siltstones (80%) and sandstones (20%)	2706	0.6	0.448
	Snadd	232.65	Claystones/siltstones (52%) and sandstones (48%)	2686	0.56	0.361
	Fruholmen	215.4	Claystones/siltstones (75%) and sandstones (25%)	2702	0.59	0.432
	Tubåen	199.87	Claystones/siltstones (10%) and sandstones (90%)	2657	0.50	0.231

Norwegian Barents Sea shelf (NPD, 2022)						
	Nordmela	187.12	Siltstones (5%) and sandstones (95%)	2653	0.5	0.215
	Stø	176	Siltstones (60%) and sandstones (40%)	2692	0.57	0.386
7229/11-1 (northeastern Finnmark Platform)	Havert	250.651	Claystones/siltstones (80%) and sandstones (20%)	2706	0.6	0.448
	Klappmyss	248.3	Claystones/siltstones (85%) and sandstones (15%)	2710	0.61	0.463
	Kobbe	244.6	Claystones/siltstones (95%) and sandstones (5%)	2716	0.62	0.494
	Snadd	232.65	Claystones/siltstones (80%) and sandstones (20%)	2706	0.6	0.448
	Fruholmen	215.4	Claystones/siltstones (50%) and sandstones (50%)	2685	0.56	0.355
	Nordmela	187.12	Claystones/siltstones (20%) and sandstones (80%)	2664	0.52	0.262
	Stø	176	Claystones/siltstones (10%) and sandstones (90%)	2657	0.50	0.231

Norwegian Barents Sea shelf (NPD, 2022)						
7335/3-1 (eastern Bjarmeland Platform)	Klappmyss	248.3	Claystones/siltstones (85%) and sandstones (15%)	2710	0.61	0.463
	Kobbe	244.6	Claystones/siltstones (90%) and sandstones (10%)	2713	0.62	0.479
	Snadd	232.65	Claystones/siltstones (73%) and sandstones (27%)	2701	0.59	0.426
	Fruholmen	215.4	Claystones/siltstones (42%) and sandstones (58%)	2679	0.55	0.330
	Tubåen	199.87	Sandstones (100%)	2650	0.49	0.2
	Nordmela	187.12	Claystones/siltstones (50%) and sandstones (50%)	2685	0.56	0.355
	Stø	176	Sandstones (100%)	2650	0.49	0.2

Table 3.4. General parameters used in RBSS calculations. Average grain densities, porosities-at-surface and compaction coefficients are from Table 3.2.

Russian Barents Sea shelf (Astafiev et al., 2008; Burguto et al., 2016)						
Well	Target sedimentary unit	Mean age (Ma)	Main lithology	Grain density (kg/m^{-3})	Porosity-at-surface	Compaction coefficient
Fersmanovskaya-1	Anisian	244.6	Claystones/siltstones (66%) and sandstones (34%)	2696	0.58	0.404
	Ladinian	239.5	Claystones/siltstones (80%) and sandstones (20%)	2706	0.60	0.448
	Carnian–Norian	222.75	Claystones/siltstones (66%) and sandstones (34%)	2696	0.58	0.404
	Hettangian–Toarcian	187.7	Claystones/siltstones (34%) and sandstones (66%)	2673	0.54	0.305
	Aalenian–Bathonian	171.2	Claystones/siltstones (34%) and sandstones (66%)	2673	0.54	0.305
Severo-Kildinskaya-80	Olenekian	249.2	Claystones/siltstones (80%) and sandstones (20%)	2706	0.60	0.448
	Anisian	244.6	Claystones/siltstones (80%) and sandstones (20%)	2706	0.60	0.448
	Ladinian	239.5	Claystones/siltstones (66%)	2696	0.58	0.404

Russian Barents Sea shelf (Astafiev et al., 2008; Burguto et al., 2016)						
			and sandstones (34%)			
	Carnian	232	Claystones/siltstones (75%) and sandstones (25%)	2702	0.59	0.432
	Norian	217.75	Siltstones (90%) and sandstones (10%)	2713	0.62	0.479
	Hettangian–Toarcian	187.7	Claystones/siltstones (20%) and sandstones (80%)	2664	0.51	0.262
	Aalenian–Bathonian	171.2	Claystones/siltstones (20%) and sandstones (80%)	2664	0.51	0.262
Arkticheskaya -1	Carnian	232	Claystones/siltstones (65%) and sandstones (35%)	2695	0.58	0.401
	Norian	217.75	Claystones/siltstones (66%) and sandstones (34%)	2696	0.58	0.404
	Rhaetian	204.9	Claystones/siltstones (60%) and sandstones (40%)	2692	0.57	0.386
	Hettangian–Toarcian	187.7	Claystones/siltstones (50%) and sandstones (50%)	2685	0.56	0.355
	Aalenian–Bathonian	171.2	Claystones/siltstones (66%)	2696	0.58	0.404

Russian Barents Sea shelf (Astafiev et al., 2008; Burguto et al., 2016)						
			and sandstones (34%)			
Murmanskaya -24	Anisian	244.6	Claystones/silt stones (100%)	2720	0.63	0.51
	Ladinian	239.5	Claystones/silt stones (80%) and sandstones (20%)	2706	0.60	0.448
	Carnian–Norian	222.75	Claystones/silt stones (66%) and sandstones (34%)	2696	0.58	0.404
	Pliensbachian–Toarcian	182.45	Claystones/silt stones (60%) and sandstones (40%)	2692	0.57	0.386
	Aalenian–Bathocian	171.2	Claystones/silt stones (30%) and sandstones (70%)	2671	0.53	0.293

Table 3.5. Main backstripping equations.

Main Backstripping equations			
Equation 1	Equation 2	Equation 3	Equation 4
$\Phi = \Phi_0 e(-cy')$	$S_d = S_i(1-\Phi_c)/(1-\Phi_0)$	$\rho_b = \Sigma_i\{[\Phi_i \rho_w + (1-\Phi_i) \rho_{sg}]/S\} y'_i$	$Y = S[(\rho_m - \rho_b)/(\rho_m - \rho_w)]$

Variables:

1) Φ = variation of porosity as a function of depth; Φ_0 = surface porosity; c = compaction coefficient; y' = depth of layer

2) S_d = decompacted thickness; S_i = compacted thickness; Φ_c = compacted porosity; Φ_0 = surface porosity

3) ρ_b = bulk density of the entire sedimentary column; Φ_i = mean porosity of the ith layer; ρ_{sg} = grain density of the same layer; S = total thickness of the column corrected for compaction; y' = thickness of the ith sediment layer

4) Y = depth of the basement corrected for sediment load; S = total thickness of the column corrected for compaction; ρ_m = mantle density; ρ_b = bulk density of the entire sedimentary column; ρ_w = water density

Table 3.6. Analyzed structural elements grouped by geometrical similarity, as well as by associated deflections and their characteristics.

Location	Group	Deflection	Approximate Age (Stage)	Duration (~Ma)	Subsidence (km)	Tectonic mechanism
HB	1	1	Induan–Olenekian	2	0.61	F
HB	1	2	Anisian–Carnian	12	1.09	Te?/E?
LH	1	3	Anisian–Carnian	12	1.24	Te?/E?
WBP	2	4	Olenekian–Carnian	18	1.29	E
EBP	2	5	Induan–Carnian	18	0.87	E
EBP	2	6	Hettangian–Pliensbachian	13	0.05	F
NB	2	7	Induan–Carnian	18	1.34	E
NFP	2	8	Wuchiapingian–Carnian	22	1.24	E
FH	3	9	Olenekian–Norian	26	0.89	F
NKMA	2	10	Induan–Carnian	20	0.78	E
SBB	4	11	Norian–Pliensbachian	30	0.81	F
SKMA	2	12	Olenekian–Norian	26	0.63	E
Standard Deviation						

Locality	Mean (Tes Mean; Tos Mean)	Standard Deviation (Tes SD; Tos SD)	Coefficient of variation (Tes SD/ Tes Mean; Tos SD; Tos Mean)
HB	0.898; 2.089	0.527; 1.312	0.586; 0.628
LH	0.412; 0.781	0.561; 1.085	1.361; 1.389
WBP	0.815; 1.599	0.411; 0.847	0.504; 0.529
EBP	0.728; 1.378	0.296; 0.576	0.406; 0.417
NB	0.914; 1.955	0.433; 0.972	0.473; 0.497
NFP	1.001; 2.185	0.413; 0.912	0.412; 0.417
FH	0.517; 0.972	0.353; 0.698	0.682; 0.718
NKMA	0.629; 1.209	0.274; 0.559	0.435; 0.462
SBB	0.562; 1.114	0.328; 0.703	0.583; 0.631
SKMA	0.462; 0.862	0.292; 0.590	0.632; 0.684

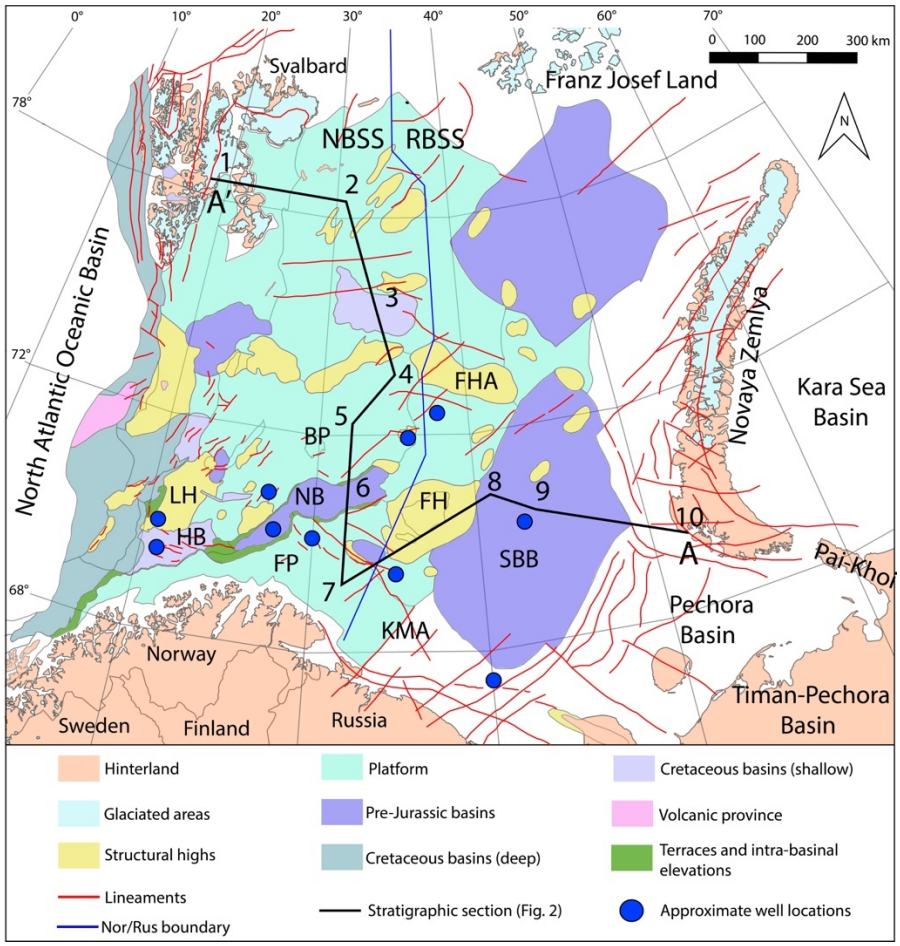

Figure 3.1. Main BSS structural elements. HB = Hammerfest Basin; LH = Loppa High; BP = Bjarmeland Platform; NB = Nordkapp Basin; FP = Finnmark Platform; FHA = Fersmanovskaya High area; FH = Fedynsky High; KMA = Kola Monocline area; and SBB = South Barents Basin (modified from Martins et al., 2022).

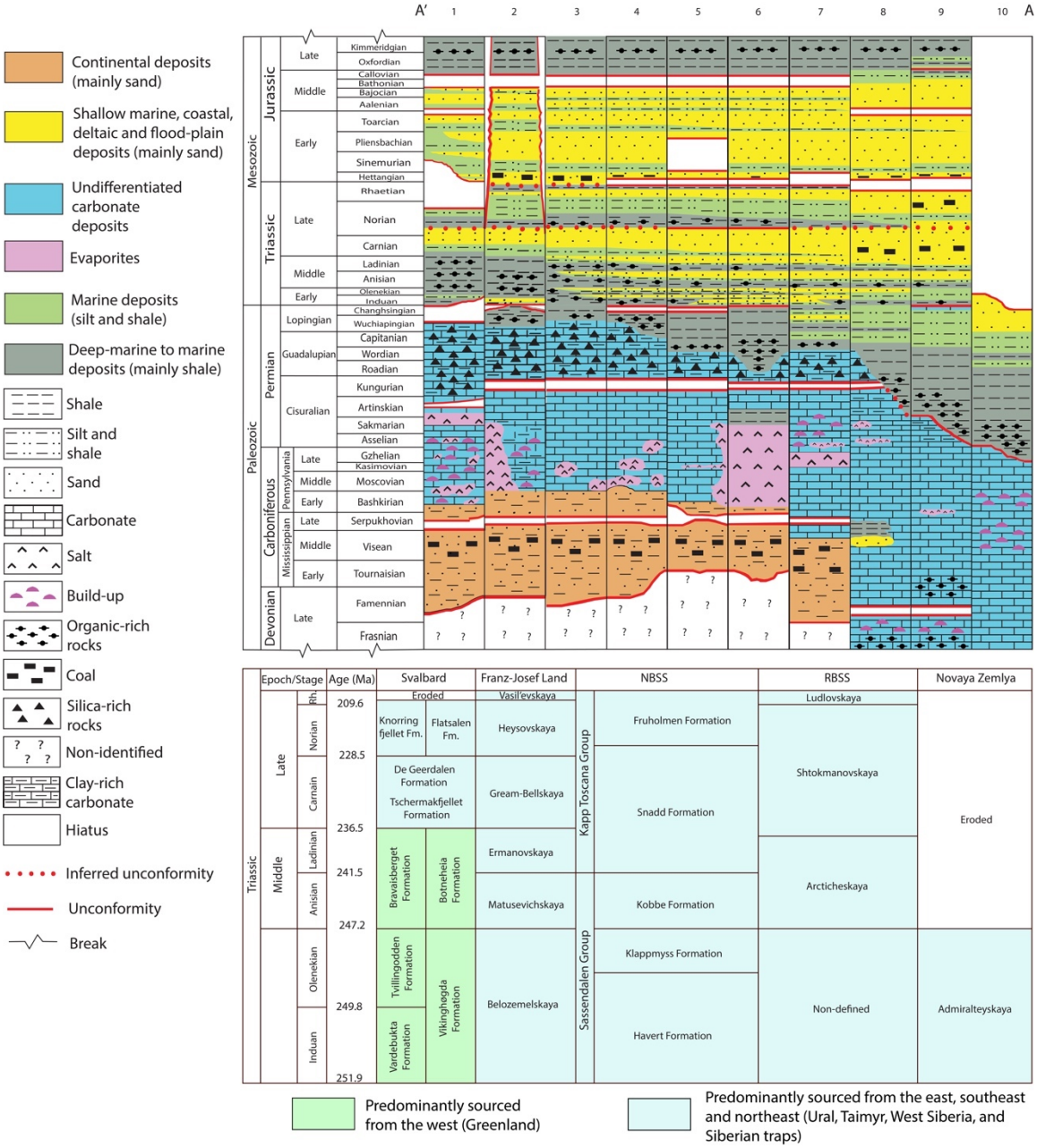

Figure 3.2. Top figure—Cross section schematically illustrating Upper Devonian–Late Jurassic strata across Svalbard (column 1), NBSS (columns 2–7), RBSS (columns 8–9); and Novaya Zemlya (column 10) (modified from Martins et al., 2022). Bottom figure—Simplified stratigraphic correlation for Triassic units across Svalbard, Franz Josef Land, NBSS, RBSS, and Novaya Zemlya (modified from Gilmullina et al., 2021).

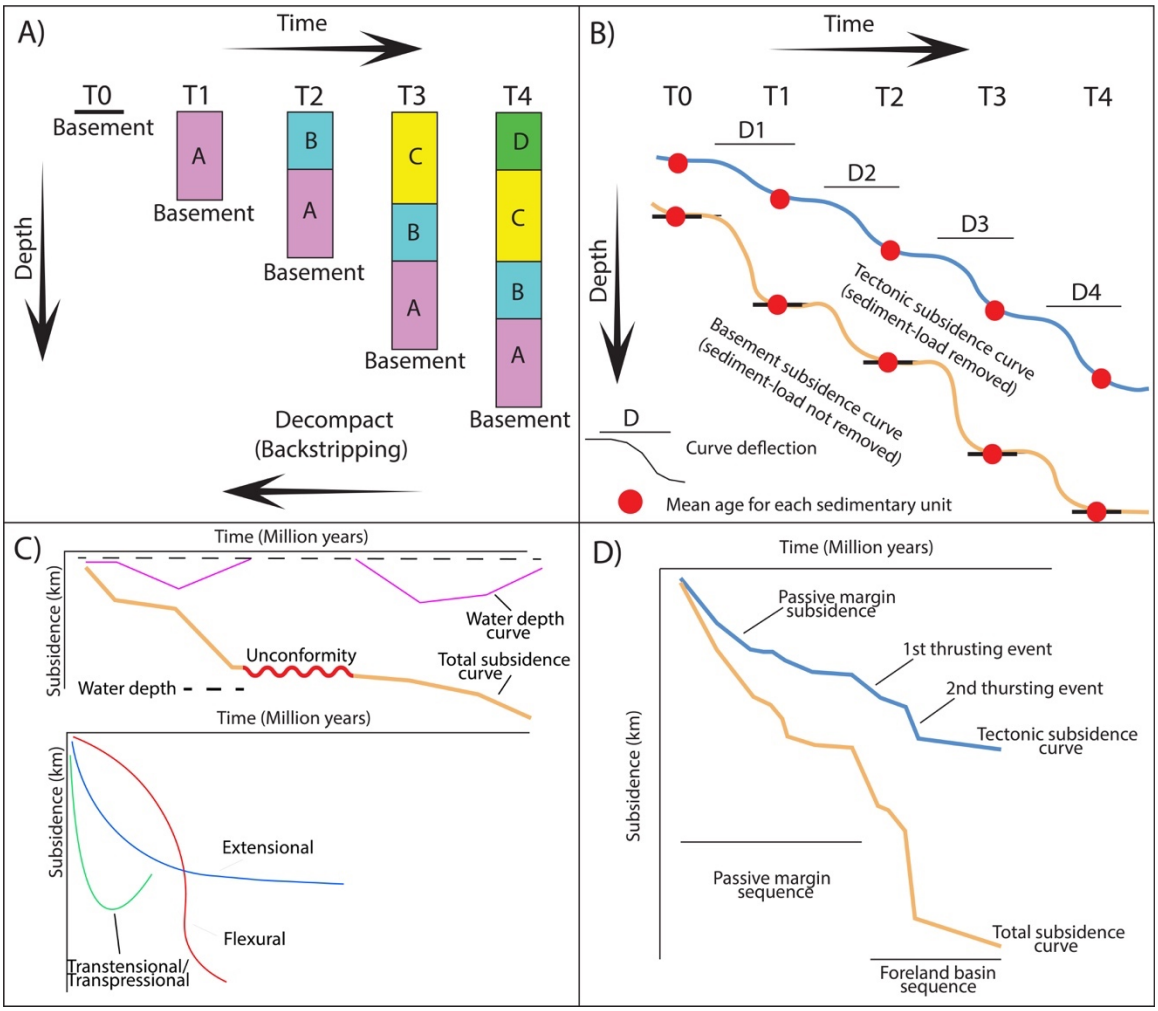

Figure 3.3. Basic concepts and outputs of the backstripping method (modified from Angevine et al., 1990; Kneller, 1991; Roberts et al., 1998; and Watts, 2012). A) Each sedimentary unit is removed from the most recent (Time 4; T4) to the oldest stratum (Time 0; T0). B) Vertical movement of the datum in time after the sedimentary load is progressively removed. C) Backstripping elements for tectonostratigraphic interpretation (modified from Angevine et al., 1990; and Kneller, 1991). D) Example of high-resolution interpretation (modified from Watts, 2012).

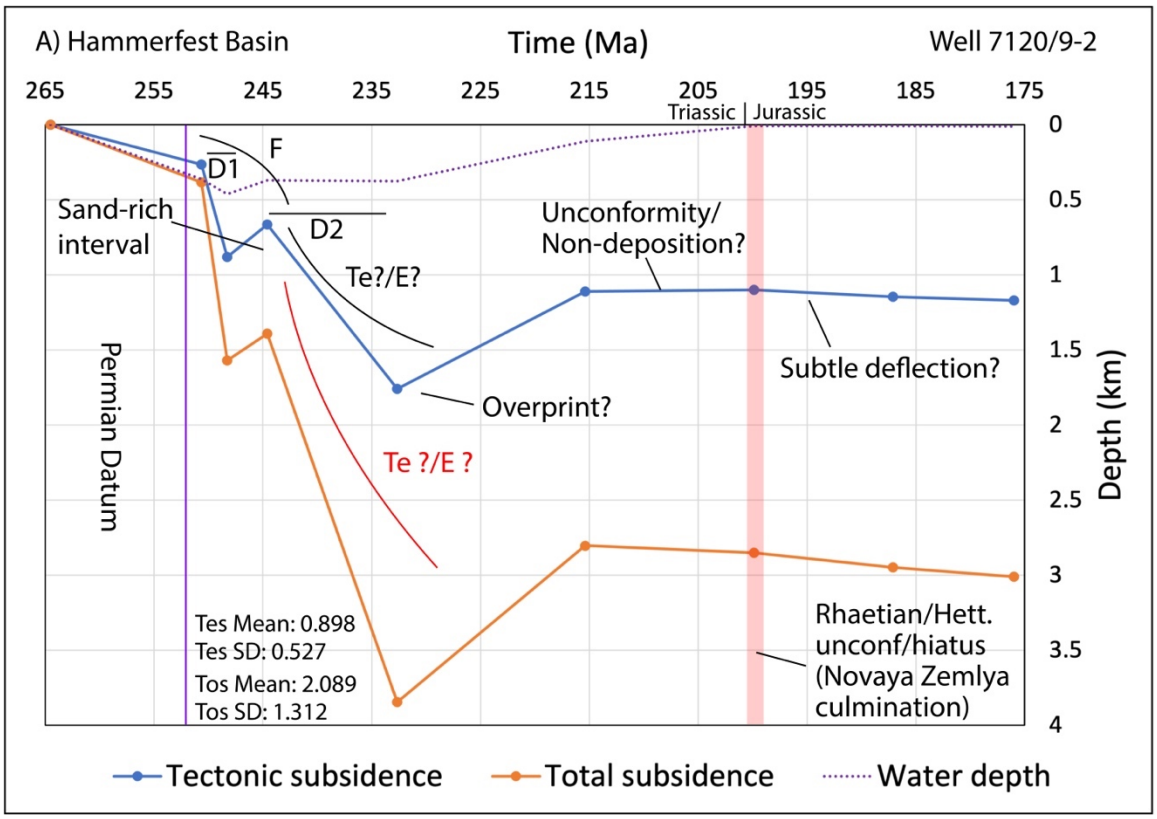
A) Hammerfest Basin
Time (Ma)
Well 7120/9-2
265
255
245
235
225
215
205
195
185
175
Triassic | Jurassic
0
0.5
1
1.5
2
2.5
3
3.5
4
Depth (km)
D1
F
D2
Sand-rich interval
Te?/E?
Unconformity/ Non-deposition?
Subtle deflection?
Overprint?
Te ?/E ?
Permian Datum
Tes Mean: 0.898
Tes SD: 0.527
Tos Mean: 2.089
Tos SD: 1.312
Rhaetian/Hett. unconf/hiatus (Novaya Zemlya culmination)
Tectonic subsidence
Total subsidence
Water depth

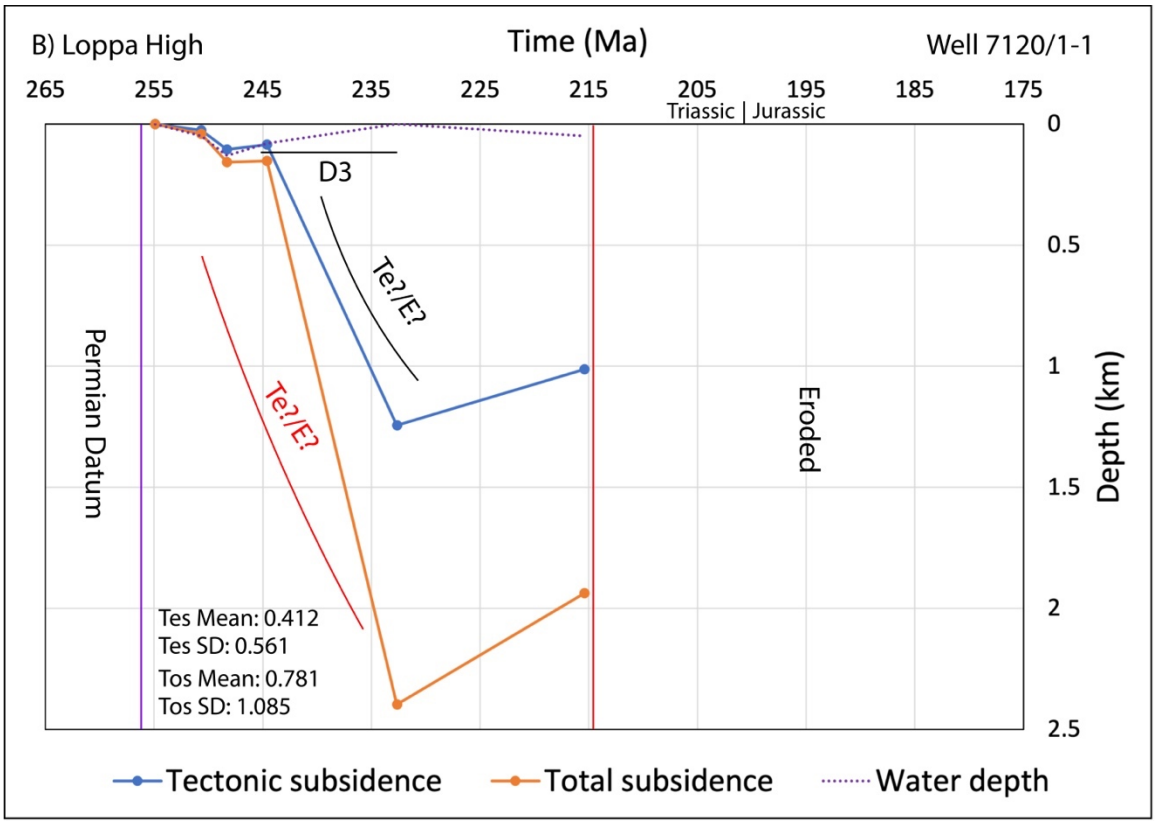
B) Loppa High
Time (Ma)
Well 7120/1-1
265
255
245
235
225
215
205
195
185
175
Triassic | Jurassic
0
0.5
1
1.5
2
2.5
Depth (km)
D3
Te?/E?
Te?/E?
Permian Datum
Eroded
Tes Mean: 0.412
Tes SD: 0.561
Tos Mean: 0.781
Tos SD: 1.085
Tectonic subsidence
Total subsidence
Water depth

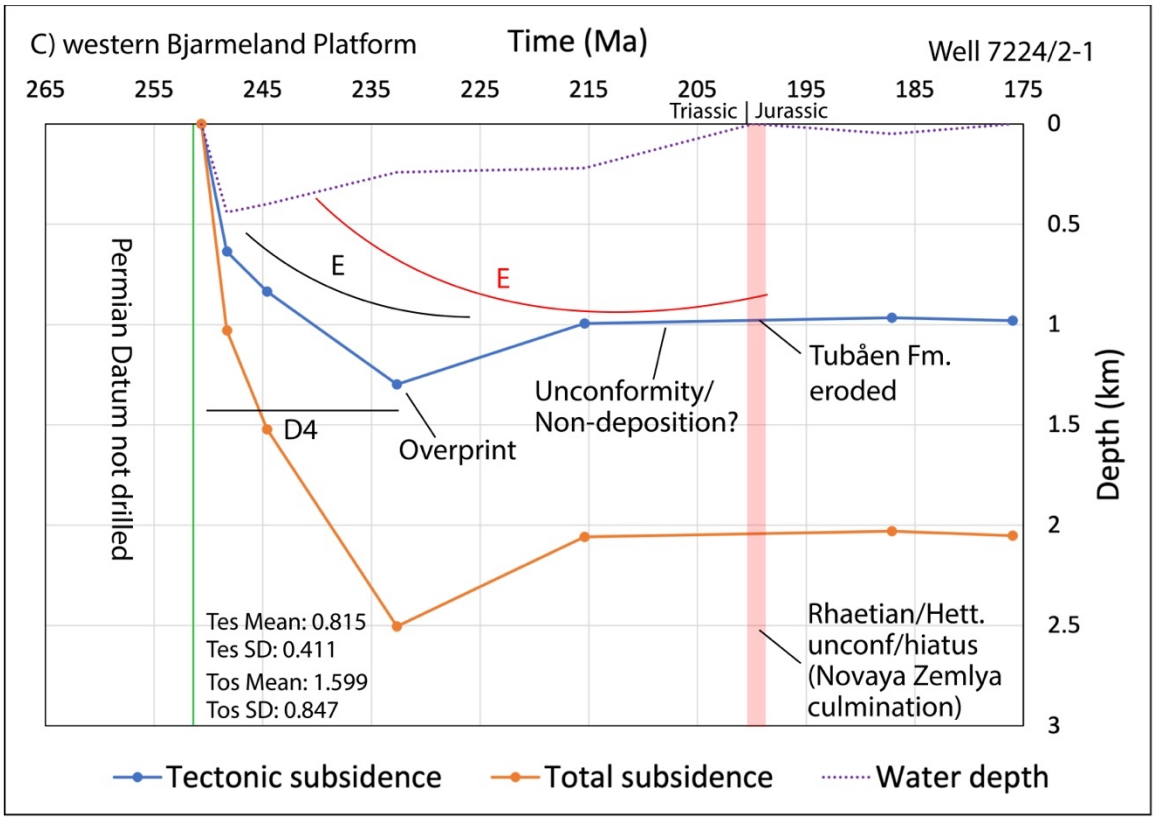
C) western Bjarmeland Platform
Time (Ma)
Well 7224/2-1
265
255
245
235
225
215
205
195
185
175
Triassic | Jurassic
0
0.5
1
1.5
2
2.5
3
Depth (km)
Permian Datum not drilled
E
E
D4
Overprint
Unconformity/
Non-deposition?
Tubåen Fm.
eroded
Tes Mean: 0.815
Tes SD: 0.411
Tos Mean: 1.599
Tos SD: 0.847
Rhaetian/Hett.
unconf/hiatus
(Novaya Zemlya
culmination)
Tectonic subsidence
Total subsidence
Water depth

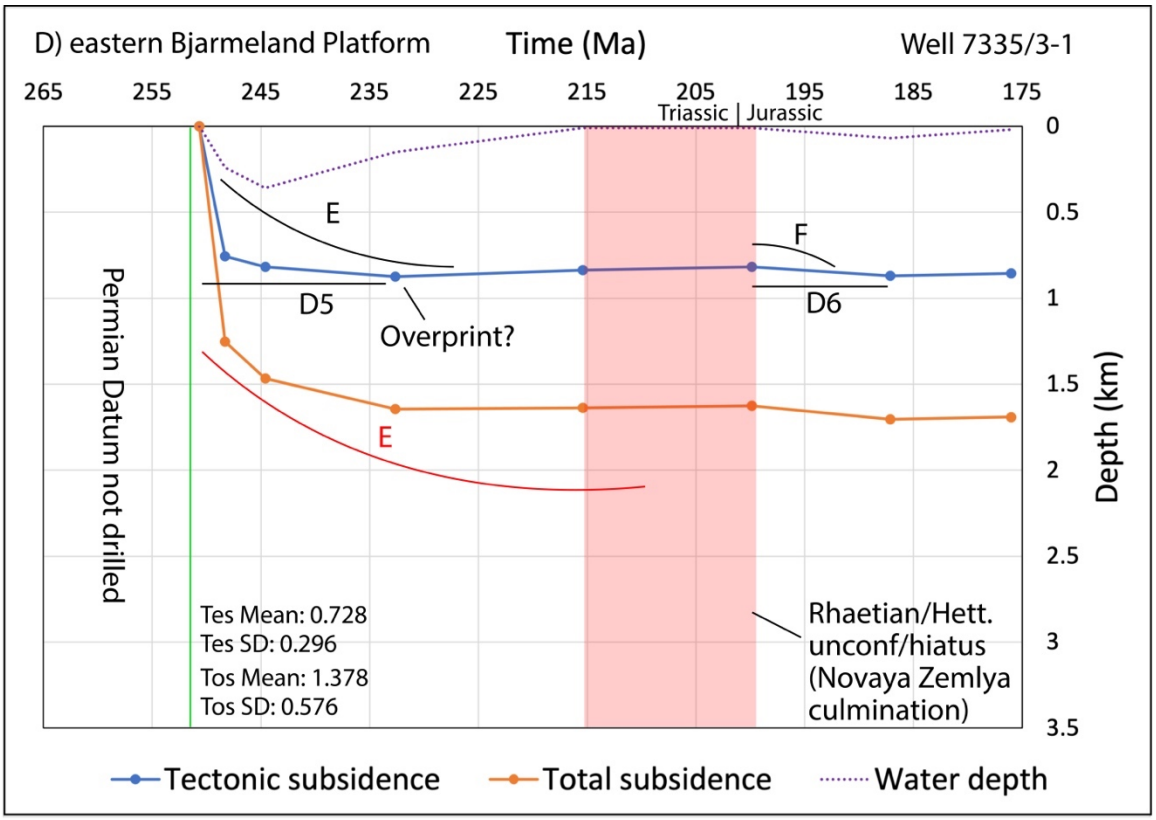
D) eastern Bjarmeland Platform
Time (Ma)
Well 7335/3-1
265
255
245
235
225
215
205
195
185
175
Triassic | Jurassic
0
0.5
1
1.5
2
2.5
3
3.5
Depth (km)
Permian Datum not drilled
E
F
D5
Overprint?
D6
E
Tes Mean: 0.728
Tes SD: 0.296
Tos Mean: 1.378
Tos SD: 0.576
Rhaetian/Hett.
unconf/hiatus
(Novaya Zemlya
culmination)
Tectonic subsidence
Total subsidence
Water depth

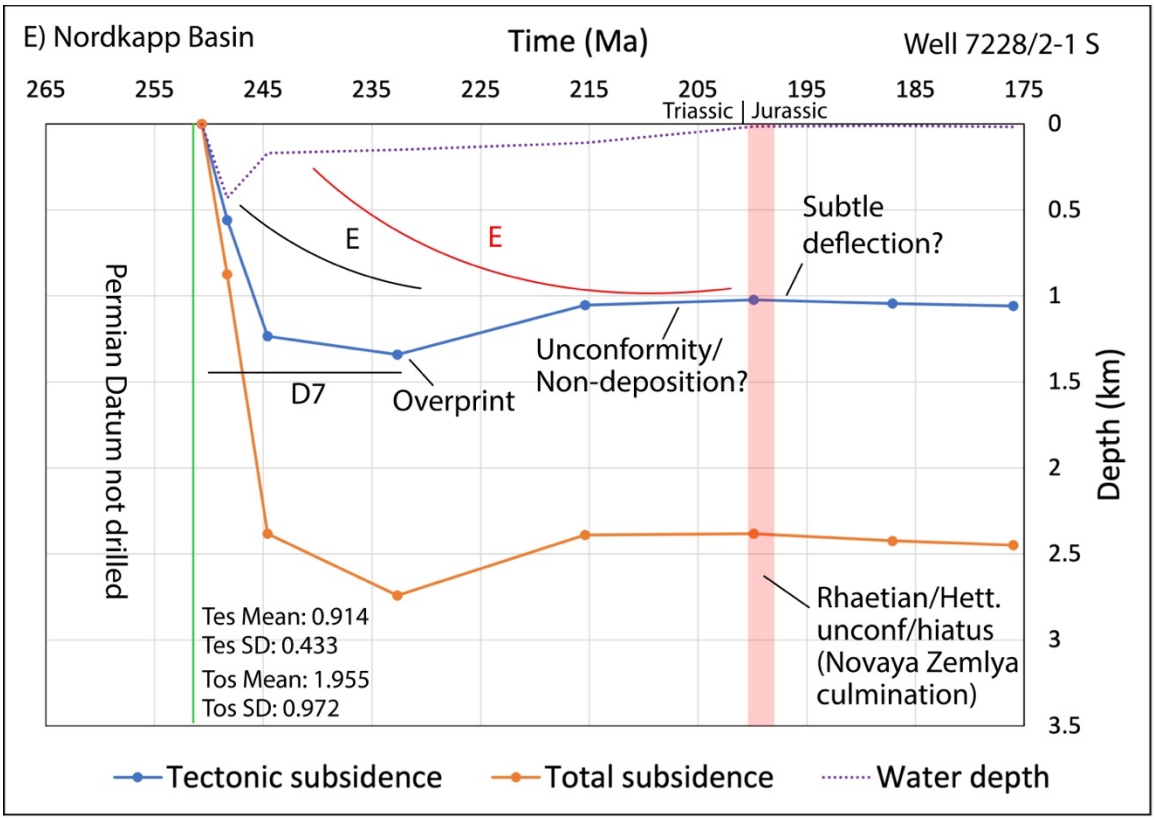
E) Nordkapp Basin
Time (Ma)
Well 7228/2-1 S
265
255
245
235
225
215
205
195
185
175
Triassic | Jurassic
0
0.5
1
1.5
2
2.5
3
3.5
Depth (km)
Permian Datum not drilled
E
E
Subtle deflection?
Unconformity/ Non-deposition?
D7
Overprint
Rhaetian/Hett. unconf/hiatus (Novaya Zemlya culmination)
Tes Mean: 0.914
Tes SD: 0.433
Tos Mean: 1.955
Tos SD: 0.972
Tectonic subsidence
Total subsidence
Water depth

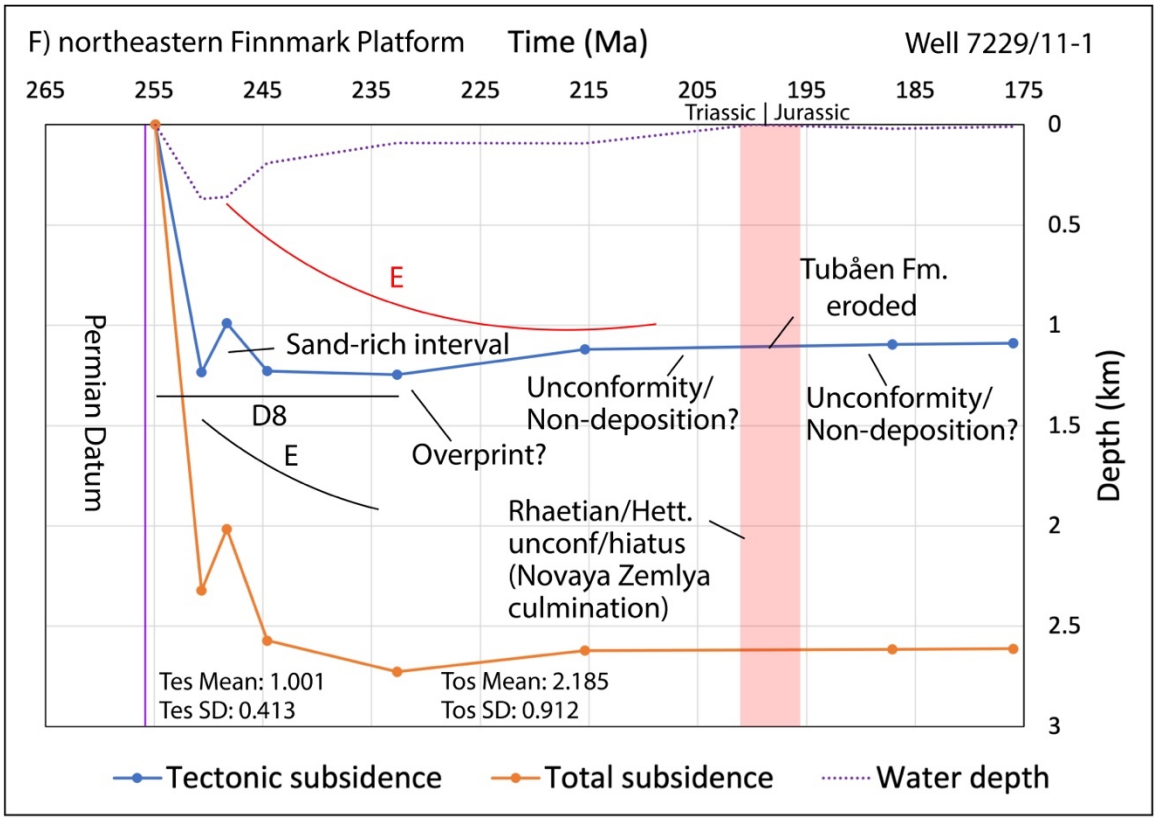
F) northeastern Finnmark Platform
Time (Ma)
Well 7229/11-1
265
255
245
235
225
215
205
195
185
175
Triassic | Jurassic
0
0.5
1
1.5
2
2.5
3
Depth (km)
Permian Datum
E
Tubåen Fm. eroded
Sand-rich interval
Unconformity/ Non-deposition?
Unconformity/ Non-deposition?
D8
E
Overprint?
Rhaetian/Hett. unconf/hiatus (Novaya Zemlya culmination)
Tes Mean: 1.001
Tes SD: 0.413
Tos Mean: 2.185
Tos SD: 0.912
Tectonic subsidence
Total subsidence
Water depth

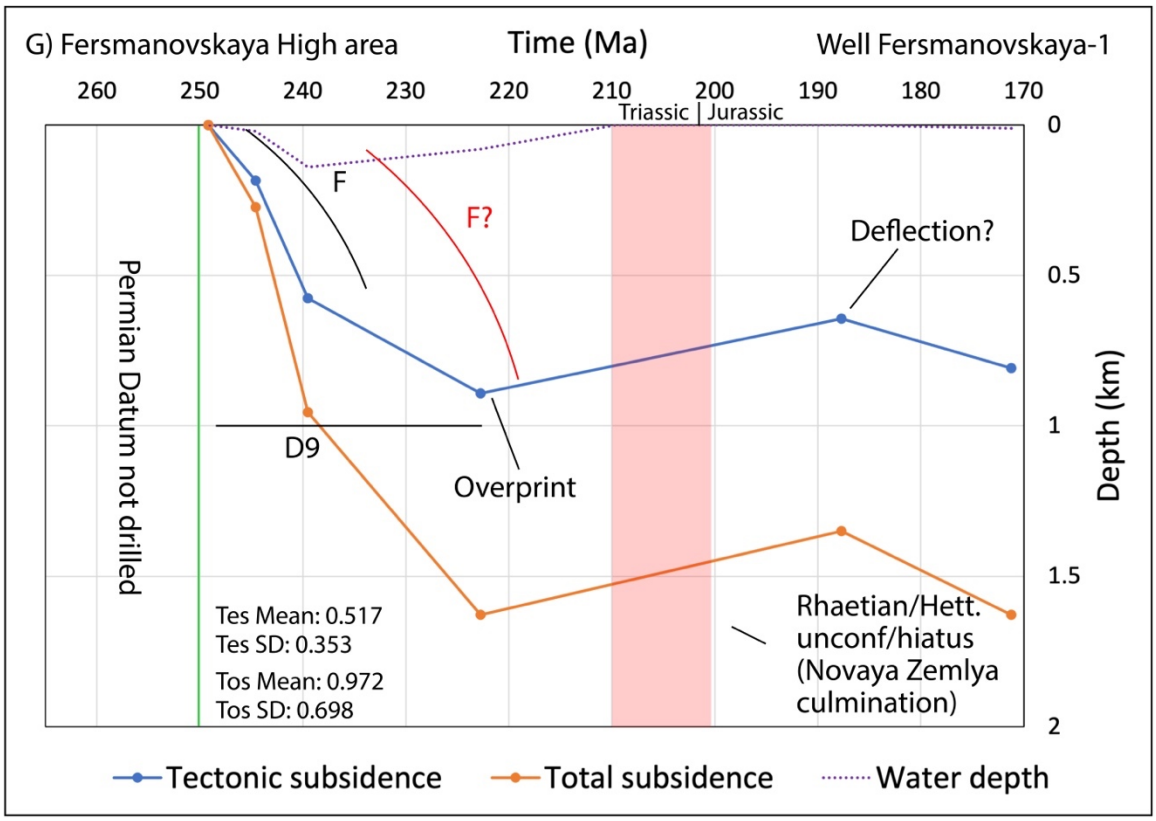
G) Fersmanovskaya High area
Time (Ma)
Well Fersmanovskaya-1
260
250
240
230
220
210
200
190
180
170
Triassic | Jurassic
0
0.5
1
1.5
2
Depth (km)
Permian Datum not drilled
F
F?
Deflection?
D9
Overprint
Tes Mean: 0.517
Tes SD: 0.353
Tos Mean: 0.972
Tos SD: 0.698
Rhaetian/Hett.
unconf/hiatus
(Novaya Zemlya
culmination)
Tectonic subsidence
Total subsidence
Water depth

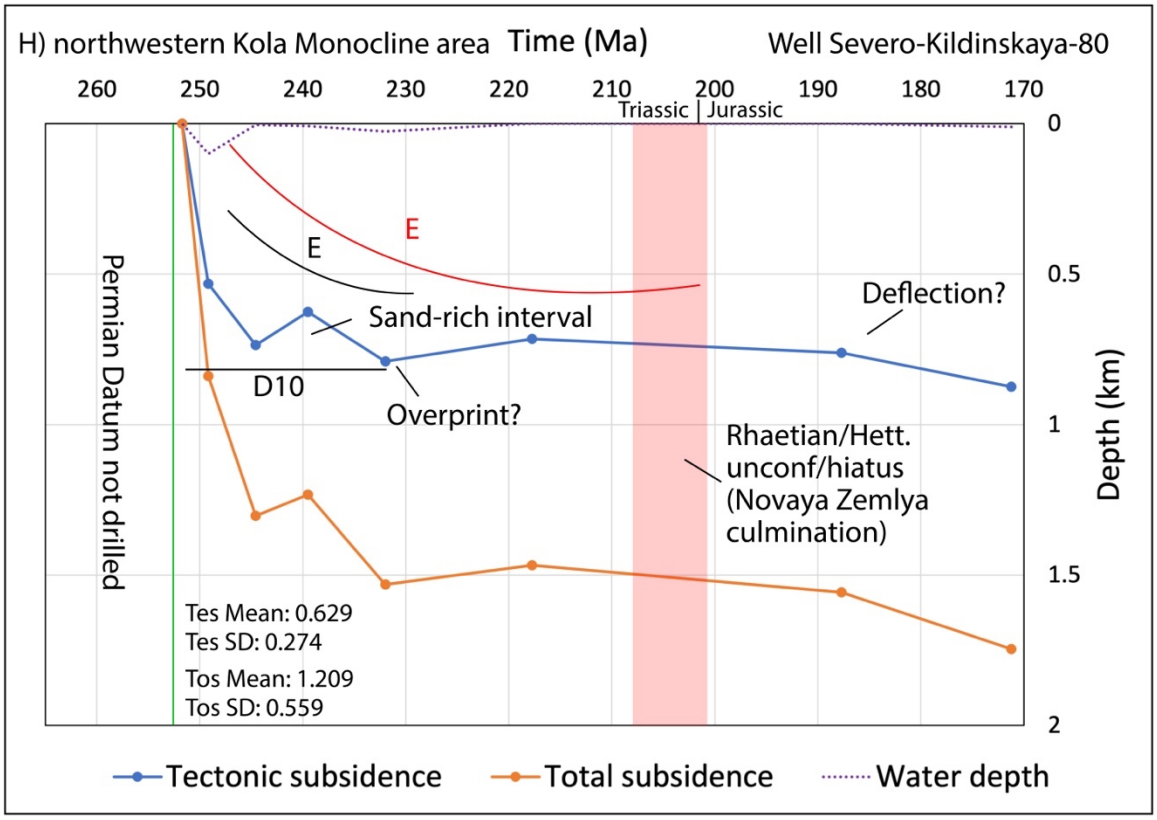
H) northwestern Kola Monocline area
Time (Ma)
Well Severo-Kildinskaya-80
260
250
240
230
220
210
200
190
180
170
Triassic | Jurassic
0
0.5
1
1.5
2
Depth (km)
Permian Datum not drilled
E
E
Sand-rich interval
Deflection?
D10
Overprint?
Rhaetian/Hett.
unconf/hiatus
(Novaya Zemlya
culmination)
Tes Mean: 0.629
Tes SD: 0.274
Tos Mean: 1.209
Tos SD: 0.559
Tectonic subsidence
Total subsidence
Water depth

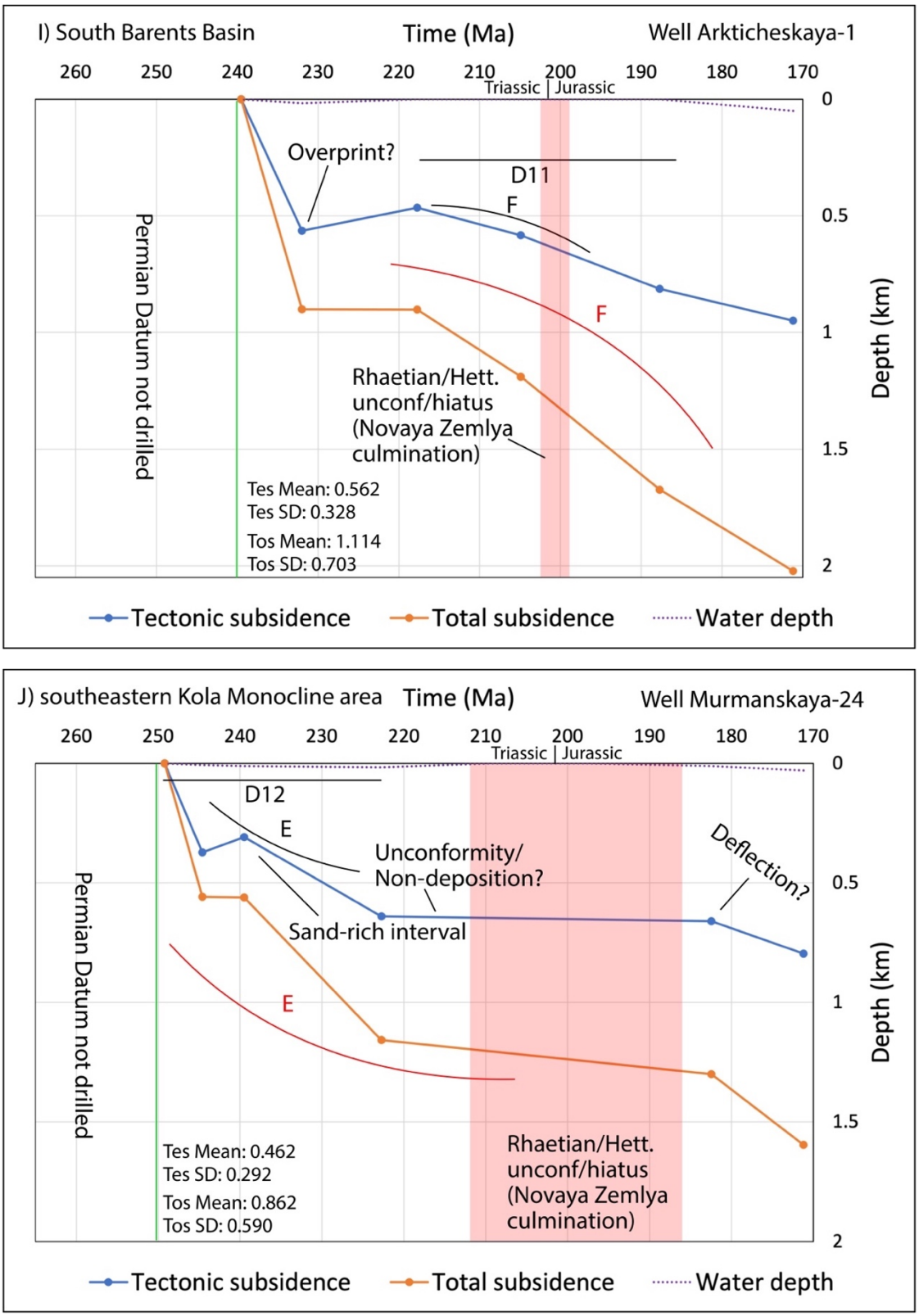

Figure 3.4. Tectonic (blue) and datum (orange) subsidence curves for target BSS structural elements.

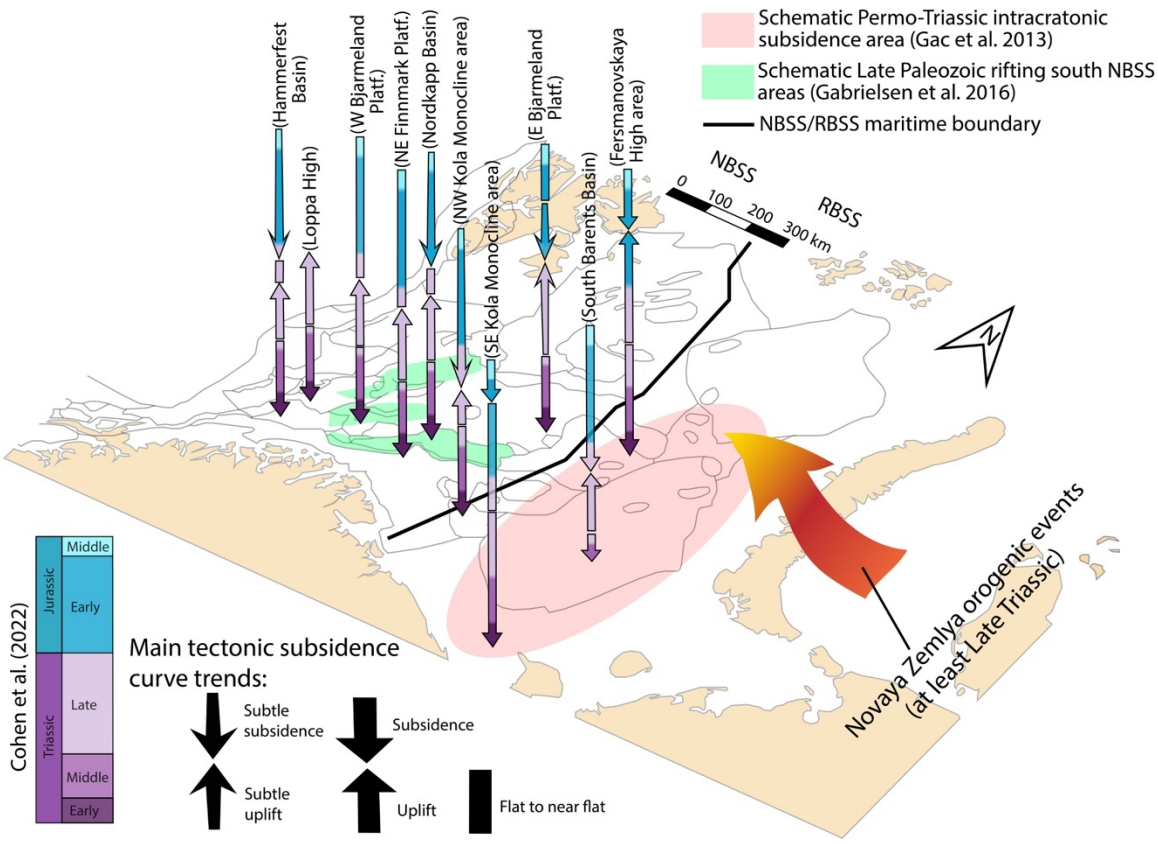

Figure 3.5. Schematic illustration showing main tectonic curve trends of targeted BSS structural elements. The lengths of the arrows and columns represent the duration of each main curve trend and are temporally correlated to the International Stratigraphic Chart (Cohen et al., 2022). The reddish arrow represents the westwardly migrating Novaya Zemlya orogenic events. The green areas represent the location of Late Paleozoic, North Atlantic, rifting events (Gabrielsen et al., 2016), whereas the red ellipse represents areas with mainly intracratonic subsidence mechanisms (Gac et al., 2013).

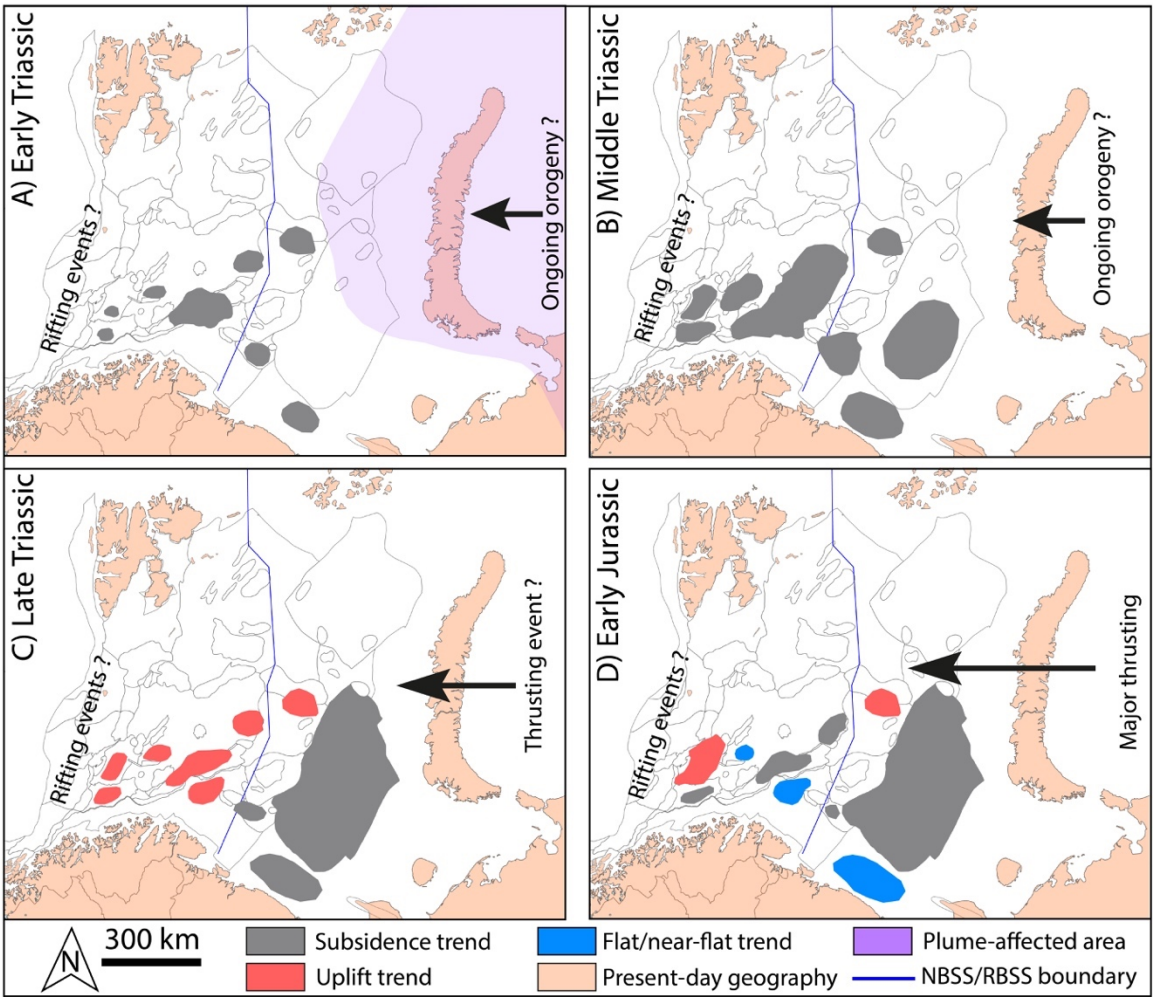

Figure 3.6. Highly schematic and extrapolated maps illustrating the main BSS structural trends observed in Fig. 3.5.) Early Triassic time; B) Middle Triassic time; C) Late Triassic time; and D) Early Jurassic time. The purple area represents the area likely affected by the Siberian Superplume (Puchkov, 2018; Puchkov et al., 2021).

CHAPTER 4. INTERPRETING THE UPPER TRIASSIC–LOWER JURASSIC SEDIMENTARY SUCCESSION ACROSS THE SOUTH-CENTRAL BARENTS SEA SHELF: AN EXERCISE IN COMPRESSIONAL, TECTONOSTRATIGRAPHIC ANALOGUE MODELLING

4.1 Introduction

The Barents Sea shelf (BSS) consists of a shallow shelf area that covers approximately 1.4 million km^2, located between northern Norway, northwestern Russia, Svalbard, Franz Joseph Land and Novaya Zemlya (Figs. 4.1A, B). The geology of the BSS reflects a complex system of sedimentary basins, platforms, and structural highs (Fig. 4.1B), which have been the sources of substantial hydrocarbon resources (e.g., Henriksen et al., 2011). In the Norwegian part of the shelf (western BSS; NBSS; Fig. 4.1B), hydrocarbon exploration has been conducted since the 1970s with the first wells drilled in the 1980s. Approximately 157 exploration wells have been drilled in the NBSS, with most of these located in south-southwestern areas. The northern NBSS sector (N of 74°30') has not yet been opened to drilling; thus, our lithologic and stratigraphic information from this sector is currently restricted to the published literature and two cores from shallow boreholes (Fig. 4.1B). On the Russian part of the shelf (eastern BSS; RBSS; Fig. 4.1B), most drilling has taken place in the southeast, where correlations with nearby wells from the better-known Pechora Sea and Timan-Pechora basins (Figs. 4.1B, C) have been attempted (e.g., Gilmullina et al., 2021).

The tectonostratigraphic development of the hydrocarbon-rich Upper Triassic–Lower Jurassic BSS succession has been interpreted as related to the evolution of the Novaya Zemlya orogeny across the eastern BSS margin (Polyakova, 2015; Olaussen et al., 2018; Müller et al., 2019; Martins et al., 2022). However, regional ties to Novaya Zemlya tectonism and associated large-scale BSS tectonostratigraphy are still debated (e.g.,

Olaussen et al., 2018; Müller et al., 2019; Gilmullina et al., 2021; Martins et al., 2023). Although various studies have addressed the influence of Novaya Zemlya compression in BSS stratigraphy, the theme remains understudied (Müller et al., 2019). Previous studies used analytical methods including seismic, thermochronologic, and lithologic analyses (e.g., Olaussen et al., 2018; Zhang et al., 2018). Detailed flexural modelling, however, is still underused in BSS tectonostratigraphy but is essential because the development of a Novaya Zemlya fold belt implies RBSS crustal loading and related flexural responses. Because obtaining BSS lithostratigraphic data can be difficult, analogues need to be used to complement the analysis (Martins et al., 2022). Tectonostratigraphic flexural models from possible analogue areas (e.g., Appalachian system of orogens and basins in eastern U.S.; Martins et al., 2022) can be useful for relating compressional tectonism to Upper Triassic–Lower Jurassic BSS stratigraphy. Though conceptual in origin, "flexural modelling" is used in this study to mean that a given tectonic process in the orogen (e.g., deformational loading) gives rise to a wave-length-like, flexural response (e.g., foreland basin and bulge) of the crust that can effect regional sedimentation (e.g., Quinlan and Beaumont, 1984).

One technique, the "tectophase model," is based on flexural concepts that tie stratigraphy to compressional tectonics in a nearby orogen (Ettensohn et al., 2019). This model has already been used in the Rocky Mountains (Johnson, 1971), South China (Su et al., 2009), the Appalachians (Ettensohn et al., 2019), and in the Uralian-Pai-Khoi-Novaya Zemlya orogen (Martins et al., 2022) to relate regional stratigraphic responses to compressional processes. Most studies using other methods tend to present orogeny as one long episode of compression, even though orogenies are widely accepted to reflect multiple

short pulses that affect different areas of the orogen at different times (e.g., Camacho et al., 2005; DiPietro, 2018). Hence, the tectophase model is useful because it can relate unconformity-bound stratigraphic sequences to smaller-order tectonic pulses.

In the Appalachian Basin, relationships between stratigraphy and compressional tectonics are relatively well-understood (e.g., Merschat and Hatcher, 2007; Hatcher, 2010; Ettensohn et al., 2019), and the tectophase model has been widely used. The Appalachians and Uralides have long been described as tectonically and geodynamically similar (e.g., Artyushkov and Baer, 1983; Kruse and McNutt, 1988; Puchkov, 2002, 2009; Martins et al., 2022), so the opportunity exists for comparative studies using the tectophase model. Moreover, intracratonic mechanisms of subsidence in the eastern BSS were proposed to be analogous to those observed in the Appalachian foreland-intracratonic compressional system (Ritzmann and Faleide, 2009; Gac et al., 2013; Martins et al., 2022). Because the evolving Novaya Zemlya fold-thrust belt must have triggered coeval far-field responses across the BSS during at least Late Triassic time (Zhang et al., 2018; Müller et al., 2019; Martins et al., 2022), we suggest that BSS lithostratigraphy in and beyond the foreland basin may be related to similar flexural responses generated in the nearby compressional orogen.

The main goal of this paper is to demonstrate the usefulness of the Appalachian tectonostratigraphic model, or tectophase model, to evaluate how compressional related flexural processes could have influenced the development of the BSS Upper Triassic–Lower Jurassic succession.

4.1.1 Sedimentary cyclicity in foreland basins

In earth sciences, the concept of cyclicity has been used to explain a myriad of physical processes in nature (e.g., Milankovitch cycle). In most large-scale sedimentary basins, sedimentary cyclicity is controlled by the interaction of tectonics, sedimentary supply, and eustacy (e.g., Miall, 1997). The systematic and cyclic repetition of depositional styles in the stratigraphic record often results in predictable stratigraphic patterns in space and time. Understanding stratigraphic sequences as cyclic responses to eustacy (sequence stratigraphic techniques; e.g., Vail and Mitchum, 1977; Vail, 1987; Posamentier and Morris, 2000; Catuneanu et al., 2011) has become a classic method in basin analysis. Even though this method was initially used in extensional settings (e.g., Brown and Fisher, 1977), the same basic concepts (e.g., retrogradation and progradation) have been used in compressional settings. However, in compressional basins, flexural models (e.g., Karner and Watts, 1983; Quinlan and Beaumont, 1984; Ettensohn, 1985; Beaumont et al., 1987, 1988; Klein and Hsui, 1987; Ziegler, 1987; Klein, 1994) are probably more appropriate at addressing the resulting relationships among deformational loading, depositional regime, and reactivation of basement structures by far-field forces (Ettensohn, 2004, 2008; Ettensohn et al., 2019).

The importance of flexural modelling lies in the well-accepted theory that the Earth's crust can exhibit regional flexural responses to orogenic loading. Hence, flexural modelling better resolves the many tectonostratigraphic nuances in compressional settings because it better uses the physical characteristics of basins developed by these mechanisms. In tectonostratigraphy, the above relationships may also be explained using tectophase cycles. Inasmuch as orogenies typically progress as a series of pulses (Johnson, 1971;

Jamieson and Beaumont, 1988; DiPietro, 2018), the tectonostratigraphic responses necessarily manifest as a series of unconformity-bound cycles related to each pulse of crustal loading and relaxation during a few millions to tens of millions (10^6–10^7) of years (Ettensohn et al., 2019).

4.1.2 The tectophase cycle

The tectophase cycle consists of seven distinct and systematic tectonostratigraphic responses produced as subsurface and surface orogenic structures load the lithosphere (Fig. 4.2). To isostatically compensate for the load, the lithosphere downwarps into a flexural foreland basin with an uplifted peripheral bulge that migrates cratonward (Fig. 4.2A). The migrating bulge typically generates a regional, sequence-bounding unconformity that defines the base of the tectophase cycle (Fig. 4.2A, C [part 1]). As deformational loading progresses, rapid subsidence ensues, and the initial response is typically a thin, transgressive, shallow-water carbonate or clastic unit (Fig. 4.2C, part 2). Because initial loads are mostly in the subsurface, siliciclastic influx is minor and subsidence outpaces sedimentation. As a result, organic matter from the water column predominates in starved-basin conditions, generating dark, organic-rich muds (Fig. 4.2A, C [part 3], D).

As deformation continues, the load eventually becomes subaerial and drainage nets develop. Once deformation has ceased and the load becomes static, drainage nets and erosion begin the transfer of sediment into adjacent basins. However, because the load is now stationary, the lithosphere relaxes in response to the static load and begins to subside while the bulge moves back towards the load (Fig. 4.2E). This process marks the beginning of the loading-type relaxation in the tectophase cycle (Fig. 4.2B). Because of crustal

relaxation and erosion (Fig. 4.2C [part 4], E), the deepening foreland basin fills with "flysch-like" sediments that might include deep-water deltaic, turbidites, contourites, and debris flows, some of which may eventually be reworked by storms (Fig. 4.2C [part 4]; E).

Once the static surface load is eroded and the rate of sediment influx exceeds the rate of basin subsidence, the foreland basin eventually fills or overflows with sediment. At this point, a brief period of elevational equilibrium between the basin and eroded load is established, allowing the deposition of a thin blanket of shallow-water carbonates or shales across the area (Fig 4.2C, part 5). This phase of equilibrium is short-lived, as parts of the former orogen and adjacent foreland basin begin to rebound in response to the lost load (Fig 4.2F). Rebound and a compensating "anti-peripheral bulge" result in brief episode of transgression followed by a cratonward prograding wedge of "molasse-like" sediments, including marginal-marine, fluvial-deltaic and alluvial sediments (Fig. 4.2C, parts 6 and 7). Because this flexural stage began at near-equilibrium, sea-level conditions, a single, cratonward paleoslope becomes established (Fig. 4.2F).

A bounding unconformity at the top of the sequence (Fig. 4.2C) can represent a new pulse of tectonism, which represents the beginning of the next tectophase cycle. The above description represents ideal deposition, but parts of the succession may be poorly developed, or truncated by an overlying cycle unconformity.

The overarching importance of the tectophase model is the use of flexural arguments to tie orogenic events to stratigraphy (Fig. 4.2). Because of the development of a Late Triassic–Early Jurassic orogen across the eastern BSS margin implies progressive crustal loading, the tectophase model can be used. Even though a few studies have used flexural analyses in the BSS (Müller et al., 2019), no study to our knowledge has analyzed the Late

Triassic–Early Jurassic BSS succession in terms of individual lithologic responses to orogenic evolution (Fig. 4.2C). If Novaya Zemlya compressional tectonism was indeed operating across the eastern BSS margin during Late Triassic–Early Jurassic time, a succession similar to that noted in Figure 4.3 would be expected in response to foreland-basin development. Hence, the existence of sequence-bounding unconformities, occurrence of key lithologies, and a regional variations in stratigraphic thicknesses at various BSS localities are expected and are indicative of responses to flexurally related structures (e.g., foreland basins and bulges). If Novaya Zemlya tectonism were not operant, then eustasy would largely control the resulting succession.

4.2 Materials and methods

This study examined the Upper Triassic–Lower Jurassic sections in exploration wells from the NBSS (78), RBSS (eight), Pechora Sea basin (southeasternmost RBSS; three) and Timan-Pechora basin (one) (Fig. 4.1C). Lower Jurassic parts of the section are already well understood (e.g., Olaussen et al., 2018) and were examined largely through the literature. However, this study will emphasize Upper Triassic parts of the section, which are less well understood and represented by the Fruholmen Formation and equivalent rocks across the NBSS and RBSS, respectively.

NBSS well data for the studied section are publicly available online from the Norwegian Petroleum Directorate (NPD, 2023), whereas Russian (RBSS, Pechora Sea and Timan-Pechora basins) well data for equivalent deposits were obtained from selected literature (Chirva et al., 1990; Astafiev et al., 2008; Gavrilov et al., 2010; Norina et al., 2014; Burguto et al., 2016; Gilmullina et al., 2021). The selected Pechora Sea and Timan-

Pechora wells (Fig. 4.1C; Table 4.1) were included to provide a more complete regional context. For the NBSS, only wells that pierced the entire Fruholmen Formation were used, whereas in the RBSS, approximately equivalent chronostratigraphic intervals were adopted from the literature. Fourteen wireline logs from selected NBSS wells were obtained from the NPD (10 are publicly available; NPD, 2023) and used for correlation (Fig. 4.1B). Wireline logs were not available for the RBSS. Thicknesses and lithologic changes across the NBSS were measured from gamma-ray (GR), density (DE), and neutron (NP) logs.

Minimum and maximum Fruholmen Formation (~Norian–Rhaetian) thicknesses were obtained from 14 NBSS wells, whereas equivalent thicknesses from 10 RBSS and adjacent areas wells are presented as obtained per individual well. The thicknesses encountered in each well are presented as interpreted by the NPD and Russian literature (e.g., Chirva et al. 1990), and were used for regional interpretation of stratigraphic patterns. Additionally, two northern NBSS cores from shallow stratigraphic boreholes (7934/8-U-1, and 7533/2-U-2) were provided by the NPD (Fig. 4.1B). These cores are equivalent to lower parts of the Fruholmen Formation in the northern NBSS and were used to illustrate key stratigraphic features. Chronostratigraphy is based on recent Barents Sea literature (e.g., Paterson and Mangerud, 2019; Gilmullina et al., 2021).

4.3 Regional setting

4.3.1 Structural development

In the BSS, the Timanian (Late Proterozoic–Early Cambrian), Caledonian (Early Paleozoic), and Uralian-Pai-Khoi-Novaya Zemlya (Late Paleozoic–Middle Mesozoic) orogenies periodically reactivated basement structures (Nikishin et al., 1996; Petrov et al.,

2008; Drachev, 2016; Smelror and Petrov, 2018; Klitzke et al., 2019). In the western NBSS area, North Atlantic extensional events may have begun as early as latest Devonian–earliest Carboniferous time (Stemmerik, 2000). In contrast, in the eastern RBSS area, Novaya Zemlya compressional events may have started as early as Late Permian (Filatova and Khain, 2010) or Middle Triassic time (Otto and Bailey, 1995; Nikishin et al., 2011; Norina et al., 2014).

Late Triassic–Early Jurassic BSS compressional stresses and associated structural reactivation have been tied to the Uralian-Pai-Khoi-Novaya Zemlya orogeny. This orogenic event is the final product of the diachronous collision between Baltica and Siberia during Early Carboniferous to at least Early Jurassic time (e.g., Ziegler, 1989; Gudlaugsson et al., 1998; Puchkov, 2009; Torsvik and Cocks, 2017; Martins et al., 2022). During at least latest Triassic–Early Jurassic time, Novaya Zemlya was thrust westward over the eastern BSS, forming a west-verging, arcuate fold belt (e.g., Lopatin et al., 2001; Drachev et al., 2010; Scott et al., 2010; Curtis et al., 2018) (Fig. 4.1B) and a foreland basin in the RBSS area (e.g., Müller et al., 2019). In contrast, the NBSS area includes several rift, strike-slip, and intracratonic basins, which may have been reactivated coevally due to Novaya Zemlya deformation and resulting far-field forces (e.g., Faleide et al., 2017).

4.3.2 Tectonostratigraphy

During Triassic time, widespread deltaic progradation, mostly derived from the southeast, generated complex offshore-marine and fluvio-deltaic sedimentation across most of the BSS (e.g., Glørstad-Clark et al., 2010; Uchman et al., 2016; Gilmullina et al., 2021). Even though this pattern of sedimentation was largely maintained during Late

Triassic time (e.g., Fleming et al., 2016) (Fig. 4.3), progradation from the east gradually became preeminent, likely because of Novaya Zemlya uplift (Klausen et al., 2016; Khudoley et al., 2019). During Late Triassic time, widespread fluvio-deltaic deposition restricted open-marine sedimentation to more northern BSS areas (Fig. 4.3, columns 3, 10, 12, 14, 18–20) (Riis et al., 2008; Sømme et al., 2018; Klausen et al., 2015, 2019).

Across the NBSS and Svalbard (Fig. 4.1), Upper Triassic marginal-marine to fluvio-deltaic sediments (Snadd Fm., Carnian; Fig. 4.3, columns 1–14) include sandstones and interbedded mudrocks overlain by coal-bearing, coastal-plain sediments and fluvial red beds (Smelror et al., 2009; Lundschien et al. 2014; Olaussen et al. 2018). In the RBSS (Fig. 4.3, columns 16–22), equivalent deposits include an alternation of dark-gray mudstones, clayey, dark-gray siltstones, fine- to medium-`grained sandstones, and coal (Gavrilov et al., 2010; Shkarubo et al., 2017). During Early Norian time, a transgressive event (Pan-Arctic Transgression) pushed the shoreline to the southern and eastern borders of the South Barents Basin (Fig. 4.1), which remained a "sediment sink" for the nearby Carnian delta (Dalland et al., 1988; Johansen et al., 1993; Embry, 1997; Klausen et al., 2015; Burguto et al., 2016; Shkarubo et al., 2017; Olaussen et al., 2018) (Fig. 4.3). A sharp shift from the deposition of immature, largely Carnian feldspathic sands to mature, orthoquartzitic sands in the overlying Fruholmen Formation was coeval with this transgression (Bergan and Knarud, 1993; Ryseth, 2014), and the resulting surface may reflect a combination of several smaller erosional events and/or ravinement surfaces (Fig. 4.3).

During Norian time across the NBSS, fluvio-deltaic sedimentation was replaced by dark, open-marine shales (Akkar Mbr.; Fig. 4.3, columns 3–13), which grade upward into

interbedded coastal to fluvial sandstones (Reke Mbr.; Norian–Rhaetian) and interfingering marine shales and delta-plain sandstones (Krabbe Mbr.; Rhaetian); these three members constitute the Fruholmen Formation (Fig. 4.3) (e.g., Mørk et al., 1999; Paterson and Mangerud, 2019). On Kong Karls Land and eastern Svalbard (Fig. 4.3, columns 1, 14), the Fruholmen equivalent Flatsalen Formation includes a prominent, basal, glauconitic, carbonate bed (Slottet Bed; Fig. 4.3, columns 1, 2, 13, 14), which is comparable to the basal Fruholmen Formation (Lord et al., 2014; Olaussen et al., 2018). This bed is overlain by dark mudstones, followed by shallow-marine to fluvial sediments, which interfinger with marine shales (Klausen et al., 2014; Lord et al., 2014; Paterson and Mangerud, 2017). The Fruholmen and Flatsalen formations are overlaid by uppermost Triassic–Lower Jurassic sandstones with subordinate shales and coals of the Tubåen and Svenskøya formations, though these deposits are eroded at some locations (Dalland et al., 1988; Lord et al., 2014, 2019; Paterson and Mangerud, 2019) (Fig. 4.3, columns 1–14).

Across the RBSS (Figs. 4.1, 4.3; columns 16–22), official stratigraphic nomenclature has not yet been defined. However, deposits comparable to the NBSS Fruholmen Formation generally consist of alternations of interbedded, black-to-brown mudstones, siltstones, and sandstones (Burguto et al., 2016; Shkarubo et al., 2017). In the Korothaika, Pechora Sea, and Timan-Pechora basins (Figs. 4.1, 4.3, columns 23–25), the Upper Triassic succession is defined as the Nar'yanmarskaya and Korothaikhinskaya formations, respectively, whereas the Lower Jurassic section is eroded. These deposits are often correlated with the RBSS succession (Mørk, 1999; Gilmullina et al., 2021). In Franz Josef Land (Fig. 4.1), the target succession is defined as the Vilchekovskaya, Vasilevskaya and Tegetkhoffskaya formations (Dibner and Krylova, 1963; Embry, 1992; Ershova et al.,

2022) (Fig. 4.3, column 15). By at least latest Triassic time, thrusting of Novaya Zemlya generated extensive compressional stresses (e.g., Faleide et al., 2017; Müller et al., 2019) (Fig. 4.3), and on top of the resulting, regional, Rhaetian unconformity (Fig. 4.3), clastics were deposited in various shallow-marine to fluvio-deltaic environments (Dalland et al., 1988; Smelror et al., 2009; Line et al., 2020). Traditionally, the Rhaetian unconformity has been tied to Novaya Zemlya compression because of its angular seismic characteristics (e.g., Astafiev et al., 2008; Smelror et al., 2009; Drachev, 2016; Müller et al., 2019).

4.4 Results

In the literature, it has been suggested that deformational loading during the Novaya Zemlya orogeny was the primary tectonic mechanism behind potential Late Triassic–Early Jurassic tectonostratigraphic responses in the BSS region (e.g., Olaussen et al., 2018; Müller et al., 2019; Martins et al., 2022, 2023). To evaluate these responses across the BSS, we examined: 1) the positional variations in Norian–Rhaetian sedimentary thickness; 2) possible far-field responses in local structures; 3) unconformities; and 4) evidence of a pre-Rhaetian orogenic pulse, relative to flexural responses in the lithosphere.

4.4.1 Thickness variations

The lithostatigraphic nature and thicknesses of the Norian-Rhaetian sediments are compiled from the 90 wells shown in Figure 4.1C. In the RBSS, very few wells were available (Fig. 4.1C; Table 4.1), and thicknesses are typically presented in terms of grouped time intervals that were interpreted to represent Norian–Rhaetian thicknesses. However, a few of these reflect incomplete sections (Table 4.1), which may be the consequence of

erosion (Fig. 4.3). The recovered succession is thickest (~730 m) in the Ludlovskaya Saddle and thinnest in the west Kola Saddle (~57 m) (Fig. 4.1B; Table 4.1). In the southeasternmost area, the succession is thickest (612 m) in the Korothaika Basin and thinnest (153 m) in the central Pechora Sea basin (Figs. 4.1, 4.3; Table 4.1).

In the NBSS, thickness values for the available 78 wells are shown individually per structural element (Figs. 4.1C, 4.4). The NBSS Norian–Rhaetian succession (Fruholmen Formation) is thickest (~580 m) near the Bjørnøyrenna Fault Complex (BFC; Figs. 4.1, 4.4) and thinnest in platform areas (~15 m) (FP and BP; Figs. 4.1, 4.4). Of these 78 wells, maximum and minimum Fruholmen Formation thicknesses per NBSS structural element are shown in Table 4.2. The Norian–Rhaetian thicknesses for all 90 wells across the BSS and adjacent areas were then plotted in Figure 4.5, where five regional thickness trends are presented: 1) increased thicknesses in the central RBSS and northern Pechora Sea areas (>~300 m); 2) moderate thickness in the southernmost RBSS, southern Pechora Sea, and Timan-Pechora areas (~130–250 m); 3) thin to moderate thicknesses in the central BSS area (~15–140 m); 4) thin to moderate thicknesses in the central NBSS area (~20–230 m); and 5) increased thickness in the westernmost NBSS area (~400 m).

4.4.2 Wireline succession analysis

One form of addressing far-field responses in foreland-basin systems is assessing variations in thickness and the lithologic compositions of included units (Ettensohn et al., 2019). For assessing these variations, gamma-ray (GR), density (DE) and neutron-porosity (NP) wireline logs were used, where available. For the NBSS, a west-east section was constructed correlated with the reference wireline section (Dalland et al., 1988) for the

Fruholmen Formation (Figs. 4.1B [green symbol], 6; Table 4.3). The tops and bottoms of the Fruholmen Formation are noted as currently adopted by the NPD (NPD, 2023). For the RBSS and adjacent areas, however, wireline logs were not available. Along this section line, the tops and bottoms of the Akkar (purple), Reke (yellow) and Krabbe (green) members of the Fruholmen Formation were picked and correlated (Figs. 4.3, 4.6). The Akkar Member represents a predominantly deep-marine succession with abundant organic-rich muds on top of glauconitic carbonate beds, and underlying fluvio-deltaic sediments (Snadd Formation; Fig. 4.3). The Reke Member includes interbedded, shallow-marine to fluvial deposits, whereas the Krabbe Member represents an intercalation of marine and fluvio-deltaic sediments (Fig. 4.3). In the wireline logs (Fig. 4.6) the Akkar Member is characterized by high gamma-ray responses and simultaneous separation between density and neutron curves, whereas the Reke Member is represented by lower gamma-ray responses and minor separation of the density and neutron curves. The Krabbe Member is exhibits oscillating, low- to high, gamma-ray responses and overall separation of the density and neutron curves.

In the section, the Fruholmen Formation is thicker in the Hammerfest (well 7120/12-1; 198 m) and Nordkapp (well 7227/10-1; 234 m) basins (Fig. 4.6), whereas thinner on the Loppa High (well 7222/11-1; 47 m). All three members of the Fruholmen Formation are apparent in the wells, except in well 7222/11-1 (Loppa High; Fig. 4.1), where the Krabbe Member is likely eroded or was not deposited (Fig. 4.6; green). Clearly, all members show variations in thickness from well to well (Figs. 4.1, 4.6), but more important are the larger-scale changes in thickness patterns as the section moves from west to east across various structures. In the four western wells, for example, the entire section

is thicker and probably reflects deposition in a basinal setting. The section then dramatically thins in well 7222/11-1 as it moves across the Loppa High, but again thickens moderately on the intervening Bjarmeland Platform. This thickness trend is maintained eastwardly until the Nordkapp Basin (well 7227/10-1; 234 m), where the section again thickens abruptly. To the south and east of this well, including the southern edges of the basin and adjacent platform areas (Finnmark Platform), thicknesses again become moderate. It is important to note that the three different members commonly vary in thicknesses independently of each other (Krabbe Mbr., Fig. 4.6), but overall, reactivated structural elements seem to control regional thickness trends per member.

Of the three members, the Akkar Member is probably the most important because it represents regional processes associated with the beginning of deformational loading as reflected in the tectophase succession (Fig. 4.2). The thicknesses of the Akkar Member and the sum of the thicknesses of the Reke and Krabbe members are illustrated in a west-to-east graphic format to better demonstrate member distribution trends (Fig. 4.7). Variations in sedimentary thicknesses of a formation deposited across different structural elements suggests episodes of structural reactivation by far-field tectonics (Ettensohn et al., 2019). Hence, Fruholmen thickness variations (Akkar, Reke and Krabbe mbrs) may indicate varying types of structural reactivation across the BSS (e.g., uplift vs. subsidence). In Figure 4.7, thicknesses of the Akkar Member are highly variable, ranging from ~10 meters (Well 7132/2-2, eastern Finnmark Platform; Fig. 4.1) to 60 meters (Well 7228/2-1 S, Nordkapp Basin; Fig. 4.1), but having an average thickness of approximately 39 meters (blue line; Fig. 4.7). The graphic presentation in Figure 4.7 is important because it illustrates that thickness variations in the basal Akkar Member are apparent from the

beginning of sequence deposition, suggesting that structures were being reactivated simultaneously at different places across the NBSS.

4.4.3 Unconformities

In the tectophase model, presence and distribution of unconformable surfaces is important because these features often indicate flexural responses to orogenic inception (Fig. 4.2). Within the Upper Triassic–Lower Jurassic BSS succession, two such surfaces are present. The first surface (Rhaetian–Hettangian) (Fig. 4.3) has been traditionally interpreted as an unconformity because of its prominent seismic angularity and regional distribution (e.g., Astafiev et al., 2008; Drachev, 2016; Müller et al., 2019). In the shallow core 7533/2-U-2 (Fig. 4.8A), this surface reflects erosional truncation of low-angle cross stratification and represents subaerial exposure and fluvial erosion (Lord et al., 2019). Below this surface, deposits are sand rich and show hummocky-like to low-angle cross stratification. Along the truncation surface, brown-colored weathering and sediments containing shale chips and siderite nodules represent a basal lag (Lord et al., 2019). Overlying grey sandstones showing wavy-like bedding that shifts to parallel low-angle cross stratification may represent a progressive decrease in energy.

Presence of a second unconformable surface (Early Norian) is debatable for some (e.g., Lundschien et al., 2014; Müller et al., 2019; Gilmullina et al., 2021), while other studies have clearly interpreted it to be an unconformity (Fig. 4.3) (e.g., Embry, 1997; Bugge et al., 2002; Riis et al., 2008; Ryseth et al., 2014; Lord et al., 2019; Olaussen et al., 2022). In the shallow core 7533/2-U-2 (Fig. 4.8B), this surface separates cross-bedded grey sandstones and grey to dark-grey mudstones from a prominent carbonate-rich lag horizon.

The contact between this carbonate lag and underlying siliciclastics is abrupt and shows evidence of scouring. In the shallow core 7934/8-U-1 (Fig. 4.8C), however, the erosional nature of this surface is less clear, though the facies shift is abrupt.

Some authors interpreted this Early Norian surface to represent a sequence boundary (Riis et al., 2008; Lord et al., 2019; Rismyhr et al., 2019), whereas others did not (Paterson and Mangerud, 2019; Gilmullina et al., 2021; Klausen et al., 2022). According to Lord et al. (2019) and Olaussen et al. (2022), the lower boundary of the Slottet Bed (Figs. 4.3, 4.8B) represents a regional subaerial unconformity. Ryseth et al. (2014) correlated this same surface in wireline logs from the Hammerfest Basin (Fig. 4.1), to approximately 250 km northeast of the basin. On Svalbard outcrops, Müller et al. (2019) indicated an Early Norian unconformable horizon between the De Geerdalen and Flatsalen formations (Fig. 4.3). In the northern BSS, Olaussen et al. (2018) noted that a similar surface is a prominent seismic horizon, and unconformable characteristics have also been suggested in the southern BSS (Bugge et al. 2002). In contrast, the contact between the carbonate lag overlying organic-rich shales (Akkar Member equivalent; Fig. 4.3) is probably conformable (Fig. 4.8D), and represents a regional transgressive event (e.g., Johansen et al., 1993; Henriksen et al., 2011; Olaussen et al., 2018; Rismyhr et al., 2019).

4.5 Discussion and conclusions

In this section, Focus is placed on the southern BSS and adjacent eastern areas because well data were only available for these regions. Even though some lithostratigraphic data from selected northern BSS locations are present (Figs. 4.1, 4.3, 4.8), lack of sufficient well data precludes in-depth flexural modelling in the northern sector.

However, we will mention northern BSS lithostratigraphy where appropriate to complement the analysis of southern and southeastern areas.

4.5.1 Tectophase sequences

Understanding the BSS Upper Triassic–lowest Jurassic succession in terms of sedimentary thicknesses, unconformity-bound sedimentary sequences, and structural reactivation leads to the presumption of multiple deformational pulses in the Novaya Zemlya orogen, like those suggested in Figure 4.9. Based on the work of Ettensohn et al. (2019), multiple orogenic pulses and resultant tectophase cycles are common in many orogenic systems. In following sections, we discuss reasons why this is the case in the Novaya Zemlya-BSS system.

4.5.2 Evidence for foreland-basin development

Across the entire BSS, only the North and South Barents basins (Fig. 4.1, SBB, NBB) have been traditionally interpreted to represent a Jurassic foreland basin, formed in response to coeval Novaya Zemlya tectonism (e.g., Faleide et al., 2017; Olaussen et al., 2018). However, others have interpreted that this orogenic event occurred as early as Norian time (e.g., Scott et al., 2010; Drachev, 2016; Zhang et al., 2018). Similarly, other authors have suggested that a major change in sandstone maturity near the Carnian–Norian boundary, which represents a shift from immature (Snadd Fm.) to mature (Fruholmen Fm.) sandstones, is indicative of major tectonism (Bergan and Knarud, 1993; Embry, 1997).

As already indicated through stratigraphic analyses, BSS sedimentary thicknesses and unconformities suggest two foreland-basin successions reflecting two Novaya Zemlya

orogenic pulses during Late Triassic–Early Jurassic time (Fig. 4.9). The Early Norian unconformity (Lord et al., 2019; Fig. 4.8B) represents inception of the first tectophase, whereas the Rhaetian unconformity (Drachev, 2016; Fig. 4.8A) represents the second (Fig. 4.9). However, our study does not preclude the possibility of pre-Late Triassic Novaya Zemlya pulses, which are beyond the scope of this work.

4.5.3 Tectophase 1 (Norian–Rhaetian)

The use of thicknesses variations across a tectonically influenced shelf is one means to illustrate geometric patterns associated with the depositional zones of a classic foreland-basin system (DeCelles and Giles, 1996) (Fig. 4.10). In the nearby and time-equivalent succession in the Pechora Sea and Timan-Pechora areas (Fig. 4.1B) a thick succession (~612 m) in the Korothaika Basin (Figs. 4.1, 4.3) becomes thin southwards (~153 m), but then slightly thicker again to the south (~248 m). Because these areas are adjacent to the northernmost Uralian and Pai-Khoi fold belts to the east, which were active during Late Triassic time (Timonin et al., 2003), the observed north-south variation in thicknesses suggests foredeep, bulge, and backbulge depozones in these areas (Fig. 4.10). This suggestion aligns with the traditional interpretation of the Korothaika Basin as a foreland basin during Late Triassic time (Prischepa et al., 2011; Sobornov, 2022).

From the Novaya Zemlya fold belt westward (Fig. 4.10), a thin Norian–Rhaetian succession (~178-m thick, yellow) on the Admiralty High (Figs. 4.1, 4.3) becomes a very thick (up to ~500–730-m thick; gray) succession in the central RBSS areas. This region with thick deposits is surrounded by areas containing much thinner accumulations (~57–198 m, light red). Even though only three wells are available, we interpret the entire linear

light-red area to be a region of reduced thicknesses. From the light-red area westward, formation thicknesses increase to ~118–130 m in the central NBSS (Fig. 4.10, blue). Toward the western NBSS, in contrast, a very sharp increase in thicknesses up to ~580 m is present (Fig. 4.10; light blue).

When compared with the foreland-basin depozones of DeCelles and Giles (1996), the thickness patterns noted above strongly suggest the presence of a Norian–Rhaetian foreland-basin system (Fig. 4.10), which aligns with the Novaya Zemlya temporal interpretations of Zhang et al. (2018). The recognized foreland depozones (Fig. 4.10) include: 1) wedge-top (easternmost RBSS, yellow); 2) foredeep (central-southern RBSS area, gray); 3) bulge (RBSS/NBSS transition, light red); and 4) back-bulge (central NBSS, blue). The sharp increase in thicknesses in westernmost areas (NBSS, light blue) probably represents overprint by North Atlantic extensional processes, which began as early as Permo-Carboniferous time (e.g., Ziegler, 1989; Stemmerik and Worsley, 2005).

Based on the above assumptions of a BSS Norian foreland basin, the following stages of an initial tectophase cycle are indicated: 1) unconformity development (Early Norian surface; Figs. 4.2, 4.8B); 2) thin, overlying carbonate-rich unit (Slottet Bed; Figs. 4.2, 4.8B); 3) organic-rich shales (Akkar Member; Figs. 4.2, 4.6, 4.8D); and 4) loading- and unloading-type siliciclastic sediments (Reke and Krabbe members; Figs. 4.2, 4.6). This section was subsequently truncated by another unconformity described below. Even though the cores and logs used to describe this tectophase cycle are largely beyond the limits of the RBSS foreland basin, tectophase sequences do onlap intracratonic areas (Ettensohn et al., 2019). Such an onlap aligns with the interpretations of Klausen et al.

(2016), who suggested that Novaya Zemlya sediments prograded well-beyond the Norian–Rhaetian RBSS foredeep as far as the western BSS area.

4.5.4 Tectophase 2 (Rhaetian–Hettangian)

Across the BSS, the Rhaetian unconformity (Fig. 4.3, 4.8A) has been confidently tied to an episode of Novaya Zemlya tectonism and coeval foreland-basin development (e.g., Drachev, 2016; Faleide et al., 2017; Müller et al., 2019). This latest Rhaetian–Hettangian stratigraphic feature represents inception of tectophase 2 (Fig. 4.9). This event was significant because it generated a hiatus of up to 40 million years in some areas and widespread truncation of previous deposits, which is easily observed in seismic data (Müller et al., 2019). This unconformity is sequence-bounding and represents the inception of the Lower Jurassic foreland-basin sequence (Faleide et al., 2017; Martins et al., 2022). This tectophase succession, however, does not contain the basal organic-rich shales (Fig. 4.2). Based in the study by Ettensohn et al. (2019), the lack of basal dark shales in a foreland succession indicates a broad, shallow foreland basin, which precludes the development of organic-rich shales. Interpretation of a shallow Jurassic RBSS foreland basin aligns with studies like Suslova (2014), Gilmullina et al. (2021), and Martins et al. (2023), who noted lesser sedimentary thickness of up to 1.2 km in this basin.

4.5.5 Limitations

In the tectophase model, presence and distribution of unconformable surfaces indicate inception of compressional tectonics. Yet, unconformity development might also

reflect sea-level variation or some combination of eustasy and tectonics, and determining which mechanism predominated is difficult (Embry, 1997).

Clearly, there is some room for uncertainty here. Ideally, tectophase cycles are better analyzed in present or former foreland basins, but that is impossible here due to lack of data and access to the RBSS. However, because every orogenic system comes with onlapping intracratonic sequences that mirror those in the foreland basin and far-field responses that extend up to 1300 km into intracratonic areas (e.g., Karner and Watts, 1983; Ziegler, 1987), evidence from intracratonic areas may support developments in the foreland basin (Ettensohn and Lierman, 2015; Ettensohn et al., 2019). Hence, likely tectophase responses across intracratonic areas, thickness variations that mirror those of typical foreland-basin depozones, and other evidence of coeval tectonism (Figs. 4.6, 4.10) all support the likelihood that our observations reflect tectonostratigraphic responses to orogeny.

4.5.6 Conclusions

Thickness variations and an Early Norian unconformable boundary with an overlying tectophase sequence suggest an initial stage of deformational loading, which supports the inception of an episode of Novaya Zemlya deformation that we interpreted here as Tectophase 1. In latest Rhaetian time, the Tectophase 1 succession was truncated by a major unconformity with an overlying thick sequence of course, largely terrestrial, clastic sediments, triggered by deformation from a second collisional event. This event continued into Early Jurassic time (Hettangian) and is identified herein as Tectophase 2. Overall, this tectonostratigraphic work aligns with other studies suggesting Late Triassic

Novaya Zemlya compressional stresses and is supported through use of the tectophase analogue. This flexural model contributes to the understanding of unconformity development, stratigraphic succession, and far-field reactivation of BSS structures in both foreland and intracratonic areas.

Table 4.1. Thicknesses for RBSS, Pechora Sea, and Timan-Pechora Late Triassic sedimentary units approximately equivalent to the NBSS early Norian–Rhaetian Fruholmen Formation.

Well	Location	Thickness (m)	Target interval
Ludlovskaya-1	Ludlovskaya Saddle	730	Norian–Rhaetian
Severo-Kildinskaya-80	west Kola Saddle	57	Norian
Arkticheskaya-1	South Barents Basin	498	Norian–Rhaetian
Shtockmanovskaya-1	South Barents Basin	299	Norian–Rhaetian
Fersmanovskaya-1	Fersmanovskaya High area	200	Norian–Rhaetian
Severo-Murmanskaya-1	South Barents Basin	212	Rhaetian
Krestovaya-1	Admiralty High	178	Norian–Rhaetian
Kurentsovskaya-1	Kurentsovskaya Steps	132	Norian
Kolguevskaya-140	Kolguyev Island	215	Norian–Rhaetian
Severo-Gulyaevskaya-1	Pechora Sea Basin	153	Norian
Severo-Donginskaya-1	Pechora Sea Basin	612	Norian
Nosovaya-1	Timan-Pechora Basin	248	Norian

Table 4.2. Maximum and minimum Fruholmen Formation thicknesses across selected NBSS structural elements.

Well	Location	Thickness (m)	Well	Location	Thickness (m)
7225/3-2	Bjarmeland Platform	17	7132/2-2	eastern Finnmark Platform	14
7335/3-1	Bjarmeland Platform	136	7229/11-1	eastern Finnmark Platform	130
7220/2-1	Bjørnøyrenna Fault Complex	425	7122/7-7 S	Hammerfest Basin	32
7220/7-2 S	Bjørnøyrenna Fault Complex	579	7120/9-2	Hammerfest Basin	262
7324/2-1	eastern Loppa High	23	7222/11-2	Loppa High	44
7324/7-3 S	eastern Loppa High	229	7120/1-1	Loppa High	414
7321/8-2 S	Fingerdjupet Basin	57	7124/4-1 S	Måsøy Fault Complex	18
7321/7-1	Fingerdjupet Basin	168	7125/4-1	Måsøy Fault Complex	120
7122/10-1 S	western Finnmark Platform	67	7228/7-1 S	Nordkapp Basin	118
7120/12-1	western Finnmark Platform	198	7227/10-1	Nordkapp Basin	234

Table 4.3. Selected wireline logs used to compose a NBSS stratigraphic and correlation section.

Well	Location	Well	Location
7120/12-1	Hammerfest Basin	7228/2-1 S	Nordkapp Basin
7120/9-2	Hammerfest Basin	7227/10-1	Nordkapp Basin
7121/5-1	Hammerfest Basin	7228/7-1 S	Nordkapp Basin
7122/4-1	Hammerfest Basin	7229/11-1	northeastern Finnmark Platform
7222/11-1	Loppa High	7132/2-2	northeastern Finnmark Platform
7224/7-1	Bjarmeland Platform	7335/3-1	eastern Bjarmeland Platform
7226/2-1	Bjarmeland Platform	7435/12-1	eastern Bjarmeland Platform

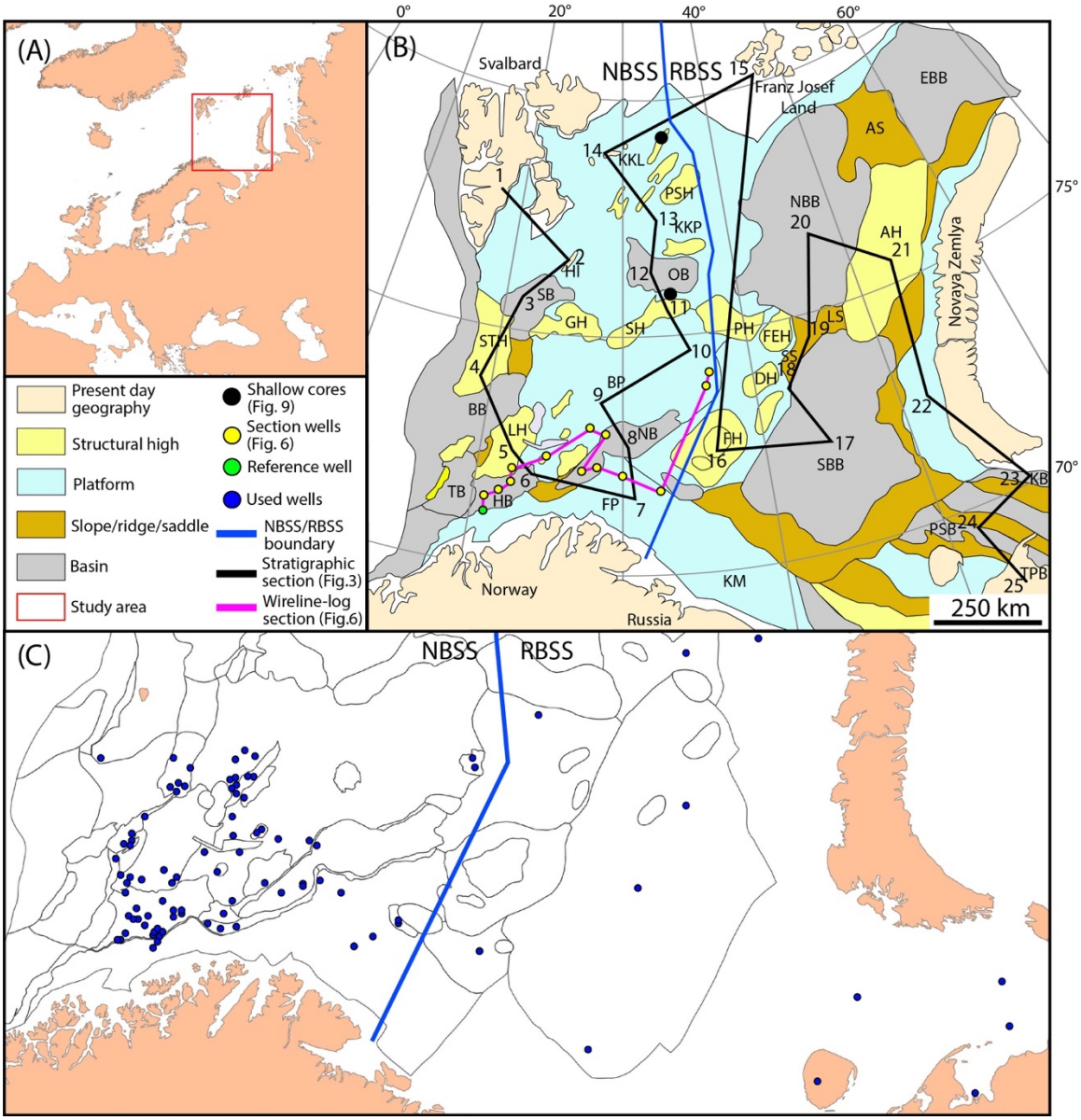

Figure 4.1. (A) Geographic location, (B) Main BSS structural elements, and (C) Hydrocarbon exploration well locations with data applied in the study. AH=Admiralty High; AS=Albanovskaya Saddle; BB=Bjørnøya Basin; BP=Bjarmeland Platform; DH=Demidovskaya High; EBB=East Barents Basin; FEH=Fersmanovskaya High; FH=Fedinsky High; ; FP=Finnmark Platform; GH=Gardarbanken High; HB=Hammerfest Basin; HI=Hopen Island; KB=Korothaika Basin; KKL=Kong Karls Land; KKP=Kong Karl Platform; KM=Kola Monocline; LH=Loppa High; LS=Ludlovskaya Saddle; NB=Nordkapp Basin; NBB=North Barents Basin; OB=Olga Basin; PH=Polarrev High; PSB=Pechora Sea Basin; PSH=Perseu High; SB=Sørkapp Basin; SBB=South Barents Basin; SH=Sentralbanken High; SS=Shtokman Saddle; STH=Stappen High; TB=Tromsø Basin; and TPB=Timan-Pechora Basin.

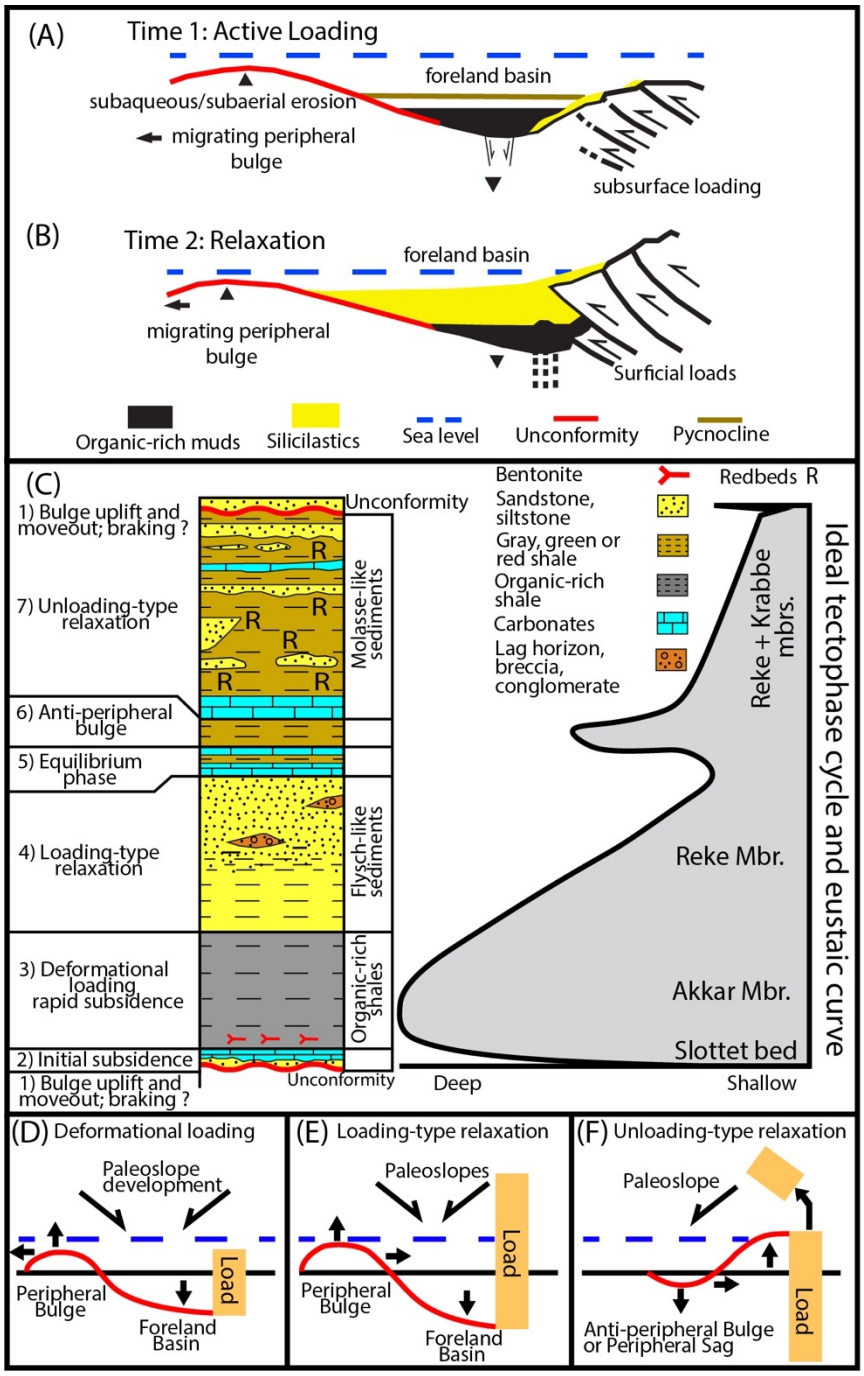

Figure 4.2. (A) and (B) Schematic tectonostratigraphic model illustrating deposition and structural reactivation during phases of active loading and relaxation. (C) Schematic lithologic succession representing an ideal tectophase cycle at outcrop scale with the associated eustatic curve. (D), (E), and (F) Schematic flexural model illustrating phases of deformational loading, loading-type relaxation, and unloading-type relaxation. Figures modified from Ettensohn et al., 2019.

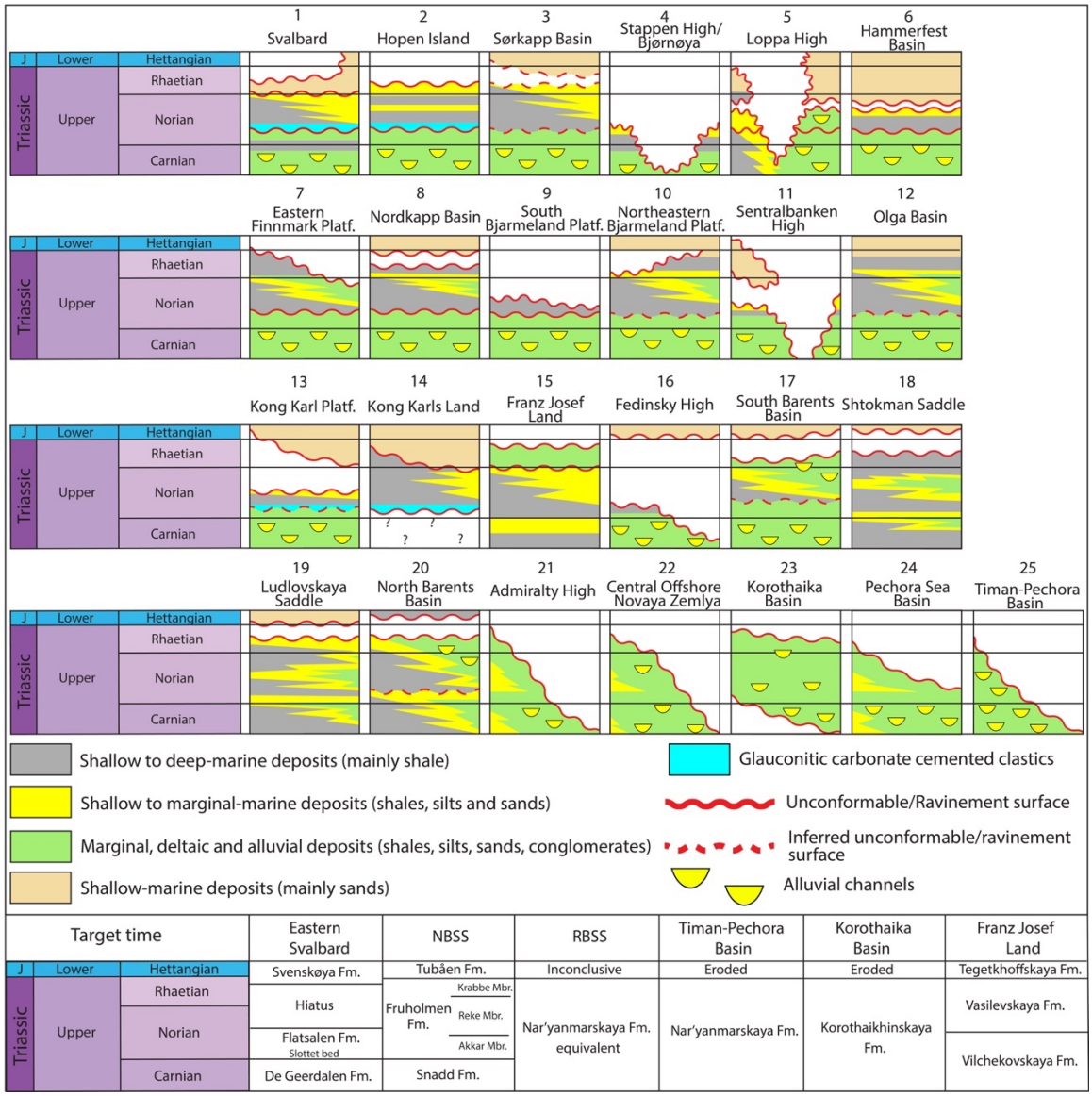

Figure 4.3. Stratigraphic compilation and interpreted depositional environments from selected BSS locations and adjacent areas. Key references include Dalland et al., (1988); Mørk (1989); Johansen et al. (1993); Grogan et al. (1999); Riis et al., (2008); Smelror et al. (2009); Stoupakova et al. (2011); Lundschien et al. (2014); Norina et al. (2014); Ryseth, 2014; Spina et al. (2015); Burguto et al. (2016); Fleming et al. (2016); Lerch et al. (2016); Sobornov and Astafiev (2017); Olaussen et al. (2018); Khudoley et al. (2019); Paterson et al. (2016); Paterson and Mangerud (2017, 2019); Line et al. (2020); Gilmullina et al. (2021); and Martins et al. (2022). Formation names and ages are compiled from Dibner and Krylova (1963); Embry (1992); Mørk (1999); Schenk (2011); Lord et al. (2014); Paterson and Mangerud (2017, 2019); Line et al. (2020); and Gilmullina et al. (2021).

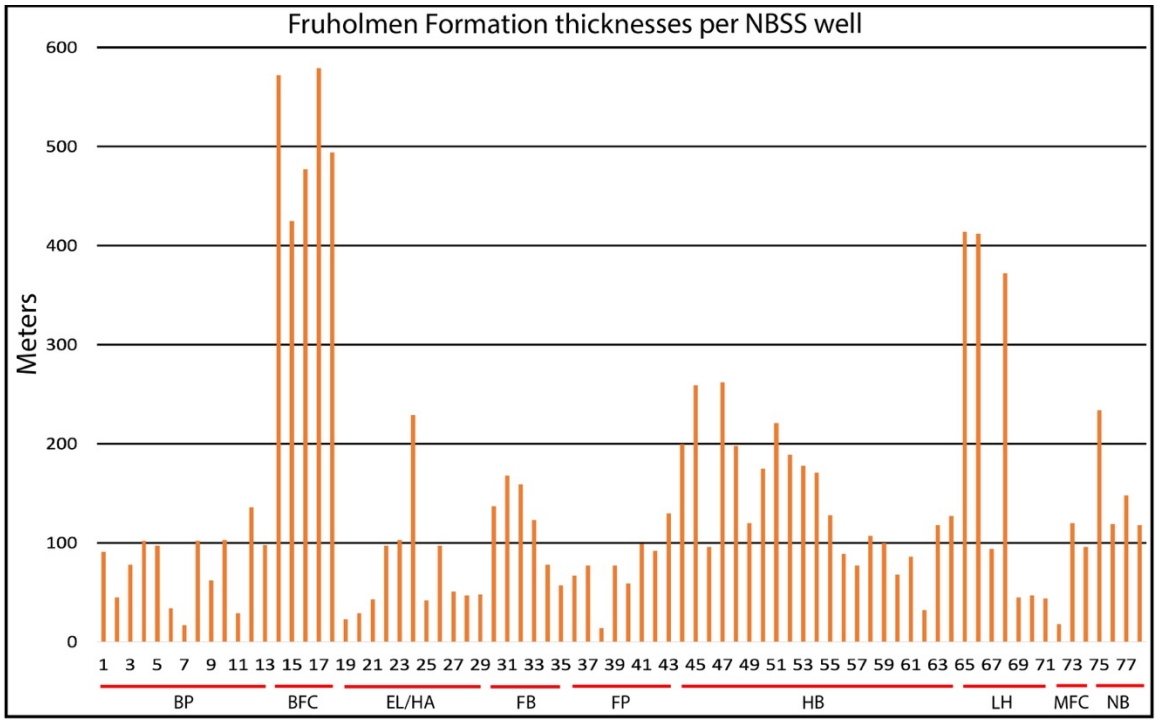

Figure 4.4. Thickness values of the Fruholmen Formation in 78 NBSS wells relative to structural elements. BP=Bjarmeland Platform; BFC= Bjørnøyrenna Fault Complex; EL/HA=East Loppa/Hoop area; FB= Fingerdjupet Basin; FP=Finnmark Platform; HB=Hammerfest Basin; LH=Loppa High; MFC= Måsøy Fault Complex; and NB=Nordkapp Basin.

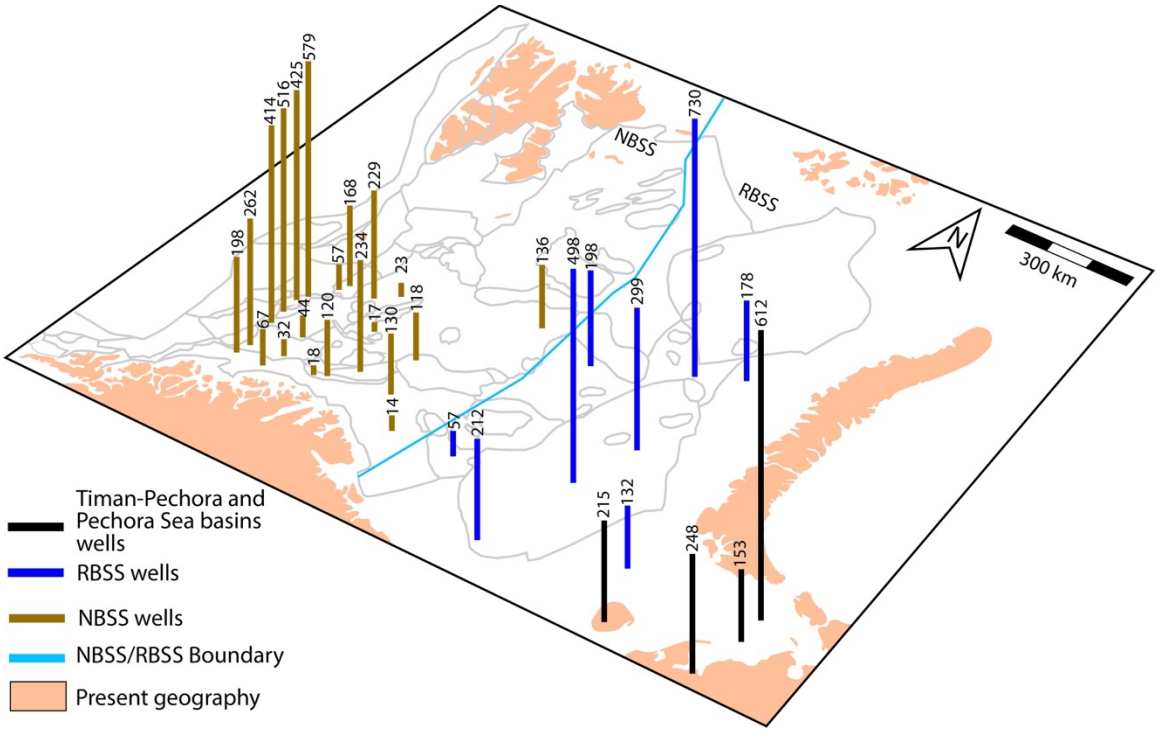

Figure 4.5. Maximum and minimum thicknesses for the Fruholmen Formation on the NBSS (brown), for approximately equivalent deposits on the RBSS (blue), and for the Pechora Sea and Timan-Pechora areas (black).

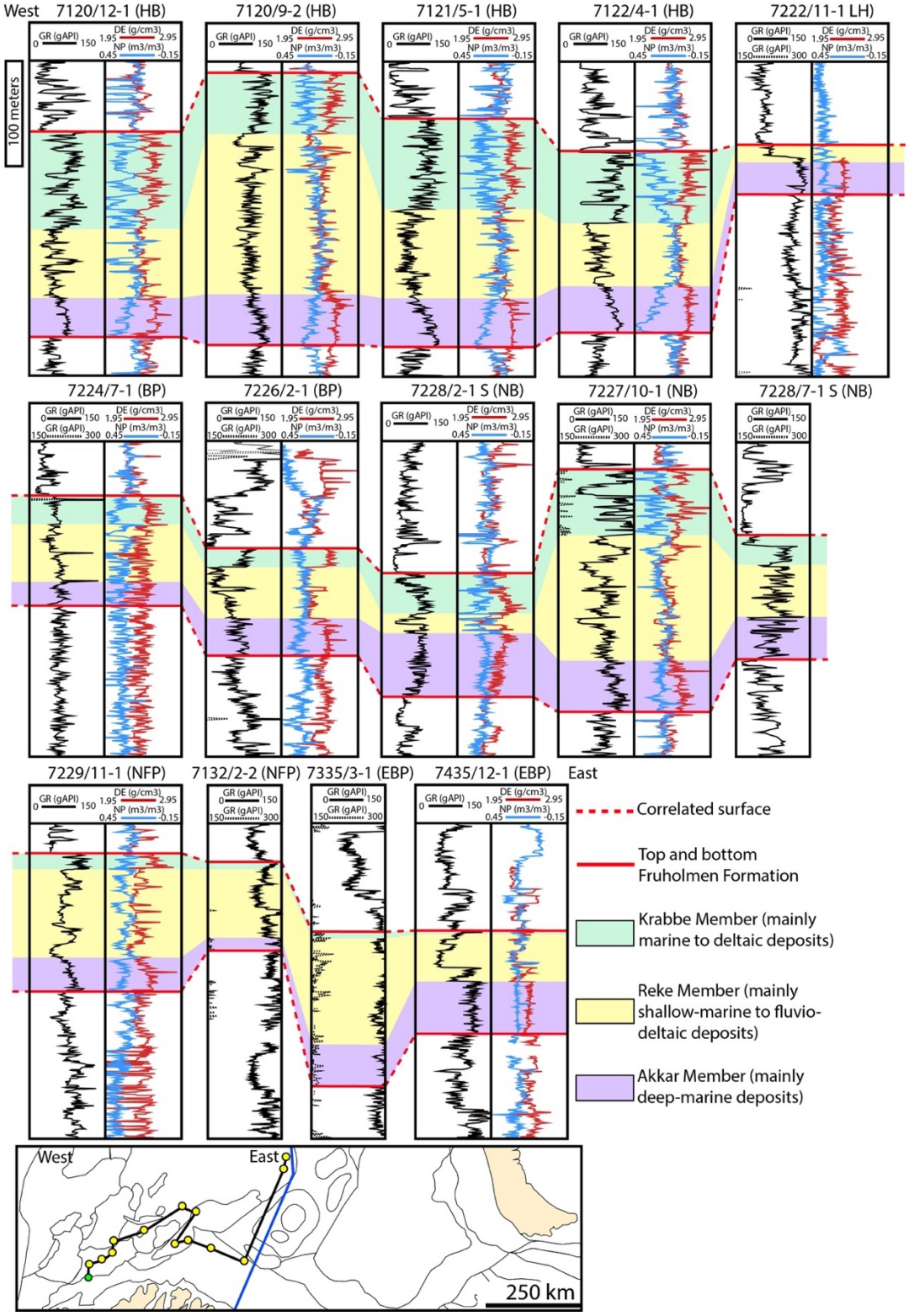

Figure 4.6. NBSS wireline-log correlation. Well 7120/12-1 is the Fruholmen reference well used for correlation. HB=Hammerfest Basin; LH=Loppa High; BP=Bjarmeland Platform; NB=Nordkapp Basin; NFP= northern Finnmark Plaftform; and EBP=eastern Bjarmeland Platform.

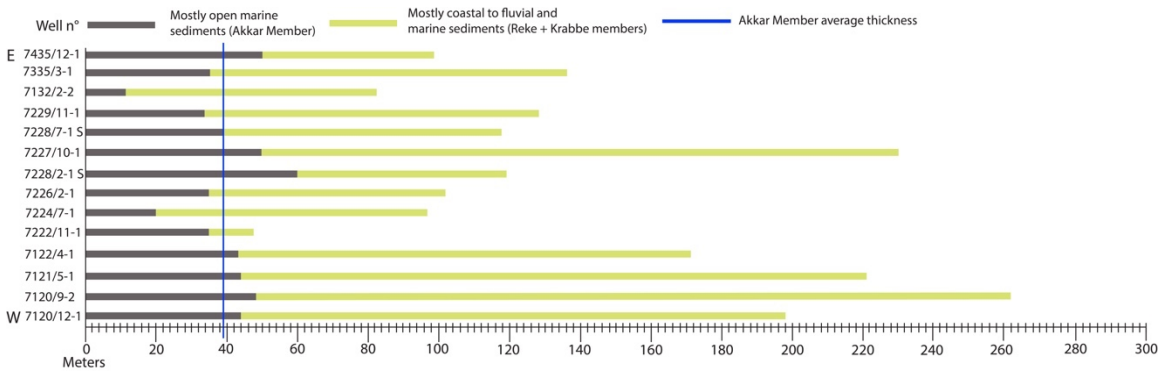

Figure 4.7. Thicknesses for the Akkar Member (dark gray) and Reke plus Krabbe members (yellow) in the various wireline logs used in the correlation line.

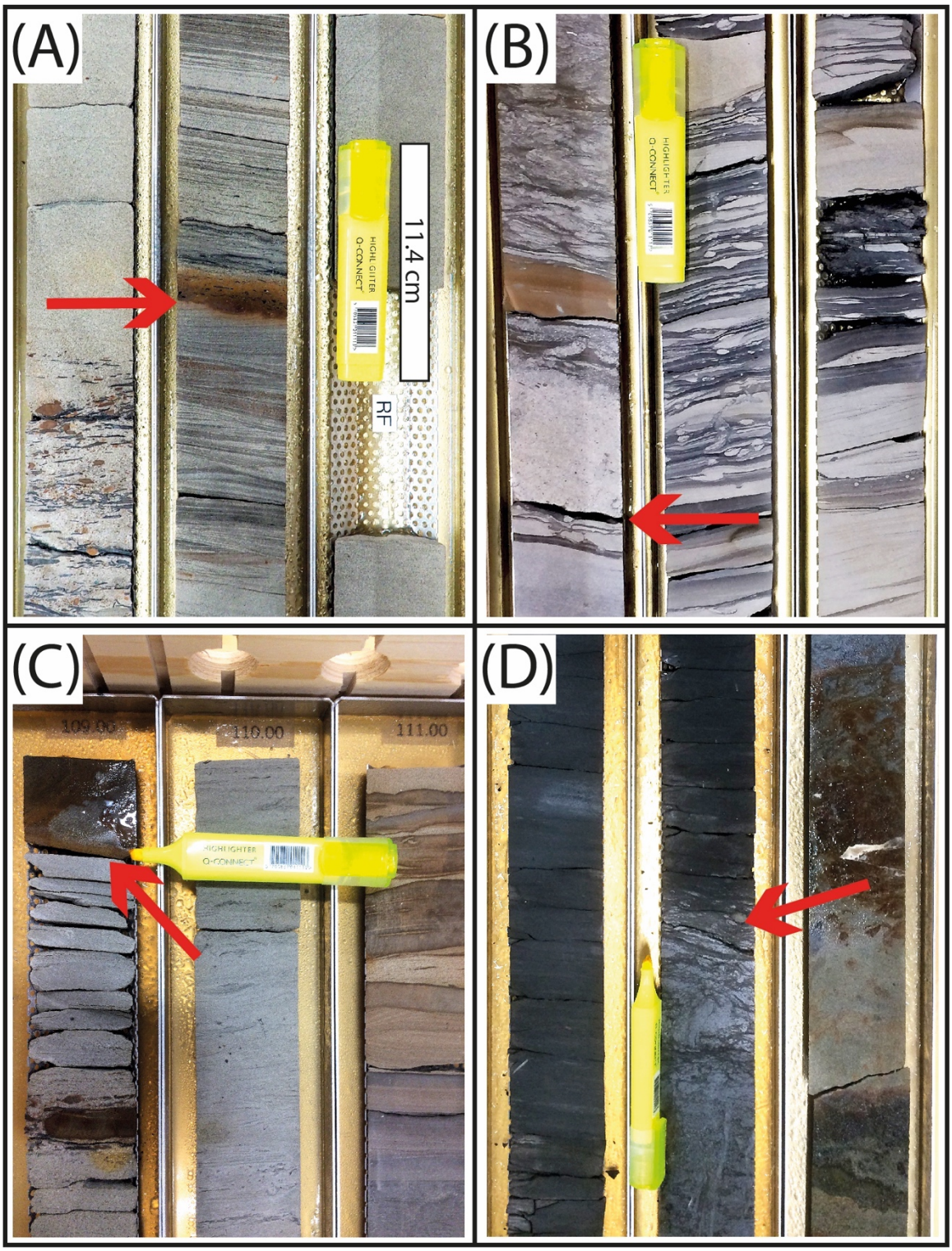

Figure 4.8. Photographs of cores from shallow boreholes 7533/2-U-2 and 7934/8-U-1 (Fig. 4.1). (A) Rhaetian-Hettangian unconformity; (B) Contact between the Slottet Bed and De Geerdalen Formation; (C) Contact between the Slottet Bed and De Geerdalen Formation; and (D) Transition between the Slottet Bed and organic-rich shales equivalent to the Akkar Member.

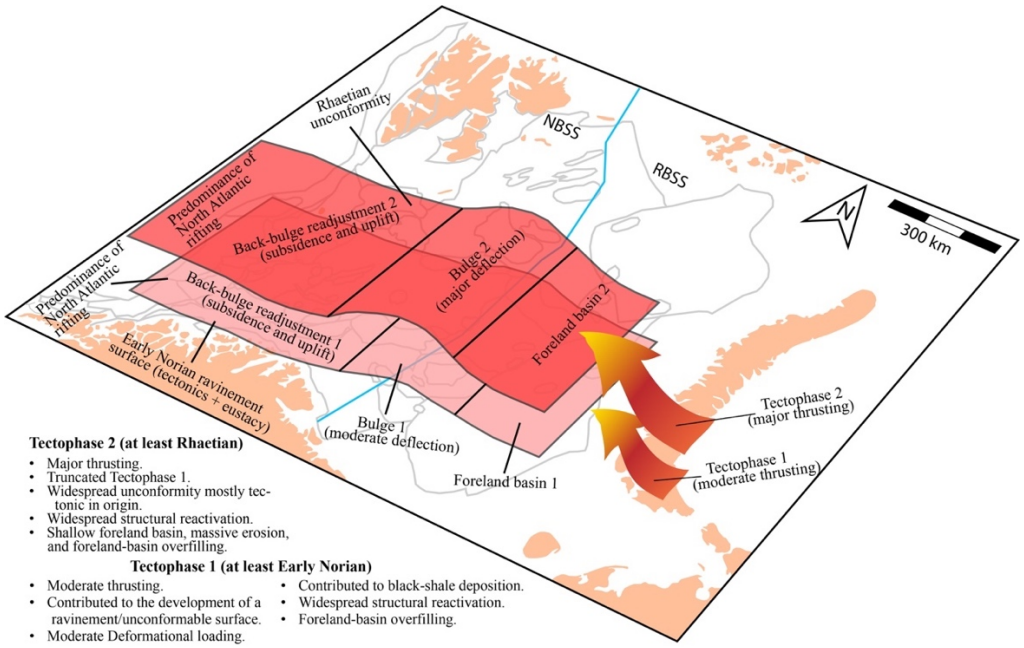

Figure 4.9. Integrative BSS map schematically illustrating the depozones associated with the two Novaya Zemlya tectophases.

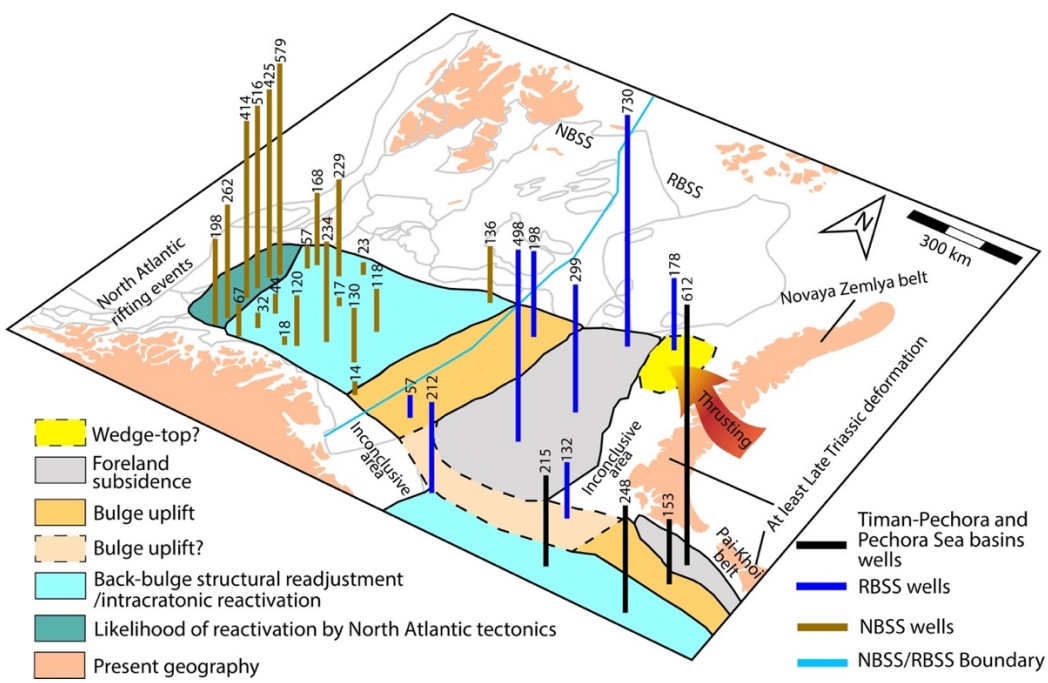

Figure 4.10 Norian–Rhaetian foreland-basin development and depozones across the southern BSS and adjacent areas. Maximum and minimum thicknesses (numbered columns) for the Fruholmen Formation on the NBSS (brown), for approximately equivalent deposits on the RBSS (blue), and the Pechora Sea and Timan-Pechora basins (black). Foreland depozone nomenclature is from DeCelles and Gilles (1996).

CHAPTER 5. CONCLUSIONS

This study shows that the Appalachian System of Basins and Platforms (ASBP) has analogue potential for the Barents Sea Shelf (BSS), because of the regional tectonic and geodynamic similarities between both areas. In Chapter 2 (Publication 1), these similarities are systematically compared, and limitations, such as timing, paleogeography, and paleoclimate, are addressed. Even though these limitations are real, very similar ASBP-BSS stratigraphic successions reflect very similar tectonostratigraphic processes and geologic history. Because of these similarities, flexural models used for the ASBP are also used for the Late Paleozoic–pre-Middle Mesozoic BSS succession in terms of the development of a regional foreland-intracratonic-basin system. As in the ASBP, the use of flexural models may help to explain how phases of the Uralian-Pai-Khoi-Novaya Zemlya orogeny, during the collision of Siberia-Kazakhstania with northern Baltican parts of Pangea, generated tectonostratigraphic responses in adjacent parts of the craton.

To refine the potential of the ASBP analogue, a more detailed analysis was done in the target BSS area to identify likely analogous processes. The ASBP is traditionally interpreted in terms of diachronous structural reactivation in space and time, which is at times coeval with deformation in the adjacent Appalachian orogen. Chapters 3 and 4 (Publications 2 and 3) investigate similar patterns across the BSS from a structural (Chapter 3) and stratigraphic (Chapter 4) point of view. In Chapter 3, backstripping analyses show that the Upper Triassic–Middle Jurassic BSS stratigraphy reflects widespread regional reactivation of basement structures due to the transmission of far-field forces related to deformation in the adjacent Uralian-Pai-Khoi-Novaya Zemlya orogen. Similarly, Chapter 4 uses Upper Triassic–Middle Jurassic stratigraphic thicknesses and unconformity analyses

as indicators for two phases of foreland-basin development and coeval intracratonic structural reactivation beyond the foreland during the Novaya Zemlya orogeny. Both structural and stratigraphic observations provide arguments suggesting that basement structures and resulting stratigraphy were controlled by far-field forces related to diachronous orogeny, similar to those in the ASBP. However, results in both chapters are limited by a dearth of wells deep enough to penetrate strata older than Triassic and the lack of access or availability of wells in Russian parts of the BSS.

Future research is needed to refine and calibrate the use of analogues in comparing ASBP and BSS processes and responses at a more local scale. These studies might include attempts to use other methodologies and techniques (e.g., quantitative modelling) beyond flexural models. It is my hope that there will be future interest among the scientific community for continued testing of the analogue. I am certain that many answers for problems in the Upper Paleozoic–Middle Mesozoic rocks below the icy waters of the Barents Sea lie hidden in analogues with the old Appalachian mountains.

APPENDIX

NBSS (source: NPD 2022)			
Well name	Location	Oldest strata (age)	Total thickness (m)
7120/1-1	Loppa High	Late Permian	2201
7120/1-3	Loppa High	Late Permian	2173
7120/2-3 S	Hammerfest Basin	Late Triassic	2284.5
7120/6-2 S	Hammerfest Basin	Late Triassic	2691
7120/9-1	Hammerfest Basin	Late Triassic	1957
7120/9-2	Hammerfest Basin	Late Permian	4753
7120/12-1	Finnmark Platform	Middle Triassic	3324
7120/12-2	Hammerfest Basin	Pre-Devonian	4491
7120/12-5	Finnmark Platform	Middle Triassic	3418
7121/1-1 R	Loppa High	Late Carboniferous	4604.2
7121/5-1	Hammerfest Basin	Late Triassic	2839

7121/5-3	Hammerfest Basin	Late Triassic	1892.5
7121/8-1	Hammerfest Basin	Late Triassic	1852
7122/4-1	Hammerfest Basin	Late Triassic	2647
7122/6-1	Hammerfest Basin	Middle Triassic	2283
7122/6-2	Hammerfest Basin	Middle Triassic	2639
7122/7-1	Hammerfest Basin	Late Triassic	1117.6
7122/7-2	Hammerfest Basin	Late Triassic	1022
7122/7-4 S	Hammerfest Basin	Early Triassic	1994
7122/7-5	Hammerfest Basin	Early Triassic	1834
7122/7-5 A	Hammerfest Basin	Middle Triassic	1580
7122/7-6	Hammerfest Basin	Early Triassic	1612

7122/7-7 S	Hammerfest Basin	Late Triassic	862
7122/10-1 S	Finnmark Platform	Middle Triassic	951
7123/4-1 A	Hammerfest Basin	Late Triassic	2190
7123/4-1 S	Hammerfest Basin	Middle Triassic	2270
7124/3-1	Hammerfest Basin	Late Carboniferous	4431
7124/4-1 S	Loppa High	Early Triassic	2388
7125/1-1	Bjarmeland Platform	Middle Triassic	1923.3
7125/4-1	Måsøy Fault Complex	Early Triassic	1299
7125/4-2	Måsøy Fault Complex	Early Triassic	1433
7130/4-1	Finnmark Platform	Early Carboniferous	2872
7131/4-1	Finnmark Platform	Middle Triassic	939
7132/2-1	Finnmark Platform	Late Triassic	559

7132/2-2	Finnmark Platform	Late Permian	3192
7219/9-1	Bjørnøyrenna Fault Complex	Late Triassic	3907
7219/12-1	Hammerfest Basin	Late Triassic	2148
7220/2-1	Bjørnøyrenna Fault Complex	Late Triassic	1121
7220/4-1	Bjørnøyrenna Fault Complex	Middle Triassic	2805
7220/7-2 S	Bjørnøyrenna Fault Complex	Late Triassic	1350
7220/8-1	Bjørnøyrenna Fault Complex	Late Triassic	1824
7220/10-1	Loppa High	Late Triassic	2030
7221/12-1	Loppa High	Late Triassic	348
7222/11-1	Bjarmeland Platform	Middle Triassic	2246
7222/11-2	Loppa High	Early Triassic	2540
7223/5-1	Bjarmeland Platform	Early Triassic	2185.6
7224/2-1	Bjarmeland Platform	Early Triassic	2502

7224/6-1	Bjarmeland Platform	Middle Triassic	2049
7224/7-1	Bjarmeland Platform	Early Triassic	2771.5
7225/3-1	Bjarmeland Platform	Early Permian	3731
7225/3-2	Bjarmeland Platform	Early Triassic	1803
7226/2-1	Bjarmeland Platform	Early Triassic	2621
7226/11-1	Bjarmeland Platform	Pre-Devonian	4939.5
7227/10-1	Måsøy Fault Complex	Middle Triassic	2863
7228/1-1	Bjarmeland Platform	Middle Triassic	1320.5
7228/2-1 S	Nordkapp Basin	Early Triassic	3627
7228/7-1 A	Nordkapp Basin	Early Triassic	2536
7228/7-1 S	Nordkapp Basin	Early Permian	1675
7228/9-1 S	Finnmark Platform	Early Permian	4175.5
7229/11-1	Finnmark Platform	Late Carboniferous	4319.7

7317/9-1	Nordkapp Basin	Late Triassic	1031
7321/4-1	Fingerdjupet Subbasin	Late Triassic	1102
7321/7-1	Fingerdjupet Subbasin	Middle Triassic	3046.5
7321/8-1	Fingerdjupet Subbasin	Late Permian	2979
7321/8-2 S	Fingerdjupet Subbasin	Late Triassic	1311
7321/9-1	Fingerdjupet Subbasin	Late Triassic	1316.5
7324/2-1	East Loppa/Hoop Area	Late Triassic	606
7324/3-1	East Loppa/Hoop Area	Late Triassic	1226
7324/6-1	East Loppa/Hoop Area	Late Triassic	1120
7324/7-1 S	Bjarmeland Platform	Middle Triassic	2039
7324/7-2	East Loppa/Hoop Area	Middle Triassic	1251.5
7324/7-3 S	East Loppa/Hoop Area	Late Triassic	271

7324/8-1	East Loppa/Hoop Area	Late Triassic	507
7324/8-2	East Loppa/Hoop Area	Middle Triassic	421
7324/9-1	East Loppa/Hoop Area	Late Triassic	646
7324/10-1	Bjarmeland Platform	Early Triassic	2488
7325/1-1	East Loppa/Hoop Area	Early Triassic	2378
7325/4-1	East Loppa/Hoop Area	Late Triassic	731
7335/3-1	Bjarmeland Platform	Early Triassic	4030
7435/12-1	Bjarmeland Platform	Middle Triassic	1254
RBSS wells (sources: Astafiev et al., 2008; Gavrilov et al., 2010; Zhuravlev et al., 2014; Burguto et al., 2016; Khudoley et al., 2019; Gilmullina et al., 2021)			
Well name	Location	Oldest strata	Total thickness (m)
Arkticheskaya-1	South Barents Basin	Ladinian	4286
Fersmanovskaya-1	Fersmanovskaya High area	Early Triassic	2945.6

Kolguevskaya-140	Kolguyev Island	Early Triassic	1450
Krestovaya-1	Admiralty High	Early Triassic	3750 (pre-Jurassic/Cretaceous strata excluded)
Kurentsovskaya-1	Kurentsovskaya Steps	Middle Triassic	3230.5
Ludlovskaya-1	Ludlovskaya Saddle	Early Triassic	2630 (pre-Middle Jurassic strata excluded)
Murmanskaya-24	Kola Monocline	Early Triassic	4270
Nosovaya-1	Timan-Pechora Basin	Early Triassic	1554 (only Triassic to Cretaceous strata included)
Severo-Dolginskaya-1	Pechora Sea Basin	Early Triassic	2396
Severo-Gulyaevskaya-1	Pechora Sea Basin	Early Triassic	2167
Severo-Kildinskaya-80	Kola Monocline	Early Triassic	3079.6
Severo-Murmanskaya-1	South Barents Basin	Late Triassic	2927
Shtockmanovskaya-1	South Barents Basin	Late Triassic	2874.2

REFERENCES

Abrams, M.A., Apanel, A.M., Timoshenko, O.M., and Kosenkova, N.N., 1999, Oil families and their potential sources in the northeastern Timan Pechora Basin, Russia: American Association of Petroleum Geologists Bulletin, v. 83, p. 553–577.

Alexander, J., 1993, A discussion on the use of analogues for reservoir geology, *in* Ashton, M., eds., Advances in Reservoir Geology: London, Geological Society Special Publication, v. 69, p. 175–194.

Allen, P.A., and Allen, J.R., 2013, Basin Analysis: Principles and Application to Petroleum Play Assessment: Wiley-Blackwell, West Sussex, 632 p.

Allen, P.A., and Armitage, J.J., 2012, Cratonic basins, *in* Busby, C., and Azor, A., eds., Tectonics of Sedimentary Basins: Recent Advances: West Sussex, Willey-Blackwell, p. 602–620.

Allen, P.A., Crampton, S.L., and Sinclair, H.D., 1991, The inception and early evolution of the north Alpine foreland basin, Switzerland: Basin Research, v. 3, p. 143–163.

Alsgaard, P.C., 1993, Eastern Barents Sea Late Palaeozoic setting and potential source rocks, *in* Vorren, T. O., Bergsager, E., Dahl-Stamnes, Ø.A., Holter, E., Johansen, B., Lie, E., and Lund, T.B., eds., Arctic Geology and Petroleum Potential: Amsterdam, NPF Special Publication, v. 2, p. 405–418.

Amantov, A., and Fjeldskaar, W., 2018, Meso-Cenozoic exhumation and relevant isostatic process: The Barents and Kara shelves: Journal of Geodynamics, v. 118, p. 118–139.

An, M., and Assumpção, M., 2006, Crustal and upper mantle structure in the intracratonic Paraná basin SE Brasil, from surface wave dispersion using genetic algorithms: Journal of South American Earth Sciences, v. 21, p. 173–184.

Anell, I., Braathen, A., and Olaussen, S., 2014, The Triassic-Early Jurassic of the northern Barents shelf: A regional understanding of the Longyearbyen CO2 reservoir: Norwegian Journal of Geology, v. 94, p. 83–98.

Anell, I., Braathen, A., Olaussen, S., and Osmundsen, P.T., 2013, Evidence of faulting contradicts a quiescent northern Barents shelf during the Triassic: First Break, v. 31, p. 67–76.

Anell, I., Faleide, J.I., Braathen, A., 2016, Regional tectono-sedimentary development of the highs and basins of the northwestern Barents shelf: Norwegian Journal of Geology v. 96, p. 27–41.

Angevine, C.L., P.L. Heller, and C. Paola. 1990. Quantitative sedimentary basin modeling. American Association of Petroleum Geologists Continuing Education Course Notes 32, 133 p.

Armitage, J.J., and Allen, P.A., 2010, Cratonic basins and the long-term subsidence history of continental interiors: Journal of the Geological Society, v. 167, p. 61–70.

Arthaud, F., and Matte, P., 1977, Late Palaeozoic strike-slip faulting in southern Europe and northern Africa: Result of a right-lateral shear zone between the Appalachians and the Urals: Geological Society of America Bulletin, v. 88, p. 1305–1320.

Artyushkov, E.V., and Baer, M.A., 1983, Mechanism of continental crust subsidence in fold belts: The Urals, Appalachians and Scandinavian Caledonides: Tectonophysics, v. 100, p. 5–42.

Artyushkov, E.V., and Baer, M.A., 1985, Mechanism of formation of deep basins in continental crust in fold belts: Journal of Geodynamics, v. 2, p. 67–84.

Artyushkov, E.V., and Baer, M.A., 1986, Mechanisms of formation of hydrocarbon basins: The West Siberia, Volga-Urals, Timan-Pechora basins and the Permian Basin of Texas: Tectonophysics, v. 122, p. 247–281.

Astafiev, B.Y., Viskunova, K.G., Voinova, O.A., Glaznev, V.N., Zhuravlev, V.A., Zhuravlev, V.I.A., Zinchenko, A.G., Kozlov, S.A., Kostin, D.A., Lopatin, B.G., Markina, N.V., Paramonova, M.S., Povysheva, L.G., Semenova, L.R., Tomilina, O.V., Chekushin, V.A., Shipilov, E.V., Shkarubo, S.I., and Yakovleva, T.V., 2008, State Geological Map of the Russian Federation (in Russian): Saint Petersburg, VSEGEI, The North-Kara-Barents Sea series, Sheets R-37 and R-38, Scale 1: 1,000,000.

Baig, I., Faleide, J.I., Jahren, J., and Mondol, N.H., 2016, Cenozoic exhumation on the southwestern Barents Shelf: estimates and uncertainties constrained from compaction and thermal maturity analyses: Marine and Petroleum Geology, v. 73, p. 105–130.

Baiyegunhi, C., Liu, K., and Gwavava, O., 2017, Sedimentation rate and subsidence history of the southeastern Karoo Basin, South Africa, using 1D backstripping method: Arabic Journal of Geosciences, v. 10, p. 1–21.Beaumont, C. , 1981, Foreland basins: Geophysical Journal of the Royal Astronomical Society, v. 65, p. 291–329. https://doi.org/10.1111/j.1365-246X.1981.tb027 15.x

Beaumont, C., Quinlan, G.M., and Hamilton, J., 1987, The Alleghanian Orogeny and its relationship to the evolution of the eastern interior, in Beaumont, C.,and Tankard, A.J., eds., Sedimentary Basins and Basin-Forming Mechanisms: Canadian Society of Petroleum Geologists Memoir v. 12, p. 425–445.

Beaumont, C., Quinlan, G.M., and Hamilton, J., 1988, Orogeny and stratigraphy: Numerical models of the Paleozoic in the eastern interior of North America: Tectonics, v. 7, p. 389–416.

Beglinger, S.E., van Wees, J.-D., Cloetingh, S., and Doust, H., 2013, Tectonic subsidence history and source-rock maturation in the Campos Basin, Brazil: Petroleum Geoscience, v. 18, p. 153–172.

Bergan, M., and Knarud, R., 1993, Apparent changes in clastic mineralogy of the Triassic–Jurassic succession, Norwegian Barents Sea:possible implications for paleodrainage and subsidence, *in* Vorren, T.O., Bergsager, E., Dahl-Stamnes, Ø.A., Holter, E., Johansen, B., Lie, E., and Lund, T.B., eds., Arctic Geology and Petroleum Potential: Amsterdam, Elsevier, v. 2, p. 363–376.

Berra, F., and Carminati, E., 2010, Subsidence history from a backstripping analysis of the Permo-Mesozoic succession of the central southern Alps (northern Italy): Basin Research, v. 22, p. 952–975.

Blaich, O.A., Tsikalas, F., and Faleide, J.I., 2017, New insights into the tectono-stratigraphic evolution of the southern Stappen High and its transition to Bjørnøya Basin, SW Barents Sea: Marine Petroleum Geology, v. 85, p. 89–105.

Blomeier, D., Scheibner, C., and Forke, H., 2009, Facies arrangement and cyclostratigraphic architecture of a shallow marine, warm-water carbonate platform: The Late Carboniferous Ny Friesland platform in eastern Spitsbergen (Pyefjellet Beds, Wordiekammen Formation, Gipsdalen Group): Facies, v. 55, p. 291–324. https://doi.org/10.1007/s1034 7-008-0163-3

Brekke, H., Sjulstad, H.I., Magnus, C., and Williams, R.W., 1999, Sedimentary environments offshore Norway — an overview, *in* Martinsen, O.J., and Dreyer, T., eds., Sedimentary Environments Offshore Norway – Palaeozoic to Recent: Bergen, Norwegian Petroleum Society, Special Publication, v. 10, p. 7–37.

Brown, L.F., and Fisher. W.L., 1977, Seismic-stratigraphic interpretation of depositional systems: Examples from Brazilian rift and pull-apart basins: Section 2. Application of seismic reflection configuration to stratigraphic interpretation, *in* Payton, C. E., eds., Applications to hydrocarbon exploration: Ann Arbor, Edward Brothers, Memoir, v. 26, p. 51–53.

Brown, D., Alvarez-Marron, J., Perez-Estaun, A., Gorozhanina, Y., and Puchkov, V., 2004, The structure of the South foreland fold and thrust belt at the transition of the Precaspian basin. Journal of the Geological Society: v. 161, p. 813–822.

Brown, D., Puchkov, V., Alvarez-Marron, J., Bea, F., and Perez-Estaun, A., 2006b, Tectonic processes in the southern and middle Urals: an overview, *in* Gee, D.G., and Stephenson, R.A., eds., European Lithosphere Dynamics: London, The Geological Society of London, Memoirs, v. 32, p. 1–15.

Brown, D., Spadea, P., Puchkov, V., Alvarez-Marron, J., Herrington, R., Willner, A.P., Hetzel, R., Gorozhanina, Y., and Juhlin, C., 2006, Arc–continent collision in the southern Urals: Earth-Science Reviews, v. 79, p. 261–287.

Buiter, S.J.H., and Torsvik, T.H., 2007, Horizontal movements in the eastern Barents Sea constrained by numerical models and plate reconstructions: Geophysical Journal International, v. 171, p. 1376–1389.

Bugge, T., Elvebakk, G., Fanavoll, S., Mangerud, G., Smelror, M., Weiss, H.M., Gjelberg, J., Kristensen, S.E., and Nilsen, K., 2002, Shallow stratigraphic drilling applied in hydrocarbon exploration of the Nordkapp Basin, Barents Sea: Marine and Petroleum Geology, v. 19, p. 13–37.

Burguto, A.G., Zhuravlev, V.A., Zavarzina, G.A., and Zinchenko, A.G., 2016, State Geological Map of the Russian Federation (in Russian): Saint Petersburg, VSEGEI, the North- Kara-Barents Sea Series, Sheets S-36 and S-37, Scale 1: 1,000,000.

Camacho, A., Lee, J.K.W., Hensen, B.J., and Braun, J., 2005, Short-lived orogenic cycles and the eclogitization of cold crust by spasmodic hot fluids: Nature, v. 435, p. 1191–1196.

Catuneanu, O., Galloway, W.E., Kendall, C.G.St.C., Miall, A.D., Posamentier, H.W., Strasser, A., and Tucker, M.E., 2011, Sequence stratigraphy: Methodology and nomenclature: Newsletters on Stratigraphy, v. 44, p. 173–245.

Cecchi, M., Markello, J., and Waite, L., 1995, Sequence stratigraphy architecture of Carboniferous–Permian sedimentary systems of the Norwegian Barents Sea with comparison to coeval systems of the USA, *in* Steel, R.J., eds., Sequence stratigraphy on the northwest European margin: Amsterdam, Elsevier, v. 5, p. 545–569.

Chirva, S.A., Morakhovskaya, E.D., Kulikova, N.K., Fedorova, V.A., and Yakovleva, S. P., 1990, Stratigraphy of the Triassic and Jurassic deposits of the Barents Sea, *in* Oknova, N. S., Slavin, V. I., and Desyatkov, V. M., eds., Geological structure and oil and gas potential of the Arctic islands: Leningrad, VNIGRI, v. 7, p. 15–30.

Cloetingh, S., and Lankreijer, A., 1992, Subsidence history analysis and forward modelling of the Cape and Karoo supergroups, *in* De Wit, M.J., and Ransome, I., eds., Inversion tectonics of the Cape fold belt, Karoo and Cretaceous basins of southern Africa: Rotterdam, Balkema, p. 239–248.

Cloetingh, S., and Burov, E., 2011, Lithospheric folding and sedimentary basin evolution: A review and analysis of formation mechanisms: Basin Research, 23, 257–290.

Cluff, R.M., and Dickerson, D.R., 1982, Natural gas potential of the New Albany Shale group (Devonian-Mississippian) in southeastern Illinois: Society of Petroleum Engineers Journal, v. 22, p. 291–300.

Coakley, B.J., and Watts, A.B., 1991, Tectonic controls on the development of unconformities: The North Slope, Alaska: Tectonics, v. 10, p. 101–130.

Cohen, K.M., Finney, S.C., Gibbard, P.L., and Fan, J.-X., 2022, The ICS International Chronostratigraphic Chart: v. 36, p. 199–204. Retrieved from. https://stratigraphy.org/ICSchart/ChronostratChart2022-02.pdf.

Colton, G.W., 1970, The Appalachian basin—Its depositional sequences and their geologic relationships *in* Fisher, G.W., Pettijohn, F.J., Reed, J.C., Jr., and Weaver, K.N., eds., Studies of Appalachian geology: Central and Southern: New York, Interscience Publishers, New York, p. 5–47.

Corfu, F., Andersen, T.B., and Gasser, D., 2014, The Scandinavian Caledonides: main features, conceptual advances and critical questions, *in* Corfu, F., Gasser, D., and Chew, D.M., eds., New Perspectives on the Caledonides of Scandinavia and Related Areas: London, The Geological Society of London, Special Publications, v. 390, p. 9–43.

Curtis, J.B., and Faure, G., 1997, Accumulation of organic matter in the Rome trough of the Appalachian basin and its subsequent thermal history: American Association of Petroleum Geologists Bulletin, v. 81, p. 424–437.

Curtis, M.L., Lopez-Mir, B., Scott, R.A., and Howard, J.P., 2018, Early Mesozoic sinistral transpression along the Phai-Khoi-Novaya Zemlya fold–thrust belt, Russia, *in* Pease, V., and Coakley, B., eds., Circum-Arctic Lithosphere Evolution: London, Geological Society, Special Publications, v. 460, p. 355–370.

Dalland, A., Worsley, D. and Ofstad, K., 1988, A lithostratigraphical scheme for the Mesozoic and Cenozoic succession, offshore mid- and northern Norway: Stavanger, Norwegian Petroleum Directorate, v. 4, 65 p.

Dallmann, W.K., Blomeier, D., Elvevold, S., Mørk, A., Olaussen, S., Grundvåg, S.-A., Bond, D., and Hormes, A., 2015, Historical Geology, *in* Dallmann, W.K., eds., Geoscience Atlas of Svalbard: Tromsø, Norsk Plarinstitutt, v. 148, p. 89–181.

DeCelles, P.G., and Giles, K.A., 1996, Foreland basin systems: Basin Research, v. 8, p. 105–123.

Dedeev, V.A., 1959, Interrelationships of the Polar Urals with neighboring folded regions: Trudy VNIGRI, Geology, v. 126, p. 371–399) (in Russian).

de Klein, G.V., and Hsui, A.T., 1987, Origin of cratonic basins: Geology, v. 15, p. 1094–1098.

Denison, R.E., 1989, Foreland structure adjacent to the Ouachita forebelt, *in* Hatcher, R.D., Jr., Thomas, W.A., and Viele, G.W., eds., The Appalachian-Ouachita Orogen in the United States, The Geology of North America: Boulder, Geological Society of America, v. F-2, p. 681–688.

Dibner, V.D., and Krylova, N.M., 1963, Stratigraphic position and material composition of coal measures in Franz Josef Land: Soviet Geology, v. 7, p. 77–89.

DiPietro, J.A., 2018, Geology and landscape evolution: Amsterdam, Elsevier, 624 p.

Drachev, S.S., 2016, Fold belts and sedimentary basins of the Eurasian Arctic: Arktos, v. 2, p. 1–30.

Drachev, S.S., Malyshev, N.A., and Nikishin, A.M., 2010, Tectonic history and petroleum geology of the Russian Arctic shelves: an overview, *in* Vining, B.A., and Pickering, S.C., eds., Petroleum Geology Conferences: London, Geological Society of London, p. 591–619.

Eide, C.H., Klausen, T.G., Katkov, D., Suslova, A.A., and Helland-Hansen, W., 2017, Linking an Early Triassic delta to antecedent topography: source-to-sink study of the southwestern Barents Sea margin: GSA Bulletin, v. 130, p. 263–283.

Embry, A.F., 1992, Mesozoic stratigraphy of Franz Josef Land archipelago, Arctic Russia – A literature review: 1992 ICAM, v. 94, p. 15–21.

Embry, A., 1997, Global sequence boundaries of the Triassic and their identification in the Western Canada sedimentary basin: Bulletin of Canadian Petroleum Geology, v. 45, p. 415–433.

Embry, A., 2009, Crockerland – The source area for the Triassic to Middle Jurassic strata of Northern Axel Heiberg Island, Canadian Arctic Islands: Bulletin of Canadian Petroleum Geology, v. 57, p. 129–140.

Embry, A.F., and Johannessen, E. P., 2017, Two approaches to sequence stratigraphy, *in* Montenari, M., eds., Stratigraphy and Timescales: Cambridge, Elsevier, p. 85–118.

Ershova, V.B., Prokopiev, A.V., and Khudoley, A.K., 2015, Integrated provenance analysis of Carboniferous deposits from northeastern Siberia: Implication for the late Paleozoic history of the Arctic: Journal of Asian Earth Sciences, v. 109, p. 38–49.

Ershova, V., Prokopiev, A., Stockli, D., Kurapov, M., Kosteva, N., Rogov, M., Khudoley, A., and Petrov, E.O., 2022, Provenance of the Mesozoic succession of Franz Josef Land (north-eastern Barents Sea): Paleogeographic and tectonic implications for the high Arctic: Tectonics, v. 41, p. 1–27.

Ettensohn, F.R., 1985, The Catskill Delta complex and the Acadian Orogeny: A model, *in* Woodrow, D.L., and Sevon, W.D., eds., The Catskill Delta: Geological Society of America Special Paper 201, p. 39–49.

Ettensohn, F.R., 1987, Rates of relative plate motion during the Acadian orogeny based on the spatial distribution of black shales: Journal of Geology, v. 95, p. 572–582.

Ettensohn, F.R., 1991, Flexural interpretation of relationships between Ordovician tectonism and stratigraphic sequences, central and Southern Appalachians, U.S.A, *in* Barnes, C.R., and Williams, S.H., eds., Advances in Ordovician Geology: Geological Survey of Canada Paper 90-9, p. 213–224.

Ettensohn, F.R., 1992, Controls on the origin of the Devonian-Mississippian oil and gas shales, east-central United States. Fuel, v. 71, p. 1487–1492.

Ettensohn, F.R., 1997, Assembly and dispersal of Pangea: Large-scale tectonic effects on coeval deposition of North American, marine, epicontinental black shales: Journal of Geodynamics, v. 23, p. 287–309.

Ettensohn, F.R., 2004, Modeling the nature and development of major Paleozoic clastic wedges in the Appalachian basin, USA: Journal of Geodynamics, v. 37, p. 657–681.

Ettensohn, F.R., 2008, Chapter 4: The Appalachian foreland basin in eastern United States, *in* Miall, A., eds., The Sedimentary Basins of the United States and Canada: Sedimentary Basins of the World: Amsterdam, Elsevier, p. 105–179.

Ettensohn, F.R., and Lierman, R.T., 2012, Chapter 4, Large-scale tectonic controls on the origin of Paleozoic, dark shale, source-rock basins: Examples from the Appalachian foreland-basin region, eastern United States, *in* Gao, D., eds., Tectonics and Sedimentation: Implications for Petroleum Systems: American Association of Petroleum Geologists Memoir 100, p. 95–124.

Ettensohn, F.R., and Lierman, R.T., 2015, Using black shales to constrain possible tectonic and structural influence on foreland-basin evolution and cratonic yoking: Late Taconian Orogeny, Late Ordovician Appalachian Basin, eastern USA, *in* Gibson, G.M, Roure, F., and Manatschal, G., eds., Sedimentary basins and crustal processes at continental margins: From hyper-extended margins to deformed ancient analogues: Geological Society of London Special Publication 413, p. 119–141.

Ettensohn, F.R., Pashin, J.C., and Gilliam, W., 2019, The Appalachian and Black Warrior Basins: Foreland basins in the eastern United States, *in* Miall, A., eds., The Sedimentary basins of the United States and Canada: Sedimentary Basins of the World: Amsterdam, Elsevier, p. 129–237.

Evdokimov, A.N., Kalenich, A.P., Kryukov, B.D., Lastochkin, A.V., and Semenov, Yu.P., 2000, Novaya Zemlya -perspective resource object on the Barents-Kara shelf: Exploration and Protection of Mineral Resources, v. 12, v. 40–43 (in Russian).

Faleide, J.I., Gudlaugsson, S. T., and Jacquart, G., 1984, Evolution of the western Barents Sea: Marine Petroleum Geology, v. 1, p. 123–150.

Faleide, J.I., Tsikalas, F., Breivik, A.J., Mjelde, R., Ritzmann, O., Egen, Ø., Wilson, J., and Eldholm, O., 2008, Structure and evolution of the continental margin off Norway and the Barents Sea: Episodes v. 31, p. 82–91.

Faleide, J.I., Pease, V., Curtis, M., Klitzke, P., Minakov, A., Scheck-Wenderoth, M., Kostyuchenko, S., and Zayonchek, A., 2017, Tectonic implications of the lithospheric structure across the Barents and Kara shelves, *in* Pease, V., and Coakley, B., eds., Circum-Arctic Lithosphere Evolution: London, Geological Society of London, Special Publications, v. 460, p. 285–314.

Filatova, N.I., and Khain, V.E., 2010, The Arctida craton and Neoproterozoic–Mesozoic orogenic belts of the circum–polar region: Geotectonics v. 44, p. 203–227.

Finney, S.C., Grubb, B.J., and Hatcher, R.D.Jr, 1996, Graphic correlation of Middle Ordovician graptolite shale, southern Appalachians: An approach for examining the subsidence and migration of a Taconic foreland basin: Geological Society of America Bulletin, v. 108, p. 355–371.

Fjeldskaar, W., and Amantov, A., 2018, Effects of glaciations on sedimentary basins: Journal of Geodynamics, v. 118, p. 66–81.

Fleming, E.J., Flowerdew, M.J., Smyth, H.R., Scott, R.A., Morton, A.C., Omma, J.E., Frei, D., and Whitehouse, M.J., 2016, Provenance of Triassic sandstones on the southwest Barents Shelf and the implication for sediment dispersal patterns in northwest Pangea: Marine Petroleum Geology, v. 78, p. 516–535.

Foucher, F., Hickman-Lewis, K., Hutzler, A., Joy, K.H., Folco, L., Bridges, J.C., Wozniakiewicz, P., Martínez-Frías, J., Debaille, V., Zolensky, M., Yano, H., Bost, N., Ferrière, L., Lee, M., Michalski, J., Schroeven-Deceunink, H., Kminek, G., Viso, M., Russel, S., Smith, C., Zipfel, J., and Westall, F., 2021, Definition and use of functional analogues in planetary exploration: Planetary and Space Science, v. 197, p. 1–13.

Gabrielsen, R.H., Færseth, R.B., Jensen, L.N., Kalheim, J.E., and Fridtjof, R., 1990, Structural elements of the Norwegian continental shelf. Pt. 1. The Barents Sea Region: Norwegian Petroleum Directorate Bulletin, v. 6, p. 1–33.

Gabrielsen, R.H., Sokoutis, D., Willingshofer, E., and Faleide, J.I., 2016, Fault linkage across weak layers during extension: an experimental approach with reference to the Hoop Fault Complex of the SW Barents Sea: Petroleum Geoscience, v. 22, p. 123–135.

Gac, S., Huismans, R.S., Simon, N.S.C., Podladchikov, Y.Y., and Faleide, J.I., 2013, Formation of intracratonic basins by lithospheric shortening and phase changes: a case study from ultra-deep East Barents Sea basin: Terra Nova, v. 25, p. 459–463.

Gac, S., Huismans, R.S., Simon, N.S.C., Faleide, J.I., and Podladchikov, Y.Y., 2014, Effects of lithosphere buckling on subsidence and hydrocarbon maturation: a case-study from the ultra-deep East Barents Sea basin: Earth and Planetary Science Letters, v. 407, p. 123–133.

Gac, S., Klitzke, P., Minakov, A., Faleide, J.I., and Scheck-Wenderoth, M., 2016, Lithospheric strength and elastic thickness of the Barents Sea and Kara Sea region. Tectonophysics: v. 691, p. 120–132.

Gao, D., Shumaker, R.C., and Wilson, T.H., 2000, Along-axis segmentation and growth history of the Rome Trough in the central Appalachian Basin: American Association of Petroleum Geologists Bulletin, v. 84, p. 75–99.

Gasser, D., 2014, The Caledonides of Greenland, Svalbard and other Arctic areas: status of research and open questions: Geological Society, v. 390, p. 93–129.

Gavrilov, V.P., Gibshman, N.B., Karnaukhov, S.M., Kholodilov, V.A., Tsemkalo, M.A., and Shamalov, Y.V., 2010, Biostratigraphy and lithofacies oil and gas bearing deposits Barents-Kara Sea region: Moscow, Nedra Publishing House, 255 p.

Gee, D. G., 2005, Timanides of Northern Russia, *in* Selley, R.C., Cocks, L.R.M., and Plimer, I.R., eds., Encyclopedia of Geology: Amsterdam, Elsevier, V. 2, p. 64–74.

Gee, D.G., Bogolepova, O.K., and Lorenz, H., 2006, The Timanide, Caledonide and Uralide orogens in the Eurasian high arctic, and relationships to the palaeo-continents Laurentia, Baltica and Siberia, *in* Gee, D.G., and Stephenson, R.A., European Lithosphere Dynamics: London, Geological Society, v. 32, p. 507–520.

Gee, D.G., Fossen, H., Henriksen, N., and Higgins, A.K., 2008, From the Early Paleozoic platforms of Baltica and Laurentia to the Caledonide Orogen of Scandinavia and Greenland: Episodes, v. 31, p. 44–51.

Gee, D.G., Juhlin, C., Pascal, C., and Robinson, P., 2010, Collisional orogeny in the Scandinavian Caledonides: GFF, v. 132, p. 29–44.

Georgiev, S.V., Stein, H.J., Hannah, J.L., Xu, G., Bingen, B., and Weiss, H.M., 2017, Timing, duration, and causes for Late Jurassic-Early Cretaceous anoxia in the Barents Sea: Earth and Planetary Science Letters, v. 461, p. 151–162.

Gernigon, L., Brönner, M., Roberts, D., Olesen, O., Nasuti, A., Yamasaki, T., 2014, Crustal and basin evolution of the southwestern Barents Sea: from Caledonian Orogeny to continental breakup: Tectonics v. 33, p. 347–373.

Gernigon, L., Brönner, M., Dumais, M.-A., Gradmann, S., Gr.nlie, A., Nasuti, A., and Roberts, D., 2018, Basement inheritance and salt structures in the SE Barents Sea: Insights from new potential field data: Journal of Geodynamics, v. 119, p. 82–106.

Gilmullina, A., Klausen, T.G., Paterson, N.W., Suslova, A., and Eide, C.H., 2021a, Regional correlation and seismic stratigraphy of Triassic strata in the greater Barents Sea: implications for sediment transport in Arctic basins: Basin Research, v. 33, p. 1546–1579.

Gilmullina, A., Klausen, T.G., Doré, A.G., Rossi, V.M., Suslova, A., and Eide, C.H., 2021b, Linking sediment supply variations and tectonic evolution in deep time, source-to-sink systems—the Triassic Greater Barents Sea Basin: GSA Bulletin, v. 0, p.1–21.

Glørstad-Clark, E., Birkeland, E.P., Nystuen, J.P., Faleide, J.I., and Midtkandal, I., 2011, Triassic platform-margin deltas in the western Barents Sea: Marine Petroleum Geology, v. 28, p. 1294–1314.

Golonka, J., and Ford, D., 2000, Pangean (Late Carboniferous-Middle Jurassic) paleoenvironment and lithofacies: Palaeogeography. Palaeoclimatology, Palaeoecology, v.161, p.1–34.

Greb, S.F., Pashin, J.C., Martino, R.L., and Eble, C.F., 2008, Appalachian sedimentary cycles during the Pennsylvanian: Changing influences of sea level, climate, and tectonics, *in* Fielding, C.R., Frank, T.D., and Isbell, J.L., eds., Resolving the Late Paleozoic Ice Age in Time and Space: Geological Society of America Special Paper 441, p. 235–248.

Grogan, P., Østvedt-Ghazi, A.-M., Larssen, G.B., Fotland, B., Nyberg, K., Dahlgren, S., and Eidvin, T., 1999, Structural elements and petroleum geology of the Norwegian sector of the northern Barents Sea, *in* Fleet, A.J., and Boldy, S.A.R., eds., Petroleum Geology of Northwest Europe: Proceedings of the 5th Conference: London, the Geological Society, v. 1, 247–259 p.

Gudlaugsson, S.T., Faleide, J.I., Johansen, S.E., and Breivik, A.J., 1998, Late Palaeozoic structural development of the South-Western Barents Sea: Marine Petroluem Geology, v. 15, p. 73–102.

Guo, L., Schekoldin, R., and Scott, R., 2010, The Devonian succession in northern Novaya Zemlya, Arctic Russia: Sedimentology palaeogeography and hydrocarbon occurrence: Journal of Petroleum Geology, v. 33, p. 105–122.

Hatcher, R.D., Jr., 2010, The Appalachian orogen: A brief summary, *in* Tollo, R.P., Bartholomew, M.J., Hibbard, J.P., and Karabinos, P.M., eds., From Rodinia to Pangea: The Lithotectonic Record of the Appalachian Region: Geological Society of America Memoir, v. 206, p. 1–19.

Hatcher, R.D.Jr., 2014, The Appalachian orogen: Reference Module in Earth Systems and Environmental Sciences, p. 1–18.

Hatcher, R.D., Jr., Thomas, W.A., Geiser, P.A., Snoke, A.W., Mosher, S., and Wiltschko, D.V., 1989, Chapter 5, Alleghanian orogen, *in* Hatcher, R.D., Jr., Thomas, W.A., and Viele, G.W., eds., The Appalachian-Ouachita Orogen in the United States, The Geology of North America: Boulder, Geological Society of America, v. F-2, p. 233–318.

Hatcher, R.D., Jr., Bream, B.R., and Merschat, A.J., 2007, Tectonic map of the southern and central Appalachians: A tale of three orogens and a complete Wilson cycle, *in* Hatcher, R.D., Jr., Carlson, M.P., McBride, J.H., and Martínez Catalan, J.R., eds., 4-D Framework of Continental Crust: Geological Society of America Memoir, v. 200, p. 595–632.

He, M., Moldowan, J.M., Nemchenko-Rovenskaya, A., and Peters, K.E., 2012, Oil families and their inferred source rocks in the Barents Sea and northern Timan-Pechora Basin, Russia: American Association of Petroleum Geologists Bulletin, v. 96, p. 1121–1146.

Heidlauf, D.T., Hsui, A.T., and Klein, G.D., 1986, Tectonic subsidence analysis of the Illinois Basin: Journal of Geology, v. 94, p. 779–794.

Henriksen, E., Ryseth, A.E., Larssen, G.B., Heide, T., Rønning, K., Sollid, K., and Stoupakova, A.V., 2011, Tectonostratigraphy of the greater Barents Sea: Implications for petroleum systems. In: Spencer, A.M., Embry, A.F., Gautier, D.L., Stoupakova, A., Sørensen, K. (Eds.), Arctic Petroleum Geology, 35. Geological Society, Memoirs, London, pp. 163–195.

Henriksen, E., Kvamme, L., and Rydningen, T.A., 2021, Hammerfest Basin composite tectono-sedimentary element, Barents Sea, *in* Drachev, S.S., Brekke, H., Henriksen, E., and Moore, T., eds., Sedimentary successions of the Arctic region and their hydrocarbon prospectivity: London, Geological Society Memoirs, v. 57, p. 2017–2023.

Howell, P.D., and van der Pluijm, B.A., 1990, Early history of the Michigan Basin: Subsidence and Appalachian tectonics: Geology, v. 18, p. 1195–1198.

Howell, J.A., Martinius, A.W., and Good, T.R., 2014, The application of outcrop analogues in geological modelling: a review, present status and future outlook, *in* Martinius A.W., Howell, J.A., and Good, T.R., eds., Sediment-body geometry and heterogeneity: Analogue studies for modelling the subsurface: London, Geological Society, Special Publications, v. 387, p. 1–25.

Indrevær, K., Gac, S., Gabrielsen, R.H., and Faleide, J.I., 2017, Crustal-scale subsidence and uplift caused by metamorphic phase changes in the lower crust: a model for the evolution of the Loppa High area, SW Barents Sea from late Paleozoic to Present: Journal of the Geological Society, v. 175, p. 1–12.

Ivanova, N.M., 1997, Prospective Paleozoic reefs in the southern part of the Barents Sea shelf: Petroleum Geoscience, v. 3, p. 153–160.

Ivanova, N.M., Sakoulina, T.S., and Roslov, Yu, 2006, Deep seismic investigations across the Barents–Kara region and Novozemelskiy fold belt (Arctic shelf): Tectonophysics v. 420, p. 123–140.

Jamieson, R.A., and Beaumont, C., 1988, Orogeny and metamorphism: A model for deformation and pressure-temperature-time paths with applications to the central and southern Appalachians: Tectonics, v. 7, p. 417–445.

Johansen, S.E., Ostisty, B.K., Birkeland, Ø, Federovsky, Y.F., Martirosjan, V.N., Bruun Christensen, O., Cheredeevm S.I., Ignatenko, E.A., and Margulis, L.S., 1993, Hydrocarbon potential in the Barents Sea region: play distribution and potential, *in* Vorren, T.O., Bergsager, E., Dahl-Stamnes, Ø.A., Holter, E., Johansen, B., Lie, E., and Lund, T.B., eds., Arctic Geology and Petroleum Potential: Amsterdam, Elsevier, v. 2, p. 273–320.

Johnson, J.G., 1971, Timing and coordination of orogenic, epeirogenic, and eustatic events: Geological Society of America Bulletin, v. 82, p. 3263–3298.

Karner, G.D., and Watts, A.B., 1983, Gravity anomalies and flexure of the lithosphere at mountain ranges: Journal of Geophysical Research, v. 88, p. 10,449–10,477.

Khudoley, A.K., Sobolev, N.N., Petrov, E.O., Ershova, V.B., Makariev, A.A., Makarieva, E.V., Gaina, C., and Sobolev, P., 2019, A reconnaissance provenance study of Triassic–Jurassic clastic rocks of the Russian Barents Sea: GFF, v. 141, p. 1–9.

Klausen, T.G., and Helland-Hansen, W., 2018, Methods for restoring and describing ancient clinoform surfaces: Journal of Sedimentary Research, v. 88, p. 241–259.

Klausen, T.G., Ryseth, A.E., Helland-Hansen, W., Gawthorpe, R., and Laursen, I., 2014, Spatial and temporal changes in geometries of fluvial channel bodies from the Triassic Snadd Formation of offshore Norway: Journal of Sedimentary Research v. 84, p. 567–585.

Klausen, T.G., Ryseth, A.E., Helland-Hansen, W., Gawthorpe, W., and Laursen, I., 2015, Regional development and sequence stratigraphy of the Middle to Late Triassic Snadd Formation, Norwegian Barents Sea: Marine Petroleum Geology, v. 62, p. 102–122.

Klausen, T.G., Müller, R., Slama, J., and Helland-Hansen, W., 2016, Evidence for Late Triassic provenance areas and Early Jurassic sediment supply turnover in the Barents Sea basin of northern Pangea: Lithosphere, v. 9, p. 14–28.

Klausen, T.G., Nyberg, B., and Helland-Hansen, W., 2019, The largest delta plain in Earth's history: Geology, v. 47, p. 470–474.

Klausen, T.G., Müller, R., Poyatos-Moré, M., Olaussen, S., and Stueland, Erik., 2022, Tectonic, provenance and sedimentological controls on reservoir characteristics in the Upper Triassic–Middle Jurassic Realgrunnen Subgroup, SW Barents Sea: Geological Society of London Special Publications, v. 495, p. 237–261.

Klein, G.de V., and Hsui, A.T., 1987, Origin of cratonic basins: Geology, v. 15, p. 1094–1098.

Klitzke, P., Faleide, J. I., Scheck-Wenderoth, M., and Sippel, J., 2015, A lithosphere-scale structural model of Barents Sea and Kara Sea region: Solid Earth, v. 6, p. 153–172.

Klitzke, P., Franke, D., Ehrhardt, A., Lutz, R., Reinhardt, L., Heyde, I., and Faleide, J.I., 2019, The Paleozoic evolution of the Olga Basin region, northern Barents Sea: a link to the Timanian Orogeny: Geochemistry, Geophysics, Geosystems, v. 20, p. 1–16.

Klug, B., 1993, Cyclic facies architecture as a key to depositional controls in a distal foredeep: Campanian Mesaverde Group, Wyoming, USA: Geol Rundsch, v. 82, p. 306–326.

Knapp, J.H., Diaconescu, C.C., Bader, M.A., Sokolov, V.B., Kashubin, S.N., and Rybalka, A.V., 1998, Seismic reflection fabrics of continental collision and post-orogenic extension in the middle Urals, central Russia: Tectonophysics, v. 288, p. 115–126. https://doi.org/10.1016/S0040 -1951(97)00288 -6

Kneller, B.C., 1991, A foreland basin on the southern margin of Iapetus: Journal of the Geological Society, v. 148, p. 207–210.

Knutsen, S.-M., and Larsen, K.I., 1997, The late Mesozoic and Cenozoic evolution of the Sørvestsnaget Basin: a tectonostratigraphic mirror for regional events along the southwestern Barents Sea margin: Marine Petroleum Geology, v. 14, p. 27–54.

Kolata, D.R., and Nelson, W.J., 1991, Tectonic history of the Illinois basin, *in* Leighton, M.W., Kolata, D.R., Oltz, D.F., and Eidel, J.J., eds., Interior Cratonic Basins: Tulsa, American Association of Petroleum Geologists, Memoir 51, p. 263–285.

Korago, E.A., Kovaleva, G.N., Schekoldin, R.A., II'in, V.F., Gusev, E.A., Krylov, A.A., and Gorbunov, D.A., 2022, Geological structure of the Novaya Zemlya archipelago (West Russian Arctic) and peculiarities of the tectonics of the Eurasian Arctic: Geotectonics, v. 56, p. 21–57.

Konyukhov, A.I., 2014, Hydrocarbon source rocks in sedimentary basins of continental margins in the Middle-Late Paleozoic: Lithology and Mineral Resources, v. 49, p. 336–358.

Konyukhov, A.I., 2016, Black shales and other sediments with high organic matter contents in Phanerozoic climatic cycles: Communication 2. Black Shales during the Pangea Existence: Lithology and Mineral Resources, v. 51, p. 42–67.

Kruse, S., and McNutt, M., 1988, Compensation of Paleozoic orogens: a comparison of the Urals to the Appalachians: Tectonophysics, v. 154, p. 1–17.

Kuznetsov, N.B., 2006, The Cambrian Baltica–Arctida Collision, Pre-Uralide–Timanide Orogen, and its erosion products in the Arctic: Doklady Earth Sciences, v. 411A, p. 1375–1380.

Larssen, G. B., Elvebakk, G., Henriksen, L. B., Kristensen, S.-E., Nilsson, I., Samuelsberg, T. J., Sv.n., T. A., Stemmerik, L., and Worsley, D., 2002, Upper Paleozoic lithostratigraphy of the southern Norwegian Barents Sea: Norwegian Petroleum Directorate, 76 p.

Lasabuda, A.P.E., Johansen, N.S., Laberg, J.S., Faleide, J.I., Senger, K., Rydningen, T.A., Patton, H., Knutsen, S.-M., and Hanssen, A., 2021, Cenozoic uplift and erosion of the Norwegian Barents Sea shelf —a review: Earth Science Reviews, v. 217, p. 1–35.

Leonchik, M.I., and Senin, B.V., 2010, Oil potential prospects for Paleozoic carbonates in the Russian sector of the Barents Sea: Neftegasovaa. Geologia / Teoria I Practika v. 5, p. 1–16. (in Russian).

Lerch, B., Karlsen, D.A., Abay, T.B., Duggan, D., Seland, R., and Backer-Owe, K., 2016, Regional petroleum alteration trends in Barents Sea oils and condensates as a clue to migration regimes and processes: AAPG Bulletin, v. 2, p. 165–190.

Lindsay, J.F., Kennard, J.M., and Southgate, P.N., 1993, Application of sequence stratigraphy in an intracratonic setting, Amadeus Basin, central Australia, *in* Posamentier, H.W., Summerhayes, C.P., Haq, B.U., and Allen, G.P., eds., Sequence Stratigraphy and Facies Associations: Cambridge, Blackwell Scientific Publications, v.18, p. 605–631.

Line, L.H., Müller, R., Klausen, T.G., Jahren, J., and Hellevang, H., 2020, Distinct petrographic responses to basin reorganization across the Triassic–Jurassic boundary in the southwestern Barents Sea: Basin Research, v. 32, p. 1463–1484.

Lobkovsky, L.I., Cloetingh, S., Nikishin, A.M., Volozh, Yu.A., Lankreijer, A.C., Belyakov, S.L., Groshev, V.G., Fokin, P.A., Milanovsky, E.E., Pevzner, L.A., Gorbachev, V.I., and Korneev, M.A., 1996, Extensional basins of the former Soviet Union – structure, basin formation mechanisms and subsidence history: Tectonophysics, v. 266, p. 251–285.

Lopatin, B.G., Pavlov, L.G., Orgo, V.V., and Shkarubo, S.I., 2001, Tectonic structure of Novaya Zemlya: Polarforschung, v. 131, p. 131–135.

Lopatin, N.V., Zubairaev, S.L., Kos, I.M., Emets, T.P., Romanov, E.A., and Malchikhina, O.V., 2003, Unconventional oil accumulations in the Upper Jurassic Bazhenov black shale formation, West Siberian basin: a self-sourced reservoir system: Journal of Petroleum Geology, v. 26, p. 225–244.

Lopes, G., Mangerud, G., Clayton, G., and Mørk, A., 2016, New insights on East Finnmark Platform palynostratigraphy and paleogeography –A study of three shallow cores from a Mississippian succession in the Barents Sea, Norway: Palaeogeography, Palaeoclimatology, Palaeoecology, v. 450, p. 60–76.

Lord, G.S., Solvi, K.H., Klausen, T.G., and Mørk, A., 2014, Triassic channel bodies on Hopen, Svalbard: Their facies, stratigraphic significance and spatial distribution: Norwegian Petroleum Directorate, v. 11, p. 41–59.

Lord, G.S., Mørk, M. B. E., Mørk, A., and Olaussen, S., 2019, Sedimentology and petrography of the Svenskøya Formation on Hopen, Svalbard: an analogue to sandstone reservoirs in the Realgrunnen Subgroup: Polar Research, v. 38, p. 1–24.

Lundschien, B.A., Høy, T., and Mørk, A., 2014, Tryassic hydrocarbon potential in the northern Barents Sea; integrating Svalbard and stratigraphic core data: Norwegian Petroleum Directorate Bulletin, v. 11, p. 3–20.

Marello, L., Ebbing, J., and Gernigon, L., 2013, Basement inhomogeneities and crustal setting in the Barents Sea from a combined 3D gravity and magnetic model: Geophys. J. Int., v. 193, p. 1–29.

Margulis, E.A., 2008, Factors of formation of a unique Shtokmanovsky-Ludlovsky gas accumulation node in the Barents Sea: Neftegasovaâ Geologiâ Teoriâ I Practika, v. 3, p. 1–15 (in Russian).

Margulis, E.A., 2009, Evolution of the Barents Sea region and its hydrocarbon systems: Neftegasovaâ Geologiâ Teoriâ I Practika, v. 4, p. 1–14 (in Russian).

Martins, G., Ettensohn, F., and Knutsen, S.-M., 2022, The Appalachian area as a tectonostratigraphic analogue for the Barents Sea shelf: Basin Research, v. 34, p. 274–299.

Martins, G., Ettensohn, F., and Knutsen, S-M., 2023a, Use of backstripping in the Triassic–Middle Jurassic, south-central Barents Sea shelf succession to understand regional tectonic mechanisms and structural responses: Tectopnophysics, v. 853, p. 1–19.

Martins, G., Ettensohn, F., and Knutsen, S-M., 2023b, Interpreting the Upper Triassic–Lower Jurassinc sedimentary succession across the south-central Barents Sea shelf: An exercise in compressional, tectonostratigraphic analogue modelling: Frontiers, v. 0, p. x-xx. (in peer-review).

Merschat, A.J., and Hatcher, R.D., Jr., 2007, The Cat Square terrane: Possible Silurian-Devonian remnant ocean basin in the Inner Piedmont, Southern Appalachians, U.S.A., in Hatcher, R.D., Jr., Carlson, M.P., McBride, J.H., and Martínez Catalan, J.R., eds., 4-D Framework of Continental Crust: Geological Society of America Memoir v. 200, p. 1252–1281.

Matte, P., 2002, Variscides between Appalachians and the Urals: Similarities and differences between Paleozoic subduction and collision belts: Geological Society of America, Special Paper, v. 364, p. 1–13).

Matysik, M., Stemmerik, L., Olaussen, S., and Brunstad, H., 2018, Diagenesis of spiculites and carbonates in a Permian temperate ramp succession –Tempelfjorden Group, Spitsbergen, Arctic Norway: Sedimentology, v. 65, p. 745–774.

McBride, J.H., and Kolata, D.R., 1999, Upper crust beneath the central Illinois basin: Geological Society of America Bulletin, v. 111, p. 375–394.

McKerrow, W.S., Mac Niocaill, C., and Dewey, J.F., 2000, The Caledonian Orogeny redefined: Journal of the Geological Society, v. 157, p. 1149–1154.

Miall, A.D., 1997, The geology of stratigraphic sequences: Berlin, Springer, 433 p.Müller, R., Klausen, T.G., Faleide, J.I., Olaussen, S., Eide, C.H., and Suslova, A., 2019, Linking regional unconformities in the Barents Sea to compression-induced forebulge uplift at the Triassic-Jurassic transition: Tectonophysics, v. 765, p. 35–51.

Miall, A.D., and Blakey, R.C., 2019, The Phanerozoic tectonic and sedimentary evolution of North America, *in* Miall, A., eds., The Sedimentary basins of the United States and Canada: Sedimentary Basins of the World: Amsterdam, Elsevier, p. 1–38.

Mørk, A, 1999, Compositional variations and provenance of Triassic sandstones from the Barents Shelf: Journal of Sedimentary Research, v. 69, p. 690–710.

Mørk, A., Embry, A.F., and Weitschat, W., 1989, Triassic transgressive–regressive cycles in the Sverdrup Basin, Svalbard and the Barents Sea shelf, *in* Collinson, J. D., eds., Correlation in Hydrocarbon Exploration: Bergen, Graham and Trotman, p. 113–130.

Mørk, A., Dallmann, W.K., Dypvik, H., Johannessen, E.P., Larssen, G.B., Nagy, J., Nøttvedt, A., Olaussen, S., Pchelina, T.M., and Worsley, D., 1999, Mesozoic lithostratigraphy, *in* Dallmann, W.K., eds., Lithostratigraphic lexicon of Svalbard. Upper Palaeozoic to Quaternary bedrock. Review and recommendations for nomenclature use: Tromsø, Norsk Polarinstitutt, p. 127–214.

Müller, R., Klausen, T.G., Faleide, J.I., Olaussen, S., Eide, C.H., and Suslova, A., 2019, Linking regional unconformities in the Barents Sea to compression-induced forebulge uplift at the Triassic-Jurassic transition: Tectonophysics, v. 765, p. 35–51

Nakrem, H.A., 2007, The 1921 O. Holtedahl Novaya Zemlya collection–geology (illustrated atlas): Oslo, Novazem, 31 p.

Nicolaisen, J.B., Elvebakk, G., Ahokas, J., Bojesen-Koefoed, J.A., Olaussen, S., Rinna, J., Skeie, J.E., and Stemmerik, L., 2019, Characterization of upper Palaeozoic organic-rich units in Svalbard: Implications for the petroleum systems of the Norwegian Barents shelf: Journal of Petroleum Geology, v. 42, p. 59–78.

Nikishin, A.M., Ziegler, P.A., Stephenson, R.A., Cloetingh, S.A.P.L., Furne, A.V., Fokin, P. A., Ershov, A.V., Bolotov, S.N., Korotaev, M.V., Alekseev, A.S., Gorbachev, V.I., Shipilov, E.V., Lankreijer, A., Bembinova, E.Yu., and Shalimov, I.V., 1996, Late Precambrian to Triassic history of the East European Craton: dynamics of sedimentary basin evolution: Tectonophysics, v. 268, p. 23–63.

Nikishin, A.M., Ziegler, P.A., Abbott, D., Brunet, M.-F., and Cloetingh, S., 2002, Permo-Triassic intraplate magmatism and rifting in Eurasia: Implications for mantle plumes and mantle dynamics: Tectonophysics, v. 351, p. 3–39.

Nikishin, V.A., Malyshev, N.A., Nikishin, A.M., and Obmetko, V.V., 2011, The Late Permian–Triassic system of rifts of the South Kara sedimentary basin: Moscow University Geology Bulletin, v. 66, p. 377–384.

Norina, D.A., Stupakova, A.V., and Kiryukhina, T.A., 2014, Depositional environments and the hydrocarbon generative potential of Triassic rocks of the Barents Sea basin: Moscow University Geology Bulletin, v. 69, p. 1–10.

Norwegian Petroleum Directorate (NPD), 2017, The Barents Sea North. Geological Assessment of Petroleum Resources in Eastern Parts of Barents Sea North: Stavanger, Norwegian Petroleum Directorate, 39 p.

Norwegian Petroleum Directorate (NPD)., 2021, Structural elements and fault lineaments of the Barents Sea shelf. https://www.npd.no/en/about -us/infor matio n-services/open-data/

Norwegian Petroleum Directorate (NPD), 2022, Factpages. https://factpages.npd.no/en/wellbore/ (accessed 02 November 2022).

O'Leary, N., White, N., Tull, S., Bashilov, V., Kuprin, V., Natapov, L., and Macdonald, D., 2004, Evolution of the Timan-Pechora and South Barents Sea basins: Geological Magazine, v. 141, p. 141–160.

Ohm, S.E., Karlsen, D.A., and Austin, T.J.F., 2008, Geochemically driven exploration models in uplifted areas: Examples from the Norwegian Barents Sea: American Association of Petroleum Geologists Bulletin, v. 92, p. 1191–1223.

Olaussen, S., Dalland, A., Gloppen, T. G., & Johannessen, E., 1984, Depositional environment and diagenesis of Jurassic reservoir sandstones in the eastern part of Troms I area, *in* Spencer, A.M., eds., Petroleum Geology of the North European Margin: Springer, Dordrecht, p. 61–79.

Olaussen, S., Larssen, G.B., Helland-Hansen, W., Johannessen, E.P., Nøttvedt, A., Riis, F., Rismyhr, B., Smelror, M., and Worsley, D., 2018, Mesozoic strata of Kong Karls Land, Svalbard, Norway; a link to the northern Barents Sea basins and platforms: Norwegian Journal of Geology, v. 98, p. 1–70.

Olaussen, S., Grundvåg, S-A., Senger, K., Anell, I., Betlem, P., Birchall, T., Braathen, A,. Dallmann, W., Jochmann, M., Johannessen, E.P., Lord, G., Mørk, A., Osmundsen, P.T., Smyrak-Sikora, A., and Stemmerik, L., 2022, The Svalbard Carboniferous to Cenozoic composite tectono-stratigraphic element: Geological Society, v. 57, p. 1–65.

Oliver, J., 1986, Fluids expelled tectonically from orogenic belts: Their role in hydrocarbon migration and other geologic phenomena: Geology, v. 14, p. 99–102.

Otto S.C., and Bailey, R.J., 1995, Tectonic evolution of the northern Ural Orogen: Journal of the Geological Society, v. 152, p. 903–906.

Palmer, C.J., and Clifford, C.W.G., 2020, Face pareidolia recruits mechanisms for detecting human social attention: Psychological Science, v. 31, p. 1–12.

Park, H., Barbeau, D.L.Jr, Rickenbaker, A., Bachmann-Krug, D., and Gehrels, G., 2010, Application of foreland basin detrital-zircon geochronology to the reconstruction of the southern and central Appalachian orogen: The Journal of Geology, 118, 23–44. https://doi.org/10.1086/648400

Paterson, N.W., and Mangerud, G., 2017, Palynology and depositional environments of the Middle–Late Triassic (Anisian–Rhaetian) Kobbe, Snadd and Fruholmen formations, southern Barents Sea, Arctic Norway: Marine and Petroleum Geology, v. 86, p. 304–324.

Paterson, W.N., and Mangerud, G., 2019, A revised palynozonation for the Middle–Upper Triassic (Anisian–Rhaetian) series of the Norwegian Arctic: Geological Magazine, v. 157, p. 1–25.

Paterson, N.W., Mangerud, G., Cetean, C.G., Mørk, A., Lord, G.S., Klausen, T.G., and Mørkved, P.T., 2016, A multidisciplinary biofacies characterization of the Late Triassic (late Carnian–Rhaetian) Kapp Toscana Group on Hopen, Arctic Norway: Palaeogeography, Palaeoclimatology, Palaeoecology, v. 464, p. 16–42.

Pease, V., Drachev, S., Stephenson, R., and Zhang, X., 2014, Arctic lithosphere – _a review: Tectonophysics, v. 628, p. 1–25.

Petrov, O.V., Sobolev, N.N., Koren, T.N., Vasiliev, V.E., Petrov, E.O., Larssen, G.B., and Smelror, M., 2008, Palaeozoic and Early Mesozoic evolution of the East Barents and Kara Seas sedimentary basins: Norwegian Journal of Geology, v. 88, p. 227–234.

Petrov, O.V., Mozorov, A., Shokalsky, S., Kashubin, S., Artemieva, I.M., Sobolev, N., Petrov, E., Ernst, R. E., Sergeev, S., and Smelror, M., 2016, Crustal structure and tectonic model of the Arctic region: Earth-Science Reviews, v. 154, p. 29–71.

Pitman, W. C. III, and Andrews, J. A., 1985, Subsidence and thermal history of small pull-apart basins, i*n* Biddle, K. T., and Christie-Blick, N., eds., Strike-slip deformation, basin formation, and sedimentation: Tulsa, SEPM, v. 37, p. 45–49.

Polyakova, I.D., 2015, Petroleum source rocks of the arctic region: Lithology and Mineral Resources, v. 50, p. 26–49.

Posamentier, H.W., and Morris, W.R., 2000, Aspects of stratal architecture of forced regressive deposits: Geological Society of London, v. 172, p. 19–46.

Price, R.A., 1973, Large-scale gravitational flow of supracrustal rocks, southern Canadian Rockies, *in* de Jong, K.A., and Scholten, R., eds., Gravity and Tectonics: New York, John Wiley, p. 491–502.

Prischepa, O.M., Bazhenova, T.K., and Bogatskii, V.I., 2011, Petroleum systems of the Timan-Pechora sedimentary basin (including the offshore Pechora Sea): Russian Geology and Geophysics, v. 52, p. 888–905.

Project Management Institute (PMI), 2017, A guide to the project management body of knowledge: Newtown Square, Project Management Institute, 976 p.

Proust, J.N., Chuvasov, B.I., Vennin, E., and Boisseau, T., 1998, Carbonate platform drowning in a foreland setting: The Mid-Carboniferous platform in western Urals (Russia): Journal of Sedimentary Research, v. 68, p. 1175–1188.

Puchkov, V. N., 1979, Bathyal complexes of the passive margins of geosynclines: Moskow, Nauka, 260 p. (in Russian).

Puchkov, V.N., 1997, Structure and geodynamics of the Uralian orogen, *in* Burg, J.P., and Ford, M., eds., Orogeny through Time: London, The Geological Society of London, Geological Society Special Publication, v. 121, p. 201–236.

Puchkov, V.N., 2002, Paleozoic evolution of the East European continental margin involved in the Uralide Orogeny, *in* Brown, D., Juhlin, C., and Puchkov, V., eds., Mountain Building in the Uralides: Washington DC, American Geophysical Union, Geophysical Monograph, v. 132, p. 9–31.

Puchkov, V.N., 2003, Uralides and Timanides: Their structural relationship and position in the geologic history of the Ural-Mongolian fold belt: Russian Geology and Geophysics, v. 44, p. 28–39.

Puchkov, V.N., 2009, The evolution of the Uralian Orogeny: Geological Society of London, Special Publications, v. 327, p. 161–195.

Puchkov, V. N., 2010, Geology of the Urals and Cis-Urals (actual problems of stratigraphy, tectonics, geodynamics and metallogeny): Ufa, Design Poligraph Service, 280 p. (in Russian)

Puchkov, V.N., 2018, The plumes – _a new world in geology of the Urals: Litosfera, v. 18, p. 483–499.

Puchkov, V.N., and Ivanov, K.S., 2020, Tectonics of the northern Urals and Western Siberia: General history of development: Geotectonics, v. 54, p. 35–53.

Puchkov, V.N., Ernst, R.E., Ivanov, K.S., 2021, The importance and difficulties of identifying mantle plumes in orogenic belts: an example based on the fragmented large igneous provinces (LIP) record in the Ural fold belt: Precambrian Research, v. 361, p. 106–186.

Quinlan, G.M., and Beaumont, C., 1984, Appalachian thrusting, lithospheric flexure, and the Paleozoic stratigraphy of the eastern interior of North America: Canadian Journal of Earth Sciences, v. 21, p. 973–996.

Rafaelsen, B., Elvebakk, G., Andreassen, K., Stemmerik, L., Colpaert, A., and Samuelsberg, T.J., 2008, From detached to attached carbonate buildup complexes –3D seismic data from the upper Palaeozoic, Finnmark Platform, Southwestern Barents Sea: Sedimentary Geology, v. 206, p. 17–32.

Reid, C.M., James, N.P., Beauchamp, B., and Kyser, T.K., 2007, Faunal turnover and changing oceanography: Late Paleozoic warm-to-cool water carbonates, Sverdrup basin, Canadian Arctic Archipelago: Palaeogeography, Palaeoclimatology, Palaeoecology, v. 249, p. 128–159.

Repetski, J.E., Robert, T.R., Anita, G.H., and Michael, H.T., 2008, Thermal maturity patterns (CAI and %Ro) in Upper Ordovician and Devonian rocks of the Appalachian Basin: A major revision of USGS Map I-917-E using new subsurface collections: United States Geological Survey, Scientific Investigations Map 3006, p. 26.

Riis, F., Lundschien, B.A., Høy, T., Mørk, A., and Mørk, M.B., 2008, Evolution of the Triassic shelf in the northern Barents Sea region: Polar Research v. 27, p. 318–338.

Rismyhr, B., Bjærke, T., Olaussen, S., Mulrooney, M.J., and Senger, K., 2019, Facies, palynostratigraphy and sequence stratigraphy of the Wilhelmøya subgroup (Upper Triassic–Middle Jurassic) in western central Spitsbergen, Svalbard: Norwegian Journal of Geology, v. 99, p. 183–212.

Ritzmann, O., and Faleide, J.I., 2009, The crust and mantle lithosphere in the Barents Sea/ Kara Sea region: Tectonophysics, v. 470, p. 89–104.

Roberts, A.M., Kusznir, N.J., Yielding, G., and Styles, P., 1998, 2D flexural backstripping of extensional basins: the need for a sideways glance: Petroleum Geoscience, v. 4, p. 327–338.

Roen, J.B., 1984, Geology of the Devonian black shales of the Appalachian basin: Organic Geochemistry, v. 5, p. 241–254.

Ryseth, A., Augustson, J. H., Charnock, M., Haugerud, O., Knutsen, S.-M., Midb.e, P.S., Opsal, J.G., and Sundsb., G., 2003, Cenozoic stratigraphy and evolution of the Sørvestsnaget Basin, southwestern Barents Sea: Norwegian Journal of Geology, v. 83, p. 107–130.

Ryseth, A., 2014, Sedimentation at the Jurassic–Triassic boundary, south-west Barents Sea: indication of climate change, *in* Martinius, W., Ravnås, R., Howell, J. A., Steel, R. J., and Wonham, J. P., eds., From Depositional systems to sedimentary successions on the Norwegian continental margin: Chichester, International Association of Sedimentologists, v. 46, p. 187–214.

Saunders, A.D., Jones, S.M., Morgan, L.A., Pierce, K.L., Widdowson, M., and Xu, Y.G., 2007, Regional uplift associated with continental large igneous provinces: The roles of mantle plumes and the lithosphere: Chemical Geology, v. 241, p. 282–318.

Schellart, W.P., and Strak, V., 2016, A review of analogue modelling of geodynamic processes: Approaches, scaling, materials and quantification, with an application to subduction experiments: Journal of Geodynamics, v. 100, p. 7–32.

Schenk, C.J., 2011, Geology and petroleum potential of the Timan-Pechora basin province, Russia, The geological evolution and hydrocarbon potential of the Barents and Kara shelves, *in* Spencer, A.M., Embry, A.F., Gautier, D.L., Stoupakova, A.V., Sørensen, K., eds., Arctic Petroleum Geology: London, The Geological Society of London Memoirs, v. 35, p. 283–294.

Sclater, J.G., and Christie, P.A.F., 1980, Continental stretching: an explanation of the post-mid-Cretaceous subsidence of the Central North Sea basin: Journal of Gephysical Research, v. 85, p. 3711–3739.

Scotese, C.R., and Wright, N., 2018, PALEOMAP paleodigital elevation models (PaleoDEMS) for the Phanerozoic. https://www.earthbyte.org/paleodem-resource-scotese-and-w right-2018/.

Scott, R.A., 2007, Eastern Barents Sea-Novaya Zemlya-Kara Sea tectonic relationships: The search for an appropriate analogue: CASP Report, Cambridge (p. 50).

Scott, R.A., Howard, J.P., Guo, L., Schekoldin, R., and Pease, V., 2010, Offset and curvature of the Novaya Zemlya fold-and-thrust belt, Arctic Russia, *in* Vining, B.A., and Pickering, S.C., eds., Petroleum Geology: From Mature Basins to New Frontiers – Proceedings of the 7th Petroleum Geology Conference: London, The Geological Society, Petroleum Geology Conferences, v. 7, p. 645–657.

Seidler, L., Steel, R.J., Stemmerik, L., and Surlyk, F., 2004, North Atlantic marine rifting in the Early Triassic: new evidence from East Greenland: Journal of the Geological Society, v. 161, p. 583–592.

Serck, C.S., Faleide, J.I., Braathen, A., Kjølhamar, B., and Escalona, A., 2017, Jurassic to Early Cretaceous basin configuration(s) in the Fingerdjupet Subbasin, SW Barents Sea: Marine Petroleum Geology, v. 86, p. 874–891.

Shatsillo, A.V., 2015, Interaction of Siberia and Baltica at the final stage of amalgamation of the Eurasian part of Pangea: Physics of the Solid Earth, v. 300, p. 300–314.

Shipilov, E.V., 2010, Role of the tectonomagmatic factor in formation of giant hydrocarbon accumulations in the East Barents Basin: Doklady Earth Sciences, v. 434, p. 1298–1302.

Shkarubo, S.I., Burguto, A.G., Zuykova, O.N., Kostin, D.A., Velichko, B.M., Zhuravlev, V.A., Zinchenko, A.G., Neupokoeva, A.A., Radchenko, M.S., and Rudenko, A.A., 2017, State geological map of the Russian Federation (in Russian): Saint Petersburg, VSEGEI, The North-Kara-Barents Sea series, Sheets S-38, Scale 1: 1,000,000.

Sims, P.K., Saltus, R.W., and Anderson, E.D., 2008, Precambrian basement structure map of the continental United States—An interpretation of geologic and aeromagnetic data: U.S. Geological Survey Scientific Investigations Map 3012, scale: 1:8,000,000.

Sinclair, H.D., Coakley, B.J., Allen, P.A., and Watts, A.B., 1991, Simulation of foreland basin stratigraphy using a diffusion model of mountain belt uplift and erosion: An example from the central Alps, Switzerland: Tectonics, v. 10, p. 599–620. https://doi.org/10.1029/90TC0 2507

Sloss, L.L., 1963, Sequences in the cratonic interior of North America: Geological Society of America Bulletin, v. 74, p. 93–114. https://doi. org/10.1130/0016-7606(1963)74[93:SITCI O]2.0.CO;2

Smelror, M., and Petrov, O.V., 2018, Geodynamics of the Arctic: from Proterozoic orogens to present day seafloor spreading: Journal of Geodynamics, v. 121, p. 185–204.

Smelror, M., Petrov, O.V., Larssen, G.B., and Werner, S.C., 2009, Geological History of the Barents Sea: Trondheim, Geological Survey of Norway, 135 p.

Sobornov, K., 2022, Korotaikha composite tectono-sedimentary element, Northwestern Russia: Geological Society, v. 57, p. 2–15.

Sobornov, K.O., and Astafiev, D. A., 2017, Structure, formation and oil and gas potential of the northern part of the Korothaika depression, Barents Sea: Vesti Gazovoy Nauki, v. 4, p. 25–37.

Sorokhtin, N.O., Lobkovsky, L.I., Kozlov, N.E., Novikov, N.G., Nikiforov, S.L., and Bogdanova, O.Y., 2015, Evolution of the Barents Sea basin and oil and gas potential of coastal zones in the Kola region: Doklady Earth Sciences, v. 465, p. 1229–1232.

Spina, V., Borgomano, J., Nely, G., Shchukina, N., Irving, A., Neumann, C., and Neillo, V., 2015, Characterization of the Devonian Kharyaga carbonate platform (Russia): Integrated and multiscale approach: AAPG Bulletin, v. 99, p. 1771–1799.

Sømme, T.O., Doré, A.G., Lundin, E.R., and Tørudbakken, B.O., 2018, Triassic–Paleogene paleogeography of the Arctic: Implications for sediment routing and basin fill: AAPG Bulletin, v. 102, p. 2481–2517.

Stemmerik L., 2000, Late Palaeozoic evolution of the North Atlantic margin of Pangea: Palaeogeography, Palaeoclimatology, Palaeoecology, v. 161, p. 95–126.

Stemmerik, L., and Worsley, D., 2005, 30 years on – _Arctic Upper Palaeozoic stratigraphy, depositional evolution and hydrocarbon prospectivity: Norwegian Journal of Geology, v. 85, p. 151–168.

Stemmerik, L., Larson, P.A., Larssen, G.B., Mørk, A., and Simonsen, B.T., 1994, Depositional evolution of Lower Permian Palaeoaplysina build-ups, Kapp Duner Formation, Bj.rn.ya, Arctic Norway: Sedimentary Geology, v. 92, p. 161–174.

Stephenson, R.A., Yegorova, T., Brunet, M.-F., Stovba, S., Wilson, M., Starostenko, V., Saintot, A., and Kuznir, N., 2006, Late Palaeozoic intra- and pericratonic basins on the East European Craton and its margins, *in* Gee, D.G., and Stephenson, R.A., eds., European Lithosphere Dynamics: London, The Geological Society of London, Memoirs, v. 32, p. 463–479.

Stockmal, G.S., Slingsby, A., and Waldron, J.W.F., 1998, Deformation styles at the Appalachian structural front, western Newfoundland: Implications of new industry seismic reflection data: Canadian Journal of Earth Sciences, v. 35, p. 1288–1306.

Stoupakova, A.V., Henriksen, E., Burlin, Yu.K., Larsen, G. B., Milne, J.K., Kiryukhina, T.A., Golynchik, P.O., Bordunov, S.I., Ogarkova, M.P., and Suslova, A.A., 2011, The geological evolution and hydrocarbon potential of the Barents and Kara shelves, *in* Spencer, A.M., Embry, A.F., Gautier, D.L., Stoupakova, A.V., Sørensen, K., eds., Arctic Petroleum Geology: London, The Geological Society of London, Memoirs, v. 35, p. 325–344.

Stoupakova, A.V., Fadeeva, N.P., Kalmykov, G.A., Bogomolov, A.K., Kiryukhina, T.A., Korobova, N.I., Shardanova, T.A., Suslova, A.A., Sautkin, R.S., Poludektina, E.N., Kozlova, E.V., Mitronov, D.V., and Korkots, F.V., 2015, Criteria for oil and gas search in domanic deposits of the Volga-Ural basin: Georesursy, v. 2, p. 77–86. (in Russian).

Stupakova, A.V., Suslova, A.A., Korobova, N.I., and Burlin, Y.K., 2012, Cyclicity and prospects of the Jurassic oil-and-gas complex on the Barents Sea shelf: Moscow University Geology Bulletin, v. 67, p. 353–360.

Su, W., Huff, W.D., Ettensohn, F.R., Liu, X., Zhang, J., and Li, Z., 2009, K-bentonite, black-shale and flysch successions at the Ordovician-Silurian transition, South China: Possible sedimentary responses to the accretion of Cathaysia to the Yangtze Block and its implications for the evolution of Gondwana: Gondwana Research, v. 15, p. 111–130.

Sun, S., Politt, D.A., Wu,S., and Leary, D.A., 2021, Use of global analogues to improve decision quality in exploration, development and production: American Association of Petroleum Geologists Bulletin, v. 105, p. 845–864.

Suslova, A.A., 2014, Seismostratigraphic analysis and prospects of the Jurassic deposits, Barents Sea shelf: Neftegasovaa. Geologia / Teoria I Practika, v. 9, p. 1–19. (in Russian).

Suvorova, E.B., and Matveeva, T.V., 2014, Lithofacies features of Carboniferous–Lower Permian strata from the Pechora Sea, *in* Stone, D.B., Grikurov, G.E., Clough, J.G., Oakey, G.N., and Thurston, D.K., eds., Proceedings of the International Conference on Arctic Margins VI: Saint Petersburg, VSEGEI, v. 1, p. 195–201.

Tankard, A.J., 1986, Depositional response to foreland deformation in the Carboniferous of eastern Kentucky: American Association of Petroleum Geologists Bulletin, v. 70, p. 853–868.

Tetra Tech, Inc., 1981, Evaluation of Devonian shale potential in Ohio. U.S. Department of Energy, Morgantown Energy Technology Center, Report DOE/METC-122, p. 61.

Thomas, W.A., 1985, The Appalachian-Ouachita connection: Paleozoic orogenic belt at the southern margin of North America: Annual Review of Earth and Planetary Sciences, v. 13, p. 175–199.

Timonin, N.I., Yudin, V.V., and Belyaev, A.A., 2003, Evolution of tectonic processes in history development of Pai-Khoi: Bull. Inst. Geol. Komi Sci. Center Ural Branch, v. 10, p. 7–9. (in Russian).

Timonin, N.I., Yudin, V.V., Belyaev, A.A., 2004, The paleogeodynamics of Pay-Khoy (In Russian): Ekaterinburg, UrD RAS, 229 p.

Tollo, R.P., Bartholomew, M.J., Hibbard, J.P., and Karabinos, P.M., 2010, From Rodinia to Pangea: The Lithotectonic record of the Appalachian region: Geological Society of America Memoir 206, 956 p.

Torsvik, T.H., and Cocks, L.R.M., 2017, Earth History and Palaeogeography: Cambridge Cambridge University Press, 324 p.

Tugarova, M., Pchelina, T., Ustinov, N., and Viskunova, K., 2008, Lithological and geochemical characteristics of Triassic sediments from the central part of the South Barents depression (Arkticheskaya-1 well): Polar Research, v. 27, p. 495–501.

U.S. Energy Information Administration (EIA)., 2021, Maps: Oil and gas exploration, resources, and production: Appalachian basin. https://www.eia.gov/maps/maps.htm?fbcli d=IwAR2 bc1KgMH2KX NdFoo ngJi7 oZZJf v24E-D79WzjaXPu lIy4O viJhi SnXxOU

Uchman, A., Hanken, N.-M., Nielsen, J.K., Grundvåg, S.-A., and Piasecki, S., 2016, Depositional environment, ichnological features and oxygenation of Permian to earliest Triassic marine sediments in Central Spitsbergen, Svalbard: Polar Research, v. 35, p. 1–21.

Ulmishek, G., 1986, Stratigraphic aspects of petroleum resource assessment, in Rice, D. D., eds., Oil and Gas Assessment: Methods and Applications, United States of America: American Association of Petroleum Geologists, p. 59–68.

Ulmishek, G.F., and Klemme, H.D., 1990, Depositional controls, distribution, and effectiveness of world's petroleum source rocks: U.S. Geological Survey Bulletin, v. 1931, p. 1–59.

Ustritskiy, V.I., and Tugarova, M.A., 2013, Barents Sea –Permian and Triassic reference section, encountered by the well Admiralteyskaya-1. Neftegasovaa. Geologia / Teoria I Practika, v. 8, p. 1–20. (in Russian)

Vail, P.R., and Mitchum, R.M.Jr., 1977, Seismic stratigraphy and global changes of sea level, part 1: Overview, *in* Payton, C.E., eds., Applications to hydrocarbon exploration: Ann Arbor, Edward Brothers, Memoir, v. 26, p. 51–53.

Vail, P.R., 1987, Seismic stratigraphy interpretation using sequence stratigraphy: Part 1: Seismic stratigraphy interpretation procedure: AAPG Special Volumes, v. 1, p. 1–10.

Viele, G.W., 1989, The Ouachita orogenic belt, *in* Hatcher, R.D., Jr., Thomas, W.A., and Viele, G.W., eds., The Appalachian-Ouachita Orogen in the United States, The Geology of North America: Boulder, Geological Society of America, v. F-2, p. 555–561.

Volkov, S.N., 1963, On the question of the relationship of the Urals, Pai-Khoy and Taimyr: VSEGUEI, v. 92, p. 25–27.

Vyssotski, A.V., Vyssotski, V.N., and Nezhdanov, A.A., 2012, Evolution of the West Siberian basin, *in* Roberts, D.G., and Bally, A.W., eds., Regional Geology and Tectonics: Phanerozoic Passive Margins, Cratonic Basins and Global Tectonic Maps: Amsterdam, Elsevier, v. 1, p. 755–801.

Walcott, R.I., 1970, Isostatic response to loading of the crust in Canada: Canadian Journal of Earth Sciences, v. 7, p. 2–13.

Watts, A.B., Karner, G.D., and Steckler, M.S., 1982, Lithospheric flexure and the evolution of sedimentary basins: Philosophical Transactions of the Royal Society of London, v. 305, p.249–281.

Weissel, J., and Karner, G.D., 1989, Flexural uplift of rift flanks due to mechanical unloading of the lithosphere during extension: Journal of Geophysical Research, v. 94, p. 13919–13950.

Wilson, J.T., 1966, Did the Atlantic close and then re-open?: Nature, v. 211, p. 676–681.

Worsley, D., 2008, The post-Caledonian development of Svalbard and the western Barents Sea: Polar Research, v. 27, p. 298–317.

Xie, X., and Heller, P.L., 2009, Plate tectonics and basin subsidence history: Geological Society of America Bulletin, v. 121, p. 55–64.

Zhang, X., Pease, V., Carter, A., and Scott, R., 2018, Reconstructing Palaeozoic and Mesozoic tectonic evolution of Novaya Zemlya: combining geochronology and thermochronology, *in* Pease, V., and Coakley, B., eds., Circum-Arctic Lithosphere Evolution: London, The Geological Society, Special Publications, v. 460, p. 335–353.

Zhuravlev, V. A., Korago, E. A., Kostin, D. A., and Zuikova, O. N., 2014, State geological map of the Russian Federation (in Russian): Saint Petersburg, VSEGUEI, The North-Kara-Barents Sea Series, Sheets R-39 and R40, Scale 1: 1,000,000.

Ziegler, P.A., 1987, Late cretaceous and Cenozoic intraplate compressional deformations in the Alpine foreland—a geodynamic model: Tectonophysics, v. 137, p. 389–420.

Ziegler, P.A., 1989, Evolution of Laurussia: Dordrecht. Kluwer Academic Publishers, 102 p.

VITA: GUSTAVO MARTINS

EDUCATION

2017: **M.S. Geology/Petroleum Geoscience**, University of Tromsø, Norway

2012: **B.S. Geology**, Federal University of Bahia, Salvador, Brazil

PROFESSIONAL POSITIONS HELD

Jan 2019 – 2023: **Research, Teaching, and Field Assistant**, University of Kentucky, United States

Sep 2016 – Nov 2016: **Scientific Assistant**, University of Tromsø, Norway.

Oct 2012 – Oct 2014: **Geophysicist**, Schlumberger, Norway, United Kingdom and United States

Aug 2011 – Aug 2012: **Geologist Intern**, Rio Tinto Minerals Development, Brazil

Jan 2011 – Mar 2011: **Geologist Intern**, Caraiba Metals, Brazil

Jul 2008 – Aug 2008: **Project Intern**, Petrobras S/A, Brazil

SCHOLASTIC AND PROFESSIONAL HONORS

2023: **Basin Research** (Impact Factor: 4.100) BREC award for best 2022 paper (*nominated)*

2021: Omicron Delta Kappa: The National Leadership Honor Society, **University of Kentucky**

2009 – Jul 2010: National Council for Scientific and Technological Development (CNPq), **Federal University of Bahia**

PROFESSIONAL PUBLICATIONS

Ettensohn, F.R., Seckinger, D. C., Eble, C. F., Clayton, G., Li, J., **Martins, G. A**., Hodelka, B. N., Lo, E. L., Harris, F. R., Taghizadeh, N., 2020, Age and tectonic significance of diamictites at the Devonian–Mississippian transition in the central Appalachian Basin. in Swezey, C.S., and Carter, M.W., eds., Geology Field Trips in and around the U.S. Capital: Geological Society of America Field Guide 57, p. 79–103. doi: https://doi.org/10.1130/2020.0057(04).

Martins, G., Ettensohn, F., and Knutsen, S. -M., 2022, The Appalachian area as a tectonostratigraphic analogue for the Barents Sea shelf: **Basin Research**, v. 34, p. 274–299. doi: https://doi.org/10.1111/bre.12619. (**Nominated for best 2022 paper/BREC award**).

Martins, G., Ettensohn, F., and Knutsen, S. -M., 2023, Use of backstripping in the Triassic–Middle Jurassic, southern-central Barents Sea shelf succession to understand regional tectonic mechanisms and structural responses: **Tectonophysics**, v. 853, p. 1–19. Doi: https://doi.org/10.1016/j.tecto.2023.229797.